THESIS FOR THE DEGREE OF DOCTOR OF PHILOSOPHY

Aging of Lean NO_X Trap Catalysts and Hydrocarbon Trapping in Cold-Start Applications

Rasmus Jonsson

Department of Chemistry and Chemical Engineering

CHALMERS UNIVERSITY OF TECHNOLOGY

Gothenburg, Sweden 2020

Aging of Lean NO_x Trap Catalysts and Hydrocarbon Trapping in Cold-Start Applications
Rasmus Jonsson
ISBN 978-91-7905-255-3

Doktorsavhandling vid Chalmers Tekniska Högskola
Ny serie nr 4722
ISSN 0346-718X

Chalmers University of Technology
Department of Chemistry and Chemical Engineering
SE-412 96 Gothenburg
Sweden
Telephone + 46 (0)31-772 1000

Printed by Chalmers Reproservice
CHALMERS UNIVERSITY OF TECHNOLOGY
Gothenburg, Sweden

Aging of Lean NO_X Trap Catalysts and Hydrocarbon Trapping in Cold-Start Applications

Rasmus Jonsson

Department of Chemistry and Chemical Engineering
Chalmers University of Technology

Abstract

It is well known that combustion processes worldwide give rise to emissions such as nitrogen oxides (NO_X), carbon monoxide (CO), hydrocarbons (HC) and particulates. For vehicles, the method for handling these emissions has been through the development of the catalytic converter. For the diesel engine, the Lean NO_X Trap (LNT) has been used since the 90s and is designed to function well in the high air/fuel ratio in which the diesel engine operates. The LNT often consist of a storage compound, e.g. barium, where NO_X is stored in lean conditions (high air/fuel ratio). During short rich pulses (low air/fuel ratio) the NO_X is released and reduced over the noble metal sites. Over time in use, these catalytic converters are exposed to the conditions that may reduce the catalytic properties of the catalyst and deactivation studies are therefore critical. Gasoline vehicles are often equipped with a hydrocarbon trap, to store HCs from the engine during the cold-start. The aim is that at higher temperature, when the catalyst is functioning, the HCs desorb and are oxidized.

Chemical poisoning of an LNT catalyst, i.e. $Pt/Ba/Al_2O_3$, was studied thoroughly. Both deactivation by phosphorus (P) as well as by zinc (Zn) was examined, because these elements can be found in the lubricant oil. The catalysts were exposed to P in two different ways. In the first study, P was introduced through gas-phase exposure by evaporating phosphoric acid. In the second study, both P and Zn were introduced to the $Pt/Ba/Al_2O_3$ catalyst through wet impregnation. The main findings were that gas-phase exposure results in an axial distribution where P can exist in different oxidation states at different positions over the washcoat. Moreover, it could be seen that Zn may help to suppress the deactivation caused by P on the LNT catalyst, and the suggested reason is due to formation of zinc phosphates. Furthermore, the main cause for deactivation of the LNT catalyst by P is attributed to the interaction between P and Ba.

The effect of catalyst composition was examined for HC Traps. The effect of promoting zeolites, by the addition of Pd, La and Fe, was studied. The addition of Fe did not show any significant effect on the toluene storage and release in comparison to zeolite beta. However, both Pd and La exhibited positive effects. The addition of La resulted in both an increase in the storage of toluene and an increase in the desorption temperature for toluene in wet conditions, which is beneficial. However, at higher La loadings, no beneficial effect of La could be seen. Lastly, during mixed-HC temperature programmed desorption experiments, an interaction mechanism between propane and toluene could be observed which resulted in higher adsorption capacity of propane on zeolite ZSM-5.

Keywords: LNT, NSR, Phosphorous, Zinc, Catalyst Deactivation, HC Trap, Cold-start, Toluene, La

Acknowledgements

The Competence Centre for Catalysis is hosted by Chalmers University of Technology and financially supported by the Swedish Energy Agency and the member companies AB Volvo, ECAPS AB, Johnson Matthey AB, Preem AB, Scania CV AB, Umicore Denmark ApS and Volvo Car Corporation AB.

Firstly, I would like to thank Louise Olsson who has been my main supervisor over these five years. She has been supportive and encouraging, together we have had many good discussions regarding the research. I value her goal-oriented and solution-oriented mind and her knowledge in the field.

I would also want to thank Magnus Skoglundh my co-supervisor for these five years. He has been engaged and provided plenty of good discussions and has been a linguistic anchor for turbulent waters. I have really valued his sharp mind and knowledge in the field.

I would also like to thank those that have assisted me during these years and taken part in the articles I have produced. So, a special thanks to Rojin, Malin, Eva, Torben, Oana, and Jungwon for your great and invaluable contribution.

I would like to thank Jonna for all the wonderful times. I am so blessed for having her in my life and it has meant so much to have her by my side. Thanks for the support over the years, you always brighten my days.

To all the co-workers over the years from KCK and KAT, the coffee, the games and the cheer. Patric my trusted and loyal squire which I shared office with for four years. The teammate during my bachelor thesis and five years of a collage, Ida. A grateful thanks to all my current colleagues Poonam, Joonsoo, Houman, Tobias, Pouya, Aiyong, Wayne, Streetama, Masood, Joby,Jesus, Salam and Diana. Seniors at the division and past colleagues such as Xavier, Prakhar, Mattias, Lidija and Kungpeng.

A great thanks to all the staff members such as Malin and Bengisu for helping me over these years.

I am grateful to my all my friends, from childhood and those that I have met later on in life, for keeping my spirit up. Finally, I would like to thank my family Rune, Elisabeth, David, Linnéa and Tobias. You support and love is irreplaceable.

List of publications and contribution

I. Gas-Phase Phosphorous Poisoning of Pt/Ba/Al_2O_3 NO_X storage Catalyst
Rasmus Jonsson, Oana Mihai, Jungwon Woo, Magnus Skoglundh, Eva Olsson, Malin Berggrund, and Louise Olsson

Catalysts 8 (2018) 155; *doi:10.3390/catal8040155*

Contribution: I am the main author. I synthesized the catalyst and performed the characterization with assistance from Lars Ilver for XPS. Jungwon Woo assisted me with ESEM and EDX mapping. I interpreted the results together with the co-authors. I wrote the manuscript.

II. Chemical poisoning by Zinc and Phosphorous of Pt/Ba/Al_2O_3 NOx storage catalysts

Rasmus Jonsson, Rojin Feizie Ilmasani, Torben Nilsson Pingel, Magnus Skoglundh, Eva Olsson, Malin Berggrund and Louise Olsson

Applied Catalysis A, General 571 (2019) 158-169
doi.org/10.1016/j.apcata.2018.11.027

Contribution: I am the main author. I synthesized the catalyst and performed the characterization and flow reactor experiments, except the STEM-EDX which was performed by Torben Nilsson Pingel. I was assisted by Rojin Feizi Ilmasani, who contributed with repetition of the findings. I interpreted the results together with the co-authors. I wrote the manuscript.

III. Zeolite beta doped with La, Fe, and Pd as a hydrocarbon trap
Rasmus Jonsson, Jungwon Woo, Magnus Skoglundh and Louise Olsson

Catalysts 10 (2020) 173; doi.org/10.3390/catal10020173

Contribution: I am the main author. I synthesized the catalyst and performed the characterization, with assistance from Jungwon Woo for STEM and EDX mapping. Eric Tam assisted with XPS measurements. I interpreted the results together with the co-authors. I wrote the manuscript.

IV. The Impact of Lanthanum and Zeolite Structure on Hydrocarbon Storage
Rasmus Jonsson, Aiyong Wang, Magnus Skoglundh and Louise Olsson

In manuscript (2020)

Contribution: I am the main author. I synthesized the catalyst with assistance from Aiyong Wang and performed the characterization and flow reactor experiments. Aiyong Wang assisted me with XRD measurements and BET surface measurements. I interpreted the results together with the co-authors. I wrote the manuscript.

Publications not included in this thesis

A. **Analysis of Particle Cloud Height Dynamics in a Stirred Tank**

Mattias Eng, Rasmus Jonsson and Anders Rasmusson, *AIChE Journal*, 62 (2016) 338-348.

List of abbreviations

BET	Brunauer Emmett Teller
CPSI	Cell per Square Inch
DOC	Diesel Oxidation Catalyst
DRIFTS	Diffusive Reflectance Infrared Fourier Transformed Spectroscopy
EDX	Energy Dispersive X-ray
ESEM	Environmental Scanning Electron Microscope
HC	Hydrocarbon
ICP-AES	Inductive Coupled Plasma Atomic Emission Spectroscopy
LNT	Lean NO_X Trap
NO_X	Nitrogen oxides (i.e. NO + NO_2)
NSR	NO_X Storage and Reduction
SAR	Silica Alumina Ratio
SCR	Selective Catalytic Reduction
SGB	Synthetic Gas Bench
STEM	Scanning Transmission Electron Microscopy
TEM	Transmission Electron Microscopy
TPD	Temperature Programmed Desorption
TPO	Temperature Programmed Oxidation
TWC	Three-Way Catalyst
XPS	X-ray Photoelectron Spectroscopy
XRD	X-ray Diffraction
ZDDP	Zinc dithiophosphate

Contents

1 Introduction

1.1 Background

In today's society, we are highly dependent on an efficient transport sector for both business and personal logistics. Most motorized vehicles use combustion engines, which can give rise to emissions of nitrogen oxides (NO_X), carbon monoxide (CO), and unburned hydrocarbons (HC). The field of exhaust abatement has been working actively to reduce these emissions in the last decades. Reducing these emissions is important for environmental and health reasons [1].

One of the earliest methods for treating these emissions that is still relevant today in gasoline-fueled vehicles is the three-way catalyst (TWC). The TWC is named for treating three components, namely NO_X, CO, and HC and converting these emissions into N_2, CO_2, and H_2O. This is made possible by the two main components of the TWC catalyst. These components are the noble metals, such as Pd or Rh and the oxygen storage component (OSC), such as CeO_2 and ZrO_2. The TWC is designed to operate in a stochiometric ratio that corresponds to a 14.6 air/fuel ratio by weight. In this stochiometric condition, the NO_X bi-product is almost eliminated due to no excess of air in the combustion process. This allows the TWC catalyst to primarily oxidize CO and HC in the exhaust, which is done efficiently. However, having the engine operate in a stochiometric condition is not good for the fuel economy. Therefore, to improve fuel economy, it is preferable to have the engine operate with excess air, in lean conditions.

In order to remove the NO_X in lean conditions, diesel vehicles mostly use either selective catalytic reduction (SCR) or a lean NO_X trap (LNT) to reduce the NO_X in the exhaust. The SCR catalyst, often equipped on trucks or heavy-duty vehicles, relies on the usage of urea, which is hydrolysed and decomposed into NH_3, which in the next step, reduces NO_X to form N_2 and H_2O. This technique requires the use of urea, therefore, LNT was introduced by Toyota in the 1990s [2–4]. The LNT catalyst is built on two essential components, a noble metal and a NO_X storage component. The engine alternates between lean phases (large excess of air) and short rich pulses (no excess of air). During the lean phase, NO_X in the exhaust is stored in the NO_X storage component, such as barium. During the rich pulses the stored NOx is released and reduced by CO and HC over the noble metal sites to form N_2 and H_2O [5–7].

New catalytic converters can efficiently reduce the NO_X to N_2 and H_2O. However, over time, catalytic converters may slowly deactivate for several reasons. Thermal aging is one deactivation mechanism that is hard to avoid. It is caused by exposure to the high temperatures that result in either the sintering of particles, which reduces the number of active sites on the

catalyst or collapse of the support material. Chemical poisoning, usually foreign substances, can deactivate the catalytic converter, resulting in blockage of active sites on the catalyst. These foreign substances are often introduced through fuel impurities or combusted oil lubricants. Deactivation of the catalyst results in an increase in the release of pollutants and is important to understand in detail and to prevent if possible.

Once catalytic converters have reached the temperature where they become active, usually called the "light-off" temperature, they operate with high efficiency. During the cold start of a vehicle, before light-off has been reached, catalytic converters are inefficient in removing pollutants from the exhaust [8–11]. For this reason, NO_X adsorbers and HC traps can be used to store the pollutants in the exhaust gas system until the light-off temperature has been reached. These trapping components are often based on zeolites that have a high surface area. These zeolites are often impregnated with a metal ion to adjust and improve the properties of the NO_X adsorber or HC trap in order to increase the temperature of desorption. Improvements in HC traps materials are important in order to steer the release temperature of the HCs to the optimum temperature window.

1.2 Objective

One of the objectives of this work is to increase the understanding of chemical poisoning by phosphorous and zinc on an LNT catalyst. Paper I focuses on the gas-phase exposure of phosphorous to $Pt/Ba/Al_2O_3$ and the effects of an uneven distribution of phosphorous onto the catalyst. Paper II reports on the effect of combining zinc and phosphorous on $Pt/Ba/Al_2O_3$ to study how these common poisoning species behave separately and in combination.

Large amount of the pollutants are released during the cold start and it is therefore critical to reduce the emissions at low temperature. Therefore, Papers III and IV focus on hydrocarbon trapping. Paper III reports on Pd/BEA impregnated with La and Fe to evaluate the synergy of different combinations of metals in the adsorption and desorption of toluene and propene during cold start applications. Paper IV mainly focuses on the effect of La in HC-trap materials. This includes different La loadings onto samples with different zeolites as the support material, such as zeolite beta, ZSM-5, and SSZ-13.

2 State of the art

2.1 NO_X storage mechanisms

2.1.1 Catalyst components

NO_X Storage and Reduction (NSR) has been a very important concept for removing NO_X from diesel vehicles since it was introduced by Toyota in 1996 [12]. The NSR catalyst, also denoted Lean NO_X trap (LNT), operates by altering between lean and rich phases. The lean phase refers to a mode in which the engine operates with a large excess of air. In the rich phase, which only lasts for a short period, the engine operates at a lower ratio air-fuel ratio. The concept of NSR is to take advantage of the reduction capacities of CO, H_2, and hydrocarbons in the rich phase to reduce the stored NO_X from the lean phase into N_2. Figure 1 depicts a schematic of this process; in the figure, NO is oxidized by O_2 on a noble metal to form NO_2 in lean conditions, after which NO_2 is stored on the storage component. After switching to rich conditions, reducing agents, marked "R," are adsorbed onto the noble metal where they react with the stored NO_X to form N_2.

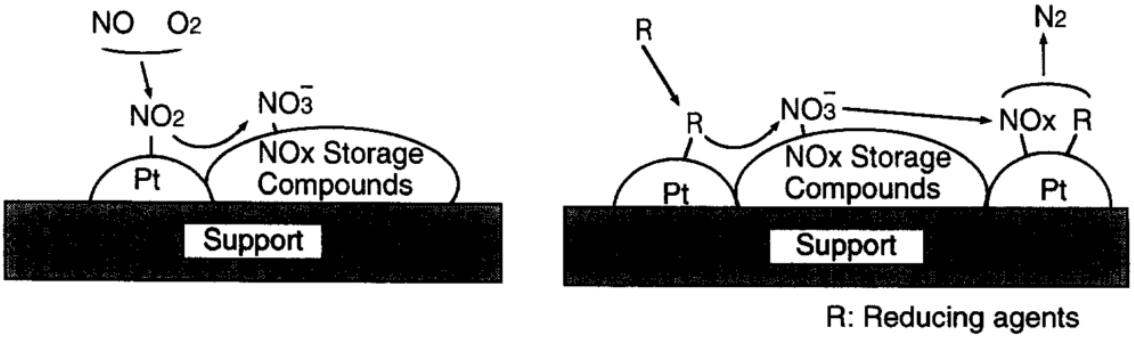

Figure 1. *An illustration of the NSR process. NO_X is stored on a NO_X storage component and thereafter reduced by reducing agents to N_2. The illustration is from Takahashi et al.* [2].

The NO_X storage compound, which is a key component in an LNT catalyst, is traditionally composed of alkali metals and alkaline earth metals, e.g. barium [3,6,13–20]. The effectiveness of such a metal correlates to the basicity of the metal. Kobayashi et al. have shown this when they studied the NO_X storage capacity of different metals [21]. They have concluded that the

order of NO_X storage capacity amongst alkali metals and alkaline earth metals followed K > Ba > Sr > Na > Ca > Li > Mg. Even if K has a higher NO_X storage capacity than Ba, it has poor stability at high temperatures [22].

Al_2O_3 is a common support material for LNT catalysts, both because of its high surface area and its NO_X storage capacity. However, NO_X storage on Al_2O_3 is more dominant in lower temperature ranges than NO_X storage on barium [23]. Shimizu et al. [24] have studied the impact of different support materials for Pt/Ba (MgO, Al_2O_3, ZrO_2, and SiO_2). Those authors found that even though Al_2O_3 did not contribute to the highest NO_X storage capacities, it contributed better than the other support materials to the reduction capacities of the catalyst, which was due to its acid-base properties.

The noble metal, where reactions take place, is of major importance for obvious reasons. A noble metal that frequently occurs in LNT catalyst formulations is Pt [2,13,14,17,18,25–29]. However, other noble metals are often used in combination with Pt, such as Pd and Rh, and different noble metals exhibit different properties [21]. Salasc et al. [30] have compared two catalyst formations, $Pt/BaO/Al_2O_3$ and $Pd/BaO/Al_2O_3$, where they found that Pd contributed to better NO_X storage capacity at 300°C, while the catalyst with Pt proved to perform better at 400°C. They explained this phenomenon with NO_X binding stronger to Pt at 300°C, resulting in a blocking of active sites on Pt, which inhibits the reduction of stored NO_X in the rich phase [30]. Andonova et al. [31] have found when comparing Pt to Rh, that Rh had better NO_X reduction abilities, however, Pt improved the NO_X storage during the lean phase.

Oxygen storage materials, such as ceria and zirconia, can be added to the LNT catalyst. Ji et al. [32] have found that the incorporation of CeO_2 into a $Pt/Rh/BaO/Al_2O_3$ catalyst enhanced NO_X conversion at temperatures in the range of 150-350°C. However, at higher temperatures, the conversion was lower with CeO_2 present in the catalyst formation [32]. For the TWC catalyst, CeO_2 has been found to promote the thermal stability of the Al_2O_3 support and increase the dispersion of the noble metal [33].

In summation, the LNT catalysts usually consist of an Al_2O_3 support with the possible addition of CeO_2. Commonly used noble metals are Pt, Rh, and Pd where Pt seems to occur more frequently than the others, either by itself or in combination with the other two. Based on literature, Ba has been found overall to be more efficient than other alkali metals and alkaline earth metals as a NO_X storage component.

2.1.2 NO_X storage and reduction mechanisms

Barium species in $Pt/Ba/Al_2O_3$ usually appear in the form of BaO, $Ba(NO_3)_2$, $Ba(OH)_2$, and $BaCO_3$. $Ba(OH)_2$ and $BaCO_3$ are formed due to H_2O and CO_2, which are the primary products of the combustion process. A study of NO_X storage performed by Lietti et al. has indicated a hierarchy between these species [34]. In the lean phase, NO_X was found to adsorb to free BaO, and, subsequently, a slip of water was observed, which indicated the storage of NO_X on $Ba(OH)_2$. A slip of CO_2 also occurred, indicating that storage on $BaCO_3$ had occurred in the last step.

In lean conditions, NO from exhaust gas reacts with O_2 on the surface of the platinum particles to form NO_2, which is then stored on BaO as $Ba(NO_3)_2$. NO_X can be stored as both nitrites and nitrates on BaO. Lietti et al. [34] have proposed that barium nitrites can be formed by 2NO + O* +BaO reacting to form $Ba(NO_2)_2$. For the storage of NO as nitrates, platinum or other noble metals must be present in order to oxidize the NO to NO_2, however, the storage of NO_2 does not require the presence of Pt since the NO_2 can adsorb directly onto the BaO and Al_2O_3 sites [35]. Several reaction pathways have been proposed for the NO_2 storage mechanism. Olsson at al. [18,36] have suggested a pathway with direct interaction with BaO sites, denoted S, where no CO_2 or H_2O is present during the experiments.

$$NO_2\ (g)\ +\ S\ \leftrightarrow S-(NO_2) \tag{1}$$

$$S-(NO_2)\ \leftrightarrow S-O+NO\ (g) \tag{2}$$

$$NO_2\ (g)\ +\ S-O\ \leftrightarrow S-(NO_3) \tag{3}$$

$$NO_2\ (g)\ +\ S-(NO_3) \leftrightarrow Ba(NO_3)_2 \tag{4}$$

$$2S-O\ \ \leftrightarrow 2S+\ O_2(g) \tag{5}$$

$$Pt-NO_2\ +\ S-(NO_3) \leftrightarrow Ba(NO_3)_2 + \text{Pt} \tag{6}$$

Reaction (1) describes the adsorption of NO_2 onto BaO, which, in Reaction (2), can lead to the formation of NO gas and BaO-O. Reaction (3) describes the formation of $BaO\text{-}NO_3$, which can further form $NO_2\text{-}BaO\text{-}NO_3$, referred to as $Ba(NO_3)_2$, through Reaction (5). The formation and decomposition of $Ba(NO_3)_2$ can be enhanced in the presence of Pt due to spillover from NO_2 adsorbed onto Pt (Reaction (6)).

Figure 2 shows the thermodynamic restrictions between NO and NO_2. At lower temperatures, NO_2 is more favored than NO, however, at higher temperatures, NO is more favored. A low amount of NO_2 was formed at low temperature in the experiment presented in Figure 2, and the reason for this is that the reaction was kinetically limited at low temperature. Since NO is favored at higher temperatures, according to thermodynamics, most NO_X in the exhaust gas from combustion processes is in the form of NO, which is about 90% of all NO_X [37]. The ratio between NO and NO_2 depends on the temperature of the catalyst [38]. This is clear from NO_2 Temperature Programmed Desorption (TPD) studies where the release of NO_X at lower temperatures favors NO_2, while at higher temperatures, NO is more favored [5,23]. Therefore, both the storage component, barium, and the noble metals, Pt, Pd, and Rh, are essential for the function of an LNT catalyst.

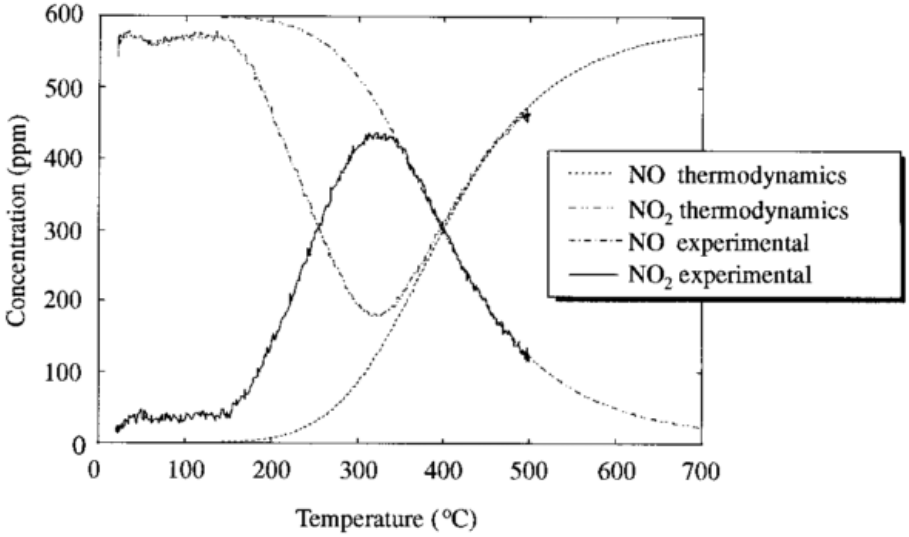

Figure 2. Temperature ramp with 600 ppm NO and 8 vol-% O_2. The image displays the experimental concentrations of NO and NO_2 compared to thermodynamic equilibrium. Image is from Olsson et al [38].

The lean phase is the desired mode of operation for both fuel economy and low CO_2 emission. Ideally, the lean phase should be as long as possible in relation to the rich phase, however, restrictions come with the NO_X storage capacity in the catalyst [3]. Perng et al. [39] have shown by comparing different lean/rich cycle lengths, all with a ratio 6:1, that the cycles with 6s lean phase and 1s rich phase exhibited the highest conversion of both NO_X and C_3H_6. The catalyst used for the study was a $Pt/Rh/BaO/CeO_2/Al_2O_3$ LNT. This shows the importance to consider both ratio and frequency, in other words, the total time spent in the lean phase and the frequency of switching between phases.

As mentioned in Section 2.1.2 regarding the hierarchy of $Ba(NO_3)_2$, $BaCO_3$, and $Ba(OH)_2$, H_2O and CO_2 affect the NO_X storage properties of the catalyst [40]. Epling et al. [40] have studied the NO_X storage capacity of a $Pt/Ba/Al_2O_3$ catalyst with and without H_2O and CO_2 in the gas mixture. They found that CO_2 strongly affected the NO_X trapping property of the catalyst at all temperatures investigated and more so at high temperatures. At lower temperatures, H_2O inhibited the NO_X trapping more than at higher temperatures. In addition, reports have shown that an increase in the concentration of H_2O may contribute to a higher conversion of NO_X [21].

CO and hydrocarbons are not fully combusted in the engine during the rich phase. Several research studies have examined regeneration during the rich phase using CO, [41,42] C_3H_6, [18,39,43–45] as well as H_2 [6,15,20,26,29,46] as the reducing agents. Abdulhamid et al. [42] have compared the properties of H_2, CO, and C_3H_6 as reducing agents on $Pt/Ba/Al_2O_3$, and they found that H_2 and CO performed better at lower temperatures than C_3H_6. The foremost products formed in the reduction of NO_X by H_2 were N_2 and NH_3, however, some N_2O was also formed. Nova et al. [29] have studied the gases formed by the reduction of NO_X with the aid of H_2 in the rich phase on the $Pt/Ba/Al_2O_3$ catalyst. Firstly, the formation of N_2 dominated the regeneration in the early stage, thereafter, the formation of NH_3 increased as the concentration of N_2 decreased. Similar to that study, Lietti et al. [17] have compared products from the reduction of NO_X with the aid of H_2 with a reduction of NO_X by NH_3. With both reducing agents, they observe the formation of N_2 early in the rich phase with a slightly higher formation

of N_2 with NH_3 as the reducing agent. They concluded from this observation that the reduction of NO_X with H_2 was caused by the formation of NH_3, which then further reacted with stored NO_X to form N_2 and H_2O. Furthermore, they concluded that $Ba(OH)_2$ was formed on the surface of the catalyst through the reduction of NO_X with H_2 and NH_3. Partridge et al. [6] have studied the reduction patterns of H_2 on $Pt/Ba/Al_2O_3$ using spaci-MS measurements. They found that NH_3 formed at the same time as N_2, indicating that NH_3 is an intermediate species in the reduction of NO_X with H_2, and the formed ammonia, therefore, reacted with the stored NO_X. These results are in good agreement with the study by Lietti et. al. [17]. C_3H_6 is also a good reducing agent, but it is not as good as H_2. Reactions between C_3H_6 and NO require higher temperatures and form CO_2, H_2O, and N_2 as the main products [18]. Another drawback with reducing NO_X with C_3H_6 is the formation of N_2O as a bi-product [43].

To summarize, BaO can react to form different compounds, such as $Ba(NO_3)_2$, $BaCO_3$, and $Ba(OH)_2$, which are associated with NO_X, CO_2, and H_2O, respectively. $Ba(OH)_2$ has been found to have less stability than $Ba(NO_3)_2$ and $BaCO_3$, both of which have a similar level of stability. There are three reducing agents commonly used in research on NSR activity on LNT catalysts; these are H_2, CO, and C_3H_6. These three reducing agents have different reaction pathways and have optimal operation at different temperatures. The products from the reduction of NO_X with H_2 are, through NH_3 as an intermediate species, N_2 and H_2O, whereas C_3H_6 forms CO_2, H_2O, and N_2.

2.2 Deactivation mechanisms

Deactivation of catalysts is a common problem that affects most catalysts regardless of type. There are different mechanisms behind catalyst deactivation, and these are often divided into groups: thermal aging, attrition/crushing, fouling, and poisoning. These four groups differ in how they affect the catalyst and the causes of deactivation.

Thermal aging causes the sintering of catalytic particles or other important compounds in the catalyst formulation. Sintering reduces the surface area and decreases dispersion, which usually results in a lowering of the catalytic activity [47–49]. The sintering rate increases drastically with increasing temperature and also increases in the presence of water vapor [49]. A common way of measuring the dispersion of catalytic particles is through Transmission Electron Microscopy (TEM) images, where it is possible to estimate particle size [48]. The dispersion of catalytic particles can also be estimated using chemisorption, where the amount of chemisorbed species is correlated to the number of available noble metal sites [47].

Attrition and crushing of the catalyst are related to damage to the structure of the catalyst. Cracks in the washcoat can appear due to pressure gradients in the cavities, shear stress caused by high velocity fluids, or physical damage to the catalyst [49].

Fouling or blockage of a catalyst is what happens when the surface of the catalyst is covered, which hinders the diffusion of molecules from the gas or liquid phase from reaching the catalyst surface. One of the more common fouling effects is the accumulation of soot. The combustion of diesel and other types of fuel generate soot, which can clog exhaust gas systems [50]. Diesel

particulate filters are commonly a part of the catalytic system to remove soot. Fouling can also be connected with the accumulation of phosphorous in the catalyst in the form of a phosphorous glaze, which can contain zinc [51].

Chemical poisoning is caused by the chemisorption of molecules onto the active sites of the catalytic particle, which results in a reduction of catalytic activity. Sulphur poisoning is one example of chemical poisoning in the field of catalysis; it causes major problems for automotive catalytic systems [2,52–55]. Other poisoning compounds on platinum and palladium catalysts are, for example, lead, phosphorous, and zinc [49].

2.2.1 Field-Aged catalysts

After years in traffic, the catalytic activity of most catalytic converters usually decreases. Characterization of field-aged three-way catalysts has shown the accumulation of several foreign species. A commonly found specie in these catalysts was sulphur, which has decreased over the years due to low sulphur levels in gasoline and diesel. However, a further decrease in sulphur is still of great interest for improving the durability of catalytic converters [52,56]. Other common species found in field-aged catalysts are phosphorous, zinc, and calcium [51,57–59]. Characterization of a field-aged catalyst containing these compounds revealed a loss of catalytic performance. Understanding the mechanisms for this and preventing poisoning or treating aged catalysts is of great interest in the research field.

The main source of phosphorous and zinc in field-aged catalysts is from oil lubricants, such as zinc dithiophosphate (ZDDP) [51,60–62]. ZDDP contains Zn, P, and S, which have a degrading effect on the properties of a catalyst. During operation, the lubricant slowly combusts, and these species accumulate slowly in the catalyst. Oil lubricants are important for the durability and functionality of an engine, therefore, they are not easily exchanged for the purpose of prolonging the durability of catalytic converters.

2.2.2 Phosphorous and Zinc poisoning

The usage of oil additives is important for the durability of combustion engines, however, additives affect catalytic converters. Williamson et al. studied the effects of oil additives on three-way catalysts in 1985 and found an accumulation of P and Zn, which reduced catalytic properties [63]. They found that the combination of both P and Zn was worse than each specie alone; components found in the additives accumulated in the catalytic converter.

Characterizations of field-aged TWCs from the late 1990s have shown a clear gradient distribution of phosphorous and zinc from the front of the catalyst to the back [57,58,64,65]. These characterization measurements revealed that phosphorous stayed on the surface of the washcoat and did not penetrate into the washcoat. It was also found that zinc formed a glass together with phosphorous, and the same was true for magnesium and calcium in field-aged catalysts. Other catalyst components that phosphorous affects are CeO_2 and Al_2O_3, due to the formation of $CePO_4$ and $AlPO_4$ [57,58,66]. The chemical poisoning of CeO_2 by phosphorous causes cerium to be locked to the oxidation state Ce(III), which hinders the functionality of

oxygen storage that is dependent on the ability of Ce to switch between Ce(III) and Ce(IV) [67–70].

The effects of ZDDP on Diesel Oxidation Catalysts (DOC) is the same as for TWCs in the sense that similar compounds accumulate in the catalyst [51]. The zinc phosphates form a glass in the front of the catalyst and more towards the surface whilst sulphur penetrates deeper into the catalyst and is more spread out. Scott et al. have found that phosphorous affects the hydrocarbon and CO oxidation of a DOC catalyst [71].

A study carried out by Kröger et al. [72] compared the wet impregnation of a phosphorous precursor, a solution of $(NH_4)_2HPO_4$, on a TWC catalyst and the gas-phase exposure of an evaporated solution of $(NH_4)_2HPO_4$ to the catalyst configuration. They concluded that the same phosphorous species formed on the catalyst regardless of method of exposure; the species found in the study was the same as the species found in field-aged catalysts. To conclude, both wet impregnation and gas-phase exposure are relevant methods for studying the phosphorous poisoning of catalysts.

There are also studies that focus on the phosphorus deactivation of SCR catalysts, such as Fe-BEA and Cu-BEA, that are exposed to evaporated H_3PO_4. Andonova et al. [73] have studied the gas-phase exposure of an evaporated solution of H_3PO_4 to a Cu/BEA NH_3-SCR catalyst. Their study revealed two different degrading effects that occurred from the exposure to the phosphoric acid solution. Firstly, they found condensation of the H_3PO_4 solution in the pores of the zeolite structure, which caused a blockage mechanism. Secondly, the redox capacity of the Cu in the catalyst configuration was reduced due to chemical poisoning by the phosphorous. Studies carried out by Shwan et al. [74,75], which focused on the phosphorous poisoning of Fe-BEA zeolite by the vapor of a phosphoric acid solution, showed clear signs of degradation. By comparing different concentrations and times of exposure of the phosphoric acid vapor to the catalyst, they could conclude that the formation of P_2O_5 tends to form early in the poisoning procedure, whilst during longer times of exposure, PO_3^- starts to form. They also found that phosphorous poisoning was more severe for the SCR reaction at low temperatures than at high temperatures.

There are ways to reduce the effect of oil additives and restore phosphorous-poisoned catalytic converters. Rokosz et al. [57] and Sumida et al. [66] have performed oxalic acid washing of phosphorous-poisoned catalysts, and they found that most of the catalytic functions could be restored using this method. They also found that it was possible to decrease the amount of phosphorous accumulated in a catalyst by using other types of oil additives. Wang et al. have compared different types of ZDDP with different levels phosphorous volatility [60]. Those authors found that oil additives that had a higher molecular weight reduced the volatility of phosphorous but were still able to maintain a low wear effect. Thus, cooperation across different research fields is important in order to solve problems with poisoning.

In summation, phosphorous has been found to have a deactivating effect on catalysts. A gradient distribution of phosphorous over a catalyst can often be observed when characterizing field-aged catalyst. $CePO_4$ and $AlPO_4$ were formed in catalysts containing Ce and Al. The addition

of Zn to a TWC catalyst has been found to increase the deactivation of the catalyst slightly, however, Zn has less effect than P on the deactivation of the TWC catalyst.

2.2.3 Aging of LNT catalysts

In the early stage of the deployment of the LNT catalyst, Takahashi et al. reported on the sensitivity of the LNT catalyst towards SO_2 [2]. Multiple studies have examined sulphur-poisoning mechanisms and also found more sulphur-tolerant materials. To inhibit the formation of $BaSO_4$, Yamazaki et al. [76] conducted a study where they exposed Pt/Ba/"X"/Al_2O_3 to SO_2, where X is different transition metals. They found higher resistance to sulphur poisoning with the addition of Fe to the Pt/Ba/Al_2O_3 configuration. Other means to affect resistance to sulphur poisoning is to use a different catalyst configuration. Le Phuc et al. [54] have compared a catalyst configuration more similar to TWCs, Pt/CexZrxO_2. Their catalyst configuration performed well as an NSR catalyst, however, it accumulated more sulphur than Pt/Ba/Al_2O_3 but had greater regeneration properties in reducing atmospheres than Pt/Ba/Al_2O_3. With traditional LNT configurations, newer studies have found that the addition of strontium to Pt/Ba/Al_2O_3 helps prevent sulphur poisoning largely through the formation of $SrSO_4$, which leaves Ba to function as initially intended [53]. These findings are not a final proposition for the issue with sulphur, however, many important findings have been revealed in this research field.

A comparison of sulphur and phosphorous shows that sulphur tends to have a greater impact on the catalyst than phosphorous [77]. However, the effects of phosphorous need to be examined more over an LNT catalyst, since oil additives cause phosphorous to accumulate in the catalyst. Galisteo et al. have studied the wet impregnation of an aqueous $(NH_4)_2HPO_4$ solution on Pt/$BaAl_2O_3$ [78] using a P/Ba ratio ranging from 0-0.7 wt-%. They observed that the NO_X storage capacity decreased almost linearly to the amount of phosphorous the catalyst was impregnated with. Moreover, the BET surface area decreased, as suspected, with a higher amount of phosphorous in the samples. Using XRD, a clear trend was observed with a lower formation of $BaCO_3$ in samples with a larger P/Ba ratio. From this result, the authors concluded that barium phosphates were likely formed. Christou et al. have studied TWCs and the effect of phosphorous alone and in combination with Ca and Zn [79]. They found that Zn and Ca added to the deactivation of a catalyst, although most of the deactivation originated from the phosphorous. To the best of our knowledge, there are no studies in the literature that consider the synergy of phosphorus and zinc during the deactivation of LNT catalysts, which was examined in the Paper II.

In summation, sulphur has been found to severely poison LNT catalysts. $BaSO_4$ is often formed when an LNT catalyst is poisoned by sulphur, however, the addition of components such as Sr has been found to decrease formation of $BaSO_4$. A linear deactivation of the LNT catalyst was found when it was impregnated with different amounts of P. High concentrations of phosphorous have been associated with high degree of deactivation.

2.3 Cold start and passive HC traps

Catalytic converters have been around for a long time and have been developed to efficiently remove NO_X, CO, and HC from exhaust during the operation of combustion engines. When the light-off temperature is reached, they perform well in the system they are designed for. However, during a cold start, it could take about 1 to 3 min to reach the light-off temperature [11,80]. The light-off temperature for a TWC catalyst varies between 250 to 400°C, which is dependent on the gas species in the exhaust [81,82]. NO_X-adsorbers and HC traps could be used to store pollutants until they can react on the activated catalytic converter in an attempt to bridge the temperature gap during the cold start. For gasoline engines, the most redundant HCs in the exhaust gas are ethene and methane, however, toluene is the largest if basing the comparison on C1 (i.e. toluene contains seven C1 species, while methane only one) [83]. Therefore, it is important for HC traps to have the ability to efficiently adsorb both large and small HC molecules. With efficient adsorption, it is also important for the HC trap to have a sufficiently high temperature of desorption for the different types of HCs in order to bridge the temperature gap of the cold start.

2.3.1 HC-trap materials and mechanism

The main component used for HC trapping is zeolites [84–87]. Zeolites have a unique structure due to pore size and channel volume. Zeolites with a smaller pore size often have a higher resistance towards dealumination at exposure to high temperature, this makes them more suitable for automotive applications [88]. Liu et al [89] have studied HC trapping on Ag-ZSM-5 using FTIR spectroscopy. They found that, after hydrothermal aging, the number of Si-OH species and non-framework alumina increased, whilst the number of Si-OH-Al framework linkages decreased, which indicates dealumination and a reduced number of Brønsted acid sites. At high temperatures, the stability of small-pore zeolites is better than for large-pore zeolites, however the small pore size contributes to steric hindrance for the adsorption of larger HC compounds such as toluene. Westermann et al [90] have compared the adsorption of unburned HC compounds on several different zeolites based on the structural properties of the zeolites. They found a correlation between the pore size of the zeolite structure where zeolites with a larger pore size adsorbed more HC than zeolites with a smaller pore size. Moreover, Park et al. [91] found the same pattern as they screened toluene adsorption over different zeolites. The larger pore size of a zeolite facilitates the adsorption of toluene.

Another important characteristic of zeolites is the acidity. The ratio between Si and Al, often mentioned as SiO_2/Al_2O_3 ratio (SAR), plays an important role since it correlates to the number of Brønsted acid sites in the zeolite structure. Hydrogen bonding has been proposed to take place between the -OH group and the C=C in alkene molecules in the adsorption of alkenes. This was suggested by Spoto et al. [92] when they studied the oligomerization of ethene and propene on zeolite H-ZSM-5 using in-situ FTIR spectroscopy. A decrease in Si/Al ratio of the zeolite, i.e. more Brønsted acid sites, has proven to aid in the adsorption of toluene. This was found by Azambre et al. [93] when they studied HC-TPDs with three different hydrocarbon species (propene, toluene, and decane) on zeolite Y. The authors found that the adsorption of

the C3 and C7 hydrocarbons increased with a low Si/Al ratio, whereas C10 decreased with a low Si/Al ratio.

The effect of water vapor on HC-trap material is relevant to understand since H_2O is one of the largest products from combustion processes. Fuel types containing ethanol that are hydrophilic, such as E85, might be helped by the presence of H_2O. The opposite is true for hydrophobic HC species, such as toluene, alkanes, and alkenes. This was shown by Park et al. [91] when they mapped toluene adsorption and desorption on different ion-exchanged zeolites in both wet and dry conditions. Those authors observed that H_2O partially inhibited toluene adsorption for all zeolites studied, indicating the importance of considering H_2O. This effect is clearly demonstrated in Figure 3, where toluene adsorption is shown for a number of zeolites in the presence and absence of water. Furthermore, Luo et al. [94] studied of the adsorption of iso-pentene on zeolite beta and found that zeolites with a low Si/Al ratio were more affected by H_2O than zeolites with a high Si/Al ratio. This was seen by that the heat of adsorption for the HC decreased more in the presence of water for beta with low Si/Al ratio, while it was similar for Si/Al ratio of 200 (with 0% H_2O present in the feed: -51.4 kJ/mol for BEA38 and -50.6 kJ/mol for BEA200; with 10.9% H_2O present in the feed: -42.9 kJ/mol for BEA38 and -50.1 kJ/mol for BEA200).

In summation, using zeolites with a smaller pore size provides thermal stability and a reduced risk of dealumination, whereas a larger pore size contributes to improved HC trapping. To further improve the zeolite, the Si/Al ratio is important to consider since it is a determining factor for the balance of Lewis acid sites and Brønsted acid sites which are the main sources of interaction between zeolite and hydrocarbons. Moreover, Brønsted acid sites are important for interaction with e.g. propene, but for a low Si/Al ratio, water inhibition has a more pronounced impact.

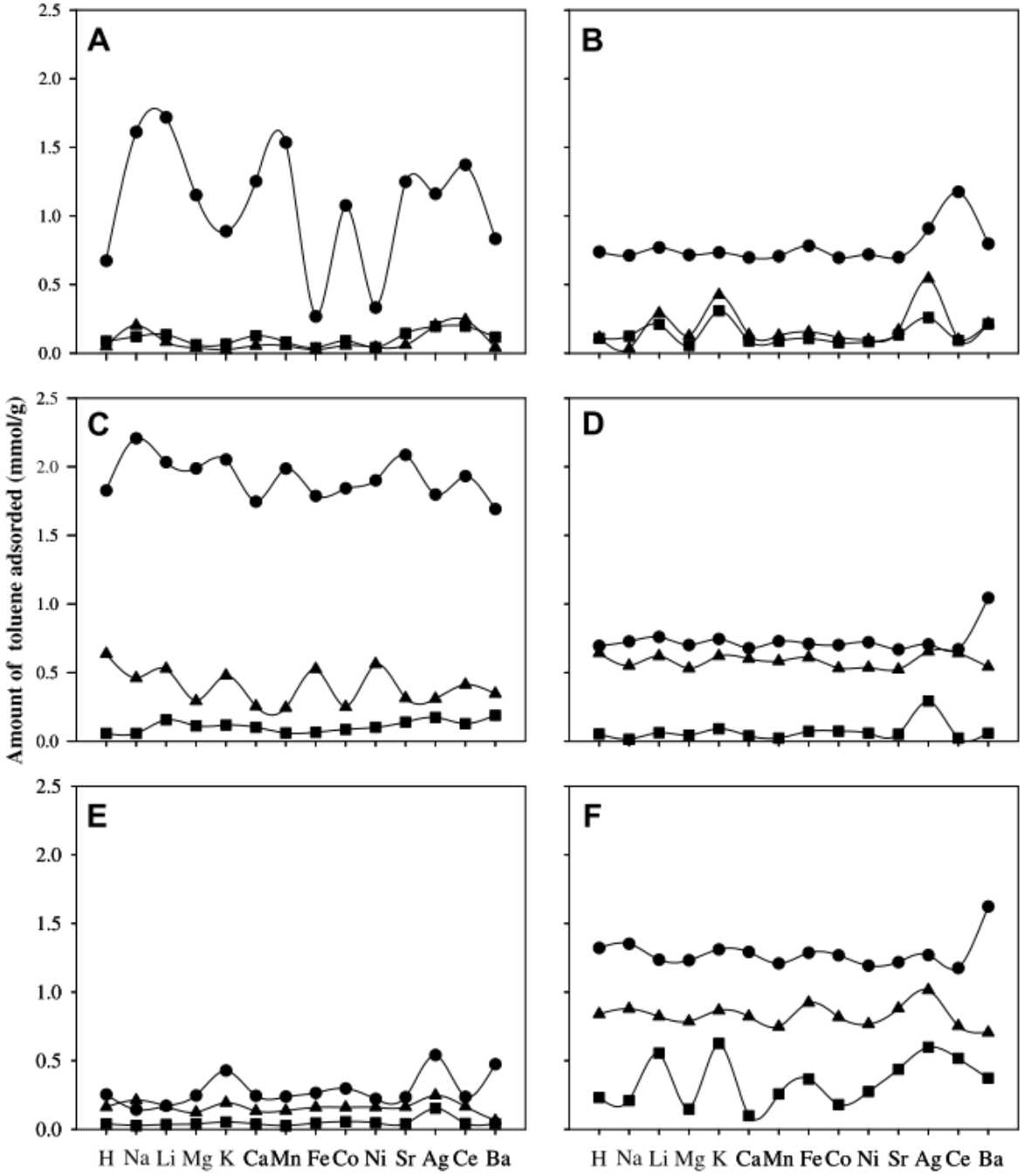

Figure 3. Amount of toluene trapped onto H, Na, Li, Mg, K, Ca, Mn, Fe, Co, Ni, Sr, Ag, Ce, and Ba ion-exchanged under dry (●), wet (▲), and temperature ramping (■) conditions: (A) X, (B) M10, (C) USY, (D) ZSM5, (E) FER760, and (F) Beta zeolites. Image and caption from Park et al. [91].

2.3.2 Adsorption properties of different hydrocarbons

The adsorption capacity of the HC trap is strongly affected by the temperature of the exhaust gas and the trapping material. Studies have been conducted on the adsorption of toluene at different temperatures [95]. These studies indicate that the adsorption capacity deceases with

an increase in temperature. Daldoul et al. [96] have studied HC trapping capacity of zeolite ZSM-12 during an accelerated heating rate (3, 6, and 9°C/s). They found evidence that the temperature of desorption is affected by the heating rate, and an increase in heating rate postpones the temperature of desorption of the hydrocarbon species. In a study by Yamamoto et al. [97], different cold-start parameters for HC traps were examined and it was found that an increase in HC-trap volume resulted in a decrease in the heating rate and a delay in light-off time and also a decrease in desorption rate. This indicates that the volume of the HC trap plays an important role in the design of a HC-trap system. Goralski et al. [98] have compared the volume of an HC trap with the storage capacity of hydrocarbon and modeled HC trapping. As the volume of the hydrocarbon trap increased, the heating rate decreased. Their result agrees well with the work by Yamamoto et al. [97] mentioned above.

Several different hydrocarbons are present in the exhaust during a cold start. Both small hydrocarbons, such as ethylene, and large aromatic hydrocarbons, such as toluene, are found in the exhaust of gasoline engines. Czaplewski et al. [99] have simulated a one-dimensional HC trap with both small and large hydrocarbons present. They found that, in multi-HC TPD, the temperature of desorption increased for smaller molecules compared to a single-HC TPD. The reason for this was attributed to the steric hinderance of the larger molecules on the smaller molecules. The adsorption of an HC mixture with C3, C7, and C10 present in the feed has been studied by Westermann et al. [81]. They found that smaller HCs adsorbed faster in the zeolite, but C3 was replaced by C7, and C7 was replaced by C10 over time. They explained this replacement effect as larger HC molecules adsorbing stronger than small molecules onto the HC trap, but the rate of adsorption was slower. Furthermore, adsorbed hydrocarbons in a zeolite framework may undergo both catalytic cracking or polymerization, leading to coking. Westermann et al. [81] have observed both of these phenomena. Those authors found that the larger hydrocarbons cracked into smaller ones during the desorption step of the TPD. Polymerization of alkenes was proposed to originate from the interaction between Brønsted acid sites and the C=C bond in the alkene molecule. These results clearly indicate that there is an inherent uncertainty when desorbed hydrocarbons from HC traps are measured.

In summation, the volume of the HC trap has been shown to play an important role in the desorption of hydrocarbons. An increase in HC-trap volume decreases the rate of desorption of trapped HC but delays the light-off of the catalyst. It has been shown that a drastically increased temperature ramping speed benefit HC traps by increasing the temperature of desorption. The interaction between hydrocarbons of different sizes and properties is important in mixed hydrocarbon adsorption. Larger hydrocarbons may replace smaller adsorbed hydrocarbons, however, larger hydrocarbons may also increase the temperature of desorption for smaller hydrocarbons, due to sterical hindrance.

2.3.3 Metal-ion incorporation into HC traps

To further increase the adsorption of hydrocarbons and improve the temperature of desorption for them, ion-exchange and the incorporation of cations into the zeolite have been proven successful in several studies [95,100–103]. Two major attributes of cations have been found to be of importance for trapping hydrocarbons. These are the Lewis acidity of a cation and its size,

as observed by Takamitsu et al. [101]. They studied ion-exchange onto zeolite beta and ZSM-5. They examined a range of different cations, and Na provided the highest temperature of desorption for the studied metal ions. Those authors concluded that if only the cation was of importance, the strongest Lewis acid would contribute to the highest temperature of desorption. If the framework oxygen of the zeolite was only of importance, the cations with a lower Lewis acidity would contribute to a higher temperature of desorption since they contribute to a higher charge on the framework oxygen. Since the cation Na is located in between these extremes, it was concluded that both Lewis acid strength and the size of a cation play an important role in the performance of an ion-exchanged HC trap.

The silver ion has been one of the more promising cations for hydrocarbon trapping. Liu et al. [89] have studied Ag^+ onto zeolite ZSM-5 for cold-start purposes and compared it to H^+ and Cu^{2+}. They concluded that, in the presence of water, the ion-exchanged Ag-ZSM-5 performed very well in contrast to Cu^{2+} and H^+, which were more affected by water inhibition. A similar conclusion was reached by Kang et al. [95] when they studied the adsorption of different hydrocarbons onto Ag-BEA. Addition of Ag was found to improve the adsorption capacity of ethylene and toluene during wet conditions. However, those authors did not observe any improvement in the adsorption and desorption of hexane in the presence of water, and this is due to the more hydrophobic by nature of hexane. One reason for the enhanced adsorption of toluene in ion-exchanged Ag-BEA was attributed to the interaction between the Ag ion and the phenyl ring of the toluene [89]. Figure 4 clearly shows that phenyl-H^+ interaction weakens in presence of water, whereas phenyl-Ag^+ remains strong.

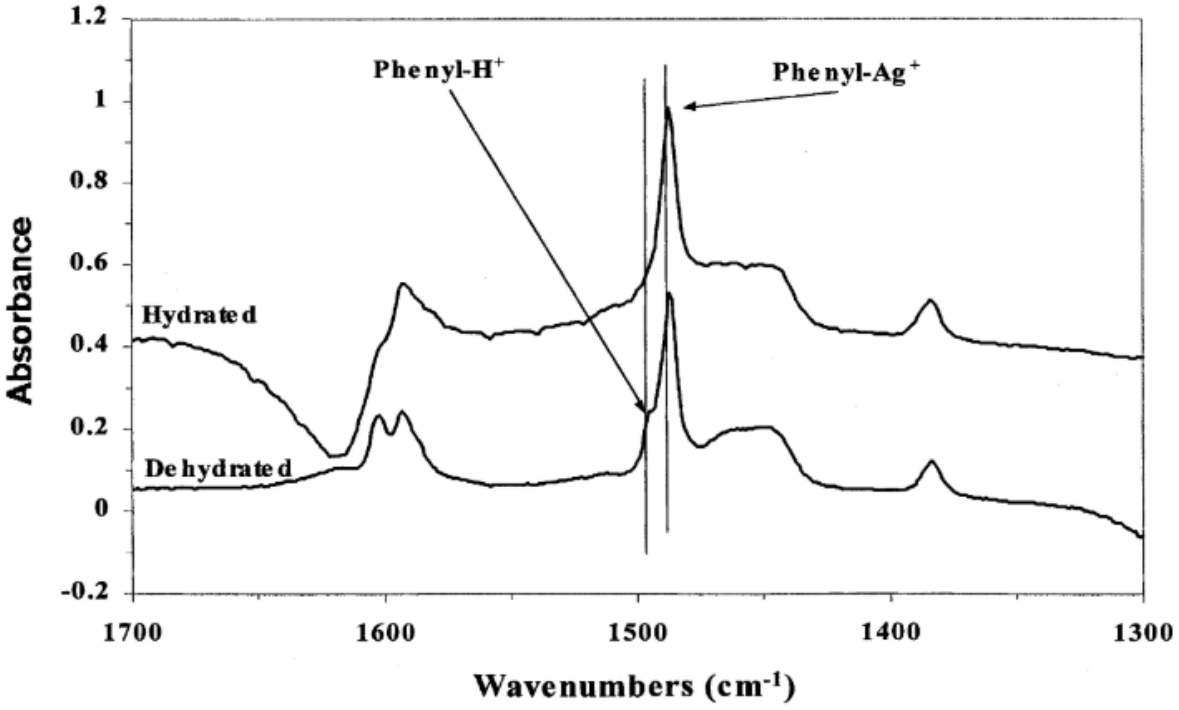

Figure 4. FT-IR spectra of toluene adsorbed in hydrated and dehydrated condition (at 350°C under vacuum) $Ag_{5.0}{}^{+}H_{0.6}{}^{+}$-ZSM-5. Image and caption from Liu et al. [89].

Palladium, similar to the silver ion, has demonstrated positive effects when added to zeolite beta for cold-start purposes. Xu et al. [104] have studied the effect of HC-trap Pd-BEA on trapping ethanol in cold-start conditions. Their results clearly showed that the addition of small quantities of Pd (0.1 to 0.2 weight percentage) provided a catalytic effect to the HC trap, which converted a significant portion of the stored ethanol to CO_2. These findings have great value since this is an alternative route for hydrocarbon trapping rather than just focusing on an increase in the temperature of desorption. Adding the ability to convert stored HC into CO_2 is highly beneficial. Moreover, Lupescu et al. [105] have studied Pd on zeolite beta as hydrocarbon trap together with a base redox active metal on a direct-injected Ford Focus. They concluded that Pd provides new adsorption sites (chemisorption), which give an HC trap with oxidation properties. They also observed that the addition of a base redox active metal helped to stabilize Pd and prevent sintering effects.

Takamitsu et al. [101] have found that Na had comparably good HC-trapping properties on zeolite beta and ZSM-5. This was attributed to Na size and Lewis acidity. However, Buke et al. [106] studied the aging of HC traps, and they compared H-BEA, N-BEA, and La-BEA and found that La, which has a relatively large atomic diameter, performed as well as Na for HC-trapping purposes. This may be an indication that there is more to be explored in regard to which factors are important for trapping hydrocarbons for cold-start purposes.

In summation, many studies indicate that Ag is a promising addition to HC traps. The motivation for Ag is that it provides a resistance to water inhibition. Two factors that are of great importance for the efficiency of a cation in an HC trap, are Lewis acidity and the ability to enhance the charge of oxygen in a zeolite framework. Usually larger cations tend to contribute to the charge of oxygen in the zeolite framework. The addition of Pd to an HC trap may contribute catalytic properties to the trap, which are useful for further minimizing the release of hydrocarbons during the cold start.

3 Experimental

3.1 Synthesis of catalyst

3.1.1 Synthesis of LNT catalyst, $Pt/Ba/Al_2O_3$

The model LNT catalyst used for both studies presented in this thesis was $Pt/Ba/Al_2O_3$ with 2 wt-% Pt and 16 wt-% Ba. Details concerning the preparation can be found in Papers I and II.

The support material, γ-Al_2O_3, was impregnated with a platinum precursor using the incipient wetness impregnation technique. Thereafter, the mixture was dried at 90°C for 2h, and then the mixture was calcined in an oven at 550°C for 2h. For the impregnation of barium with Pt/Al_2O_3 powder, a procedure similar to the one for the impregnation of platinum was used, however, due to limitations in the solubility of barium acetate, the impregnation was performed in three steps with calcination between each impregnation step. Impregnation with platinum before barium is based on the study by Lindholm et al. [23], where higher NO_X storage capacity was found when Al_2O_3 was impregnated with platinum before being impregnated with barium.

The synthesized catalyst material was coated on a honeycomb-shaped ceramic monolith substrate (20 mm in length, 21 mm in diameter with 400 cpsi). The catalyst powder was mixed with 10 wt-% boehmite as a binder material, and to further improve adhesiveness during coating, the powder mixture was mixed in a solution of 50 vol-% ethanol and 50 vol-% MilliQ water. The targeted washcoat weight for each monolith was 700 mg, and they were calcined at 550°C for 2h with a temperature ramp of 5°C/min.

3.1.2 Synthesis of HC-Trap material for cold-start purposes

The hydrocarbon trapping material for Paper III and Paper IV was based on zeolite beta, ZSM-5, and SSZ-13. These zeolites were ion-exchanged for enhanced trapping properties. See Papers III and IV for more details.

The zeolites used as support material for the HC traps had the targeted SiO_2/Al_2O_3 ratio of approximately 25 to facilitate comparison of the zeolite structure. Incipient wetness impregnation was done for all samples for the ion exchange of zeolite supports. After the impregnation step, samples were dried at 90°C for 24h followed by calcination in an oven at 550°C for 2h. This procedure was repeated for samples containing two impregnated metal components in which a second metal component was added. HC trap samples were washcoated

following the same procedure as for the NSR catalyst ($Pt/Ba/Al_2O_3$) with 5 wt-% boehmite binder material instead of 10 wt-%.

3.2 Flow reactor

A Synthetic Gas Bench (SGB) reactor was used in Papers I and II for the NO_X storage and reduction activity tests and NO_2 Temperature Programmed Desorption (TPD) measurements. Gas flow, gas concentrations, and vapor were regulated using Bronkhorst mass flow controllers and a Bronkhorst CEM system. A coated monolith was wrapped in quartz wool to avoid the by-pass of gases, and then it was placed inside a quartz tube, which was 750 mm with an inner diameter of 22 mm. Thereafter, the quartz tube was placed in a heating coil, which was covered in insulation. Two thermocouples were used; one measured the catalyst temperature, and the other measured the gas temperature in front of the catalyst and was used to regulate the temperature. An MKS Multigas 2030 FTIR spectrometer was used to measure gas concentrations after the catalyst, and all lines were covered in insulation and heated to 200°C to avoid vapor condensation in the system.

Before any measurements in the flow reactor, freshly coated monoliths were pretreated and degreened to avoid the sintering of catalyst particles during measurements. The procedure and conditions for pretreatment and degreening are described in the experimental sections in Papers I and II.

The samples were studied in lean/rich cycling conditions to measure NO_X storage and reduction. The temperature in the cycles was either 300, 350, or 400°C, and the length of the cycles varied in the papers, 4 min lean/1 min rich or 8 min lean/2 min rich. The gas composition in lean conditions for both papers was 400 ppm NO/NO_2, 5 vol-% CO_2, 8 vol-% O_2, and 5 vol-% H_2O with balance Ar. The gas composition for rich conditions was 400 ppm NO/NO_2, 1 vol-% H_2/1000ppm C_3H6, 5 vol-% CO_2, and 5 vol-% H_2O with balance Ar. More details on the activity tests are provided in Papers I and II. An overview of the experimental sequences of the flow reactor is shown in Table 1.

Table 1. An overview of the experimental sequences in the activity tests in the flow reactor. 5 vol-% CO_2 and 5 vol-% H_2O were present in the gas mixture for all lean and rich phases.

	Cycle segment 1	Cycle segment 2	Cycle segment 3
300°C	***Lean:*** 400 ppm NO and 8% O_2	***Lean:*** 400 ppm NO and 8% O_2	
	Rich: 400 ppm NO and 1% H_2	***Rich:*** 400 ppm NO and 1000 ppm C_3H_6	
350°C	***Lean:*** 400 ppm NO and 8% O_2	***Lean:*** 400 ppm NO_2 and 8% O_2	***Lean:*** 400 ppm NO and 8% O_2
	Rich: 400 ppm NO and 1% H_2	***Rich:*** 400 ppm NO_2, and 1% H_2	***Rich:*** 400 ppm NO and 1000 ppm C_3H_6
400°C	***Lean:*** 400 ppm NO and 8% O_2	***Lean:*** 400 ppm NO and 8% O_2	
	Rich: 400 ppm NO and 1% H_2	***Rich:*** 400 ppm NO and 1000 ppm C_3H_6	

NO_2 TPD experiments were conducted, where NO_2 adsorption occurred in 500 ppm NO_2 and 5 vol-% H_2O with balance Ar at 100°C for 60 min followed by flushing in 5 vol-% H_2O and Ar for 10 min. Thereafter, the temperature was increased to 500°C, with a heating rate of 10°C/min.

The same equipment as for Papers I and II was used in Papers III and IV for flow-reactor experiments. However, a Bronhorst CEM system for toluene was added for flow-reactor experiments in Papers II and IV.

Temperature Programmed Desorption (TPD) experiments were performed in both Papers III and IV under similar conditions. At 80°C, samples were loaded with either toluene, propene, or propane, depending on the type of TPD performed. The sample was exposed to hydrocarbons for 60 min followed by a flush in Ar for 20 min. After flushing, the temperature was increased to 500°C in the presence of Ar with a heating rate of 20°/min. The steps were identical in the wet-TPD experiments, as mentioned above, but with the addition of 5 vol% H_2O. The flow reactor experiments reported in both papers consisted of four different TPD measurements. Table 2 shows the different TPD experiments and their chronological sequencing for the papers.

Table 2. An overview of the experimental sequences in the HC-TPD experiments that were performed. A pre-oxidation in 10 vol-% O_2 at 500°C for 20 min was performed before and between TPD experiments.

	1st TPD	2nd TPD	3rd TPD	4th TPD
Paper III	Dry Toluene	Dry Propene	Wet Toluene	Wet Propene
Paper IV	Wet Toluene	Wet Propene	Wet Propane	Wet HC mixture

3.3 Poisoning procedure

Two different poisoning procedures were used: a gas-phase exposure to phosphorous, with results in Paper I; and wet impregnation of dissolved phosphorous and zinc salts on coated and degreened monoliths, with results in Paper II.

The first method of poisoning, gas-phase exposure, was performed by evaporating diluted phosphoric acid. The coated and degreened monoliths were placed in a quartz tube with a setup similar to the one for flow reactor experiments, with the addition of a syringe pump that injected diluted phosphoric acid into the front of the heated quartz tube. Two different cases were studied for gas-phase poisoning: one in which the sample was exposed to 50 ppm phosphoric acid, 8 vol-% O_2 and 5 vol-% H_2O with balance Ar in the gas flow for 34 h; and the other in which the sample was exposed to 100 ppm phosphoric acid, 8 vol-% O_2 and 5 vol-% H_2O with balance Ar in the gas flow for 34h.

The second method of poisoning, wet impregnation, was performed by dipping the coated monolith and allowing capillary forces absorb the solution into the channels. Ammonium phosphate and zinc acetate salt were mixed in a pre-estimated amount of MilliQ water to prepare the solutions, and the amount of salt correlated to the weight percentage of the washcoat. Thereafter, the monoliths were dried at 90°C for 2h followed by calcination at 550°C for 2h. For samples containing both zinc and phosphorous, Zinc was impregnated first, then the sample was dried and calcined before impregnation with phosphorous. Six different poisoning conditions were used: 1 wt-% P; 1 wt-% Zn; 1 wt-% P and 1 wt-% Zn; 2 wt-% P; 2 wt-% Zn; 2 wt-% P and 2 wt-% Zn. Inductively Coupled Plasma Atomic Emission Spectroscopy (ICP-AES) was used to measure the amount of zinc and phosphorous impregnated on the washcoat of the catalysts, and the ICP-AES results are shown in Table 3. Measurements were made of crushed monoliths, and the concentrations were calculated for the washcoat by assuming a uniform washcoat.

Table 3. Amount of Zn and P in weight percentage of washcoat estimated from crushed monoliths. Measurements collected with ICP-AES performed by ALS Scandinavia. Crushed monolith was used, and the concentrations were estimated for the washcoat assuming uniform washcoat distribution.

Element \Sample	**1 wt-% P**	**1 wt-% Zn**	**1 wt-% P, 1 wt-% Zn**	**2 wt-% P**	**2 wt-% Zn**	**2 wt-% P, 2 wt-% Zn**	**Fresh**
wt-% P	1.2	-	1.2	2.4	-	2.4	-
wt-% Zn	-	1.0	0.9	-	1.6	1.6	-

3.4 Characterization

3.4.1 In-situ DRIFTS

Diffusive Reflectance Infrared Fourier Transformed Spectroscopy (DRIFTS) is a method for studying surface species in-situ, for instance, during catalytic reactions. A VERTEX70 spectrometer from Bruker, equipped with a liquid N_2-cooled mercury cadmium telluride

detector, was used for the measurements. A high-temperature stainless steel reactor chamber by Harrick Scientific Products Inc and a diffusive reflectance accessory by Praying Mantis™ were used. The DRIFTS technique was used in Paper III and IV.

Powder scraped off the wash-coated monoliths was used for in-situ DRIFTS in Paper III. Prior to the scraping of the washcoat, the samples were pre-oxidized and loaded with toluene in the flow reactor followed by flushing and cooling to room temperature. The DRIFTS TPD experiment consisted of two heating ramps with an oxidation step in between. The first heating ramp consisted of the desorption of toluene, and the second consisted solely of peaks associated with the sample, therefore, the second spectra was subtracted from the first in order to see the shifts related to toluene. For further details on the in-situ DRIFTS experiments, see the experimental section of Paper III and IV.

3.4.2 X-ray photoelectron spectroscopy (XPS)

In Paper I, the surface species of samples exposed to phosphorous in the gas phase were measured using X-ray Photoelectron Spectroscopy (XPS), and the positions measured were the front, the middle, and the back. The instrument used was a Perkin Elmer 5000 ESCA system equipped with an EDS elemental mapping system. The X-ray source for the measurements was monochromatic Al Kα radiation at 1486.6 eV. The measurement was normalized to the C 1s peak at 284.6 eV to correct for the charging effect of the insulating samples [107]. The P 2p peaks were deconvoluted by fitting a Gaussian function under observed peaks and subtracting the baseline under the peaks. In Paper III, XPS was also used, these results are however not presented in this thesis. For more details regarding that see experimental section in Paper III.

3.4.3 BET surface area

The specific surface area and pore volume of the samples exposed to phosphorous in the gas phase in Paper I were measured using N_2-physisorption isotherms at -195°C and were collected using a TriStar 3000 gas adsorption analyzer. The same methodology was used in Paper IV, however, these results are not presented in this thesis. For more information, see experimental section of Paper IV. Coated monoliths were divided into three sections, inlet, middle, and outlet, which were crushed and ground to a powder. Approximately 300 mg powder from each section was thermally dried at 90°C in N_2 gas flow for 4h and used to measure the specific surface area and pore-volume.

3.4.4 ICP-AES

Inductive Coupled Plasma Atomic Emission Spectroscopy (ICP-AES) was used in Paper I and II for elemental analysis and was performed by ALS Scandinavia AB. The coated monoliths of samples exposed to phosphorous in the gas phase were divided into three sections, inlet, middle, and outlet, and these sections were crushed and ground to powder. Coated monoliths exposed to zinc and phosphorous through wet impregnation were crushed and ground to powder in a similar manner, however, not divided into different sections. The reported wt-% is based on washcoat and was estimated assuming uniform washcoat thickness.

3.4.5 STEM and ESEM-EDX mapping

A cross-section overview of the location of different elements in the catalytic washcoat was acquired using ESEM in Paper I. The instrument used for imaging and X-ray analysis was a

Quanta200 ESEM FEG from FEI. The EDX analysis was performed in low vacuum with an acceleration voltage of 20 kV. An Oxford X-max 80 X-ray detector for energy dispersive X-ray analysis, with INCA software for the evaluation of data, was used for elemental mapping to show the spatial distribution of the different elements. The sample, exposed to 50 ppm phosphorous in the gas phase, was measured at two different axial positions. The axial positions analyzed were 2 mm from the front of the catalyst and 2 mm from the back. Scanning transmission electron microscopy (STEM) was used in Paper II for the samples containing 2 wt.% of poisons. Crushed catalyst samples were placed on a carbon grid and the instrument used for EDX measurements were FEI Titan 80-300 TEM/STEM instrument operated at 300 kV from FEI. The STEM imaging was performed using High-Angle Annular Dark-Field (HAADF) detector.

3.4.6 X-ray-diffraction (XRD)

X-ray diffraction (XRD) was used in Papers II and IV to measure the crystallinity of the samples. The instrument used for the measurements was a Siemens D5000 diffractometer operated at 40kV and 40mA. The diffraction spectra in Paper II were collected in intervals of 10-80° with a 2θ increase of 0.03°/s. The intervals in Paper IV were collected between 5-40° at the same rate as for Paper II.

4 Results and Discussion

4.1 Poisoning of LNT with Phosphorous and Zinc

Papers I and II examine the chemical poisoning of an LNT catalyst ($Pt/Ba/Al_2O_3$), which is used for removing NOx from diesel and lean burn gasoline exhausts. The poisons were, however, exposed to the catalyst in different ways. In Paper I, the P was introduced to the catalyst through evaporated phosphoric acid. In Paper II, the P and Zn were introduced through wet impregnation. Coated monoliths were measured in both papers before exposure to the poison, and afterwards to track the individual effects of the poisoning.

After the coating procedure in Paper I, the NO_X storage and reduction activity were measured for both samples before the gas-phase exposure to phosphorous. The time of exposure to phosphorous, for both samples, was 34 h, and the gas phase concentration was 5 vol-% H_2O, 8 vol-% O_2 and 50 ppm or 100 ppm of phosphoric acid. Therefore, the samples were denoted “50 ppm, 34h” and “100 ppm, 34h” in the figures.

Before the wet impregnation of the coated and degreened catalysts in Paper II with P and Zn, we measured NO_X storage and reduction activity and NO_2 desorption behavior during TPD in a flow reactor. Six different aging cases were studied. They contained either 1 or 2 wt-% of each poisoning species to provide insight into the magnitude of individual poisons and to reveal interactions between them. The targeted weight percentage of each species impregnated was based on the washcoat amount on the coated monolith. The six cases studied were: 1% P, 2% P, 1% Zn, 2% Zn, (1%P and 1% Zn), and (2%P and 2% Zn).

4.1.1 Effect of Zn and P on LNT capacity

NO_X storage and reduction were measured at 300 and 400°C in Paper I. Two different lean/rich cycle segments were studied for each temperature, and each cycle segment consisted of five lean/rich cycles. The reducing agent used in the rich phase differed for the cycle segments, either 1 vol-% H_2 or 1000 ppm C_3H_6. The lean phase (400 ppm NO, 5 vol-% CO_2, 8 vol-% O_2, and 5% H_2O) was the same for both segments. The rich phase (400 ppm NO, 5 vol-% CO_2, 1 vol-% H_2/1000 ppm C_3H_6, and 5% H_2O) composition strongly affected the products and bi-products formed and the regeneration ability of the catalyst. This was due to the different reaction pathways associated with the reducing agent [17,18,34].

Figure 5 shows a comparison of sample “100 ppm, 34h” before and after exposure to phosphorous, with H_2 as the reducing agent in the rich phase at 400°C. A loss of NO_X storage in the lean phase is showed by an increase in slip of both NO and NO_2. The breakthrough of NO_X occurred earlier in the poisoned sample than in the fresh one. There was higher formation of NH_3 in the poisoned sample in the rich phase than in the fresh one. Immediately after the switch from lean to rich phase, some formation of N_2O occurred as a bi-product, and as the formation of N_2O decreased, the formation of NH_3 began to dominate the rich phase. We can conclude from the comparison of sample “100 ppm, 34h” before and after exposure to phosphorous that exposure to phosphorous in the gas phase affected the NO_X storage capacity of the catalyst, which is seen in the earlier breakthrough of NO_X. Not only did the breakthrough occur earlier, but we also observed an increase in the slip of NO and NO_2 over the remainder of the lean phase, which shows a decrease in NO_X storage capacity. These results indicate that phosphorous affects access to the NO_X storage component, BaO, which is in agreement Galisteo et al. [73] Interestingly, the formation of NH_3 increased in the rich phase after exposure to phosphorous. De Abreu Goes et al. [108] observed similar behavior when comparing a fresh LNT catalyst with a field-aged one and an oven-aged catalyst at 800°C. Both the field-aged and the oven-aged catalysts exhibited an increase in the formation of NH_3 in most cases. It is possible that the increase in the formation of NH_3 in the rich phase that was observed in our experiments was caused by some poisoning of the noble metal, which would change the selectivity between the formation of N_2 and NH_3. However, this may also be due to a reduced NO_X storage caused by phosphorous affecting giving less barium nitrates that can react with the ammonia in an SCR reaction.

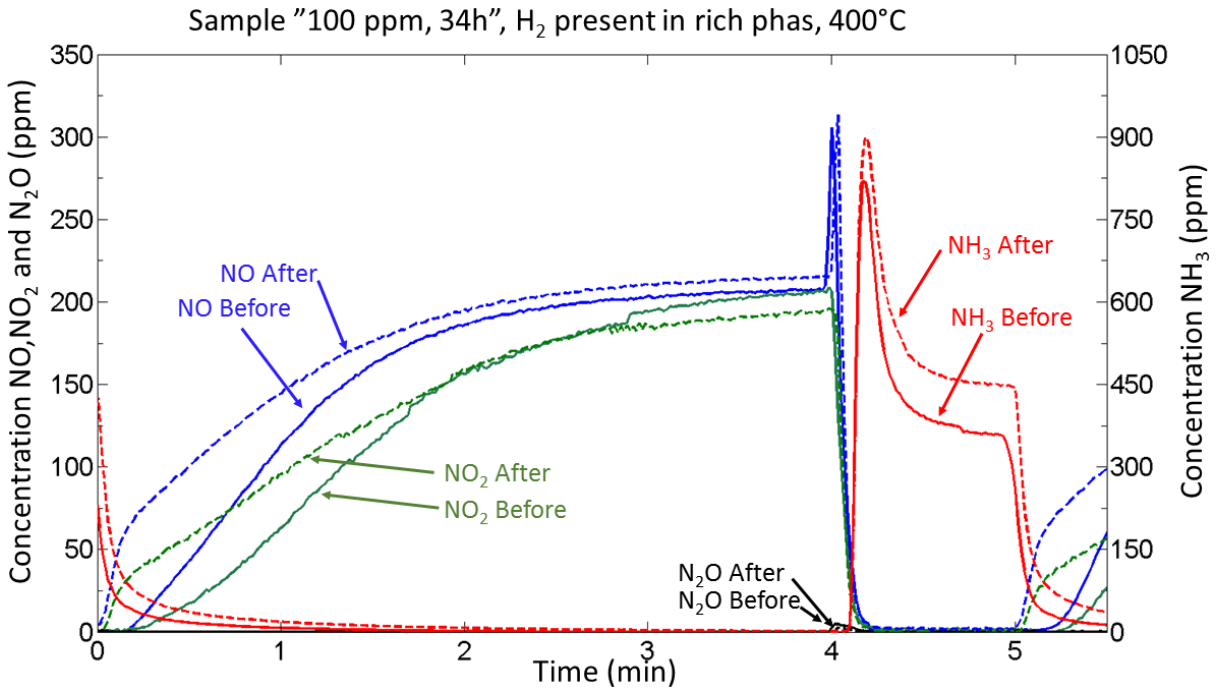

Figure 5. Measured outlet concentrations of the Pt/Ba/Al_2O_3 sample “100 ppm, 34h” before and after exposure to phosphorous (100 vol.-ppm H_3PO_4, 8 vol.-% O_2, 5 vol.-% H_2O at 200°C) at 400°C. Lean phase: 400 vol.-ppm NO, 5 vol.-% H_2O, 5 vol.-% CO_2, and 8 vol.-% O_2. Rich phase: 400 vol.-ppm NO, 5 vol.-% H_2O, 5 vol.-% CO_2, and 1 vol.-% $H_{2.\,Gas}$ concentrations were measured using FTIR.

Figure 6 shows one cycle from each cycle segment for both samples, “50 ppm, 34h” and “100 ppm, 34h,” before and after phosphorus exposure, at both 300 and 400°C. A significant loss of NO_X storage capacity was observed in all four lean/rich cycles and for both samples. The loss of NO_X storage capacity appeared the highest for the sample with 1% H_2 in the rich phase at 300°C (Figure 6 **A**), and the lowest for the sample with 1000 ppm C_3H_6 in the rich phase at 300°C (Figure 6 **B**). The reason for the minor effect observed for the propene sample is the poor reduction properties of C_3H_6 at 300°C, as shown by Olsson et al. [18]. This resulted in low NO_X storage, and the poisoning was less visible. The similarities between results at 400°C (Figure 6 **C** and **D)** indicate that the reduction properties of H_2 and C_3H_6 in the rich phase at this higher temperature are comparable. We observed that the loss of NO_X storage was approximately the same for both sample “50 ppm, 34h” and sample “100 ppm, 34h.” These results indicate that the concentration was not so critical for the degree of poisoning. This finding is in agreement with Shwan et al. [74], who have studied the effect of gas-phase poisoning of phosphorous on Fe-BEA and found that time appeared to be a more significant factor for the degradation of the catalyst than P concentration.

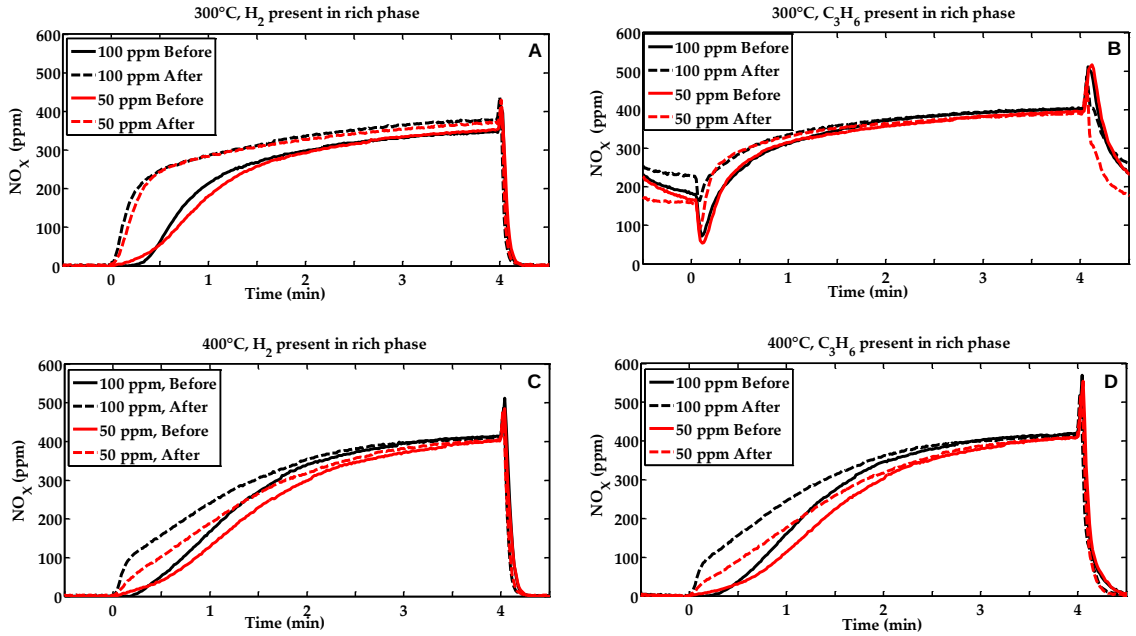

Figure 6. Measured outlet NO_x before and after exposing $Pt/Ba/Al_2O_3$ to 50 or 100 vol.-ppm H_3PO_4, 8 vol.-% O_2 and 5 vol.% H_2O for 34 h. The lean phase (400 vol.-ppm NO, 5 vol.-% H_2O, 5 vol.-% CO_2 and 8 vol.-% O_2) starts at time=0. The rich phase consists of 400 vol.-ppm NO, 5 vol.-% H_2O, 5 vol.-% CO_2 and H_2 or C_3H_6, where **A)** 300°C with 1 vol.-% H_2 in the rich phase, **B)** 300°C with 0.1 vol.-% C_3H_6 in the rich phase, **C)** 400°C with 1 vol.-% H_2 in the rich phase, and **D)** 400°C with 0.1 vol.-% C_3H_6 in the rich phase.

By assuming that all gas-phase nitrogen-containing molecules in the system during a lean/rich cycle were NO, NO_2, N_2, NH_3, and N_2O we could estimate the formation of N_2 since the concentration of the remaining molecules were quantified using FTIR. Figure 7 shows the estimated N_2 and the other measured components. In agreement with the results in Figure 6 **A**, we observed that the greatest increase in NO_X slip after poisoning occurred at 300°C with 1% H_2 as the reducing agent (Figure 7 **A**). We also observed that the formation of NH_3 increased slightly after exposure to phosphorous, and the formation of N_2 decreased significantly (Figure 7 **A**). At 400°C with 1% H_2 as the reducing agent (Figure 7 **C)**, the same trends were observed as for the 300°C case (Figure 7 **A**), however, a smaller NO_X slip and a smaller decrease in the formation of N_2 was found. Figure 7 **B** and **D** show the results of C_3H_6 as the reducing agent, and it was found that the formation of N_2 dominated compared to NH_3 and N_2O. A small amount of N_2O was formed at 300°C (Figure 7 **B**), whereas we observed the formation of some NH_3 at 400°C (Figure 7 **D**).

To summarize, the effect of phosphorous in the catalyst was observed in NO_X storage during the lean phase, which leads to an increase in NH_3 formation and a significant decrease in N_2 due to less stored NO_X, which NH_3 can react with.

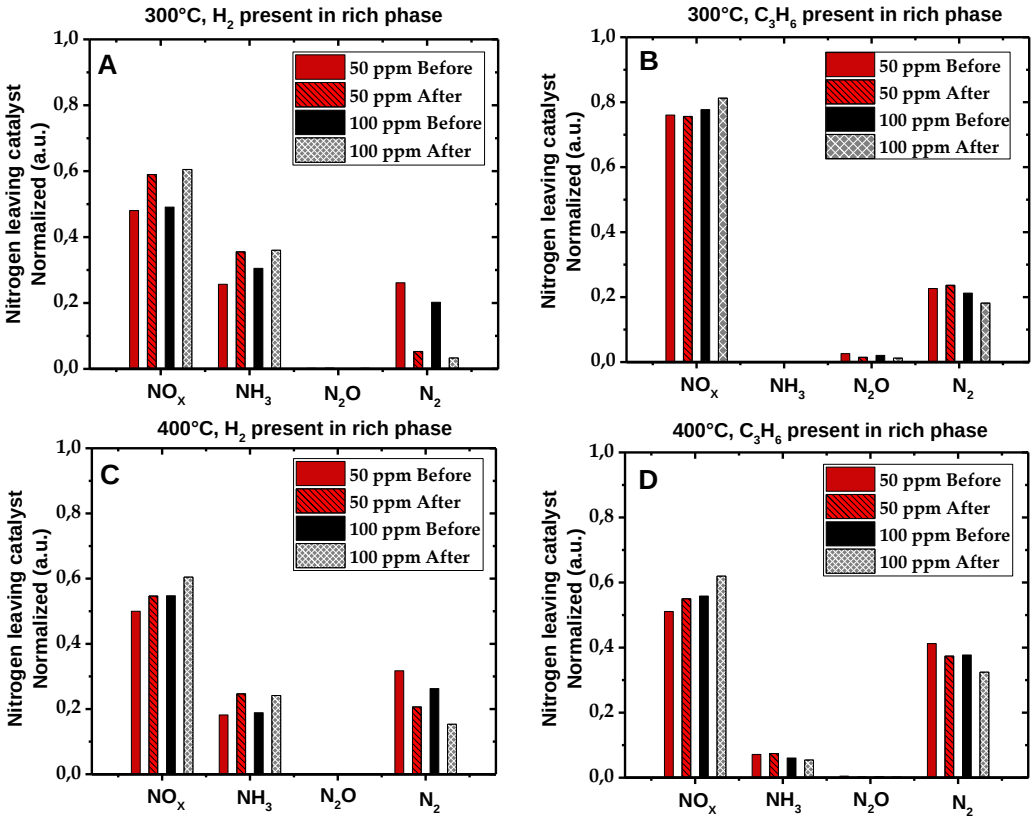

Figure 7. Balance over outlet nitrogen atoms over a lean/rich cycle before and after exposing $Pt/Ba/Al_2O_3$ to 50 and 100 vol.-ppm phosphorous for 34 h, assuming that all nitrogen leaving the catalyst is either in the form of NO_x, NH_3, N_2O, or N_2. The lean phase (400 ppm NO, 5 vol.-% CO_2, 8 vol.-% O_2 and 5 vol.-% H_2O) has the same gas composition in all four graphs. **A)** 300°C with 1 vol.-% H_2, 5 vol.-% CO_2, and 5 vol.-% H_2O in the rich phase, **B)** 300°C with 0.1 vol.-% C_3H_6, 5 vol.-% CO_2, and 5 vol.-% H_2O in the rich phase, **C)** 400°C with 1 vol.-% H_2, 5 vol.-% CO_2, and 5 vol.-% H_2O in the rich phase, **D)** 400°C with 0.1 vol.-% C_3H_6, 5 vol.-% CO_2, and 5 vol.-% H_2O in the rich phase

The effect of P and Zn, individually and in combination were investigated through wet impregnation in Paper II. The advantage with wet impregnation is that it is easy to precisely control the amount of poison, which facilitate the comparison. However, with wet impregnation, the P and Zn were more evenly distributed over the entire washcoat, while for the gas-phase exposure in Paper I a distribution of P over the monoliths was received.

The activity tests in the flow reactor in Paper II consisted of three different lean/rich cycle segments. Each segment consisted of five lean/rich cycles with a unique gas mixture combination. The lean/rich cycles were conducted at 350°C in a total flow of 1000 ml/min with Ar balance. The first cycle segment featured NO as the NO_X source in the lean phase (400 ppm NO, 5% CO_2, 8% O_2, and 5% H_2O) and H_2 as the reducing agent in the rich phase (400 ppm NO, 5% CO_2, 1% H_2, and 5% H_2O). The second cycle segment consisted of NO_2 as the NO_X source in the lean phase (400 ppm NO_2, 5% CO_2, 8% O_2, and 5% H_2O) and H_2 as the reducing agent in the rich phase (400 ppm NO_2, 5% CO_2, 1% H_2, and 5% H_2O). The third cycle segment included NO as the NO_X source in the lean phase (400 ppm NO, 5% CO_2, 8% O_2, and 5% H_2O)

and C_3H_6 as the reducing agent in the rich phase (400 ppm NO_2, 5% CO_2, 1000 ppm C_3H_6, and 5% H_2O).

Figure 8 shows the first cycle segment for samples containing 1wt-% of poisoning species. It can be seen in the figure that there was almost no deactivation of the NO_X storage and reduction capacities of the catalyst with the impregnation of 1wt-% Zn (Figure 8 **B**). In contrast, the samples containing 1wt-% P (Figure 8 **A** and **C**) showed a significant loss of NO_X storage capacity during the lean phase, where (1wt-% P + 1wt-% Zn) exhibited somewhat more deactivation than 1wt-% P. These results are in line with observations by Christou et al. [79] when they impregnated a TWC catalyst with P, Zn, and Ca. They found some deactivation associated with Zn and Ca, however, they found a significantly larger deactivation caused by phosphorous. Deactivation of the $Pt/Ba/Al_2O_3$ catalyst caused by phosphorous was also found by Galisteo et al. [78] when they impregnated the same model catalyst with $(NH_3)_3PO_4$ dissolved in water. They found an almost linear relationship between the P/Ba ratio and NO_X storage capacity. There was a significant increase in NO_X slip related to an increase in slip of NO_2 for the samples impregnated with phosphorous (Figure **A** and **C**). In contrast, the slip of NO remained almost unchanged. Olsson et al. [36] have proposed a NO_X storage mechanism in which NO is oxidized by O_2 on the Pt sites to form NO_2, after which NO_2 is stored on barium as $Ba(NO_3)_2$. The increased slip of NO_2 after impregnation with phosphorous could indicate that the barium sites were more affected by the presence of phosphorous than the Pt sites since NO oxidation capacity remained high.

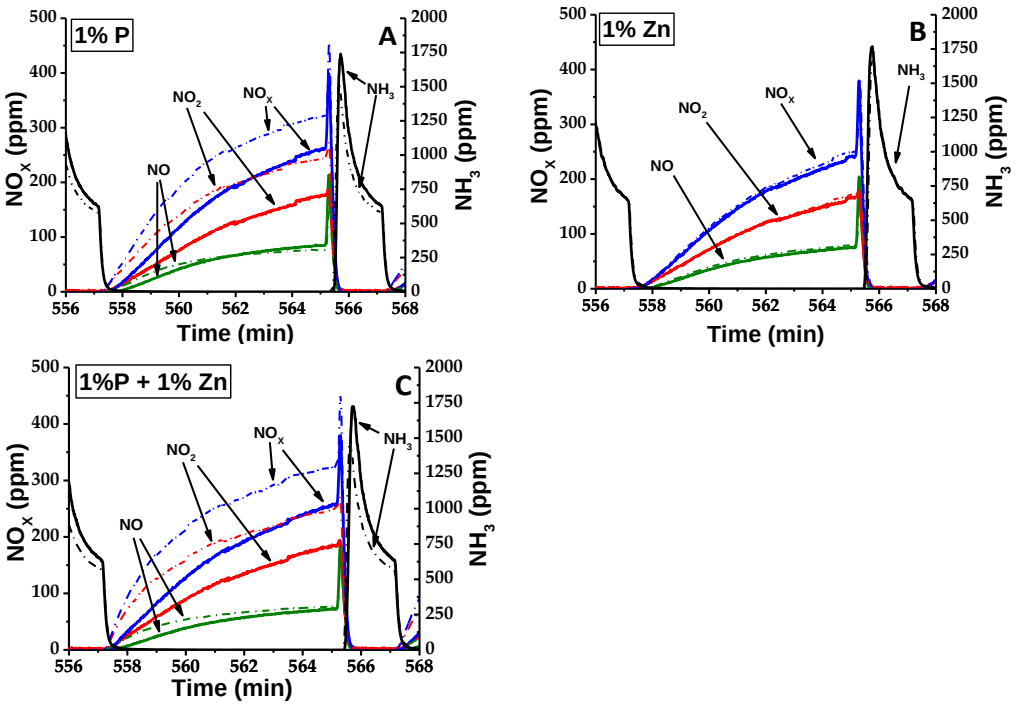

Figure 8. Lean/rich cycle at 350°C. Gas mixture lean phase: 400 ppm NO, 5% CO_2, 8% O_2, and 5% H_2O. Gas mixture rich phase: 400 ppm NO, 5% CO_2, 1% H_2, and 5% H_2O. **A)** Fresh and 1wt-% P, **B)** Fresh and 1wt-% Zn, and **C)** Fresh and (1wt-% P+1wt-% Zn).

Figure 9 shows a lean/rich cycle from the first cycle segment in which NO was the NO_X source and H_2 was the reducing agent with samples containing 2 wt-% of poisoning species. Compared to the results in Figure 8, Figure 9 shows greater deactivation for all three samples with a higher concentration of poisoning species. Figure 9 **A** and **C** shows a large slip of NO_X for samples containing phosphorous, 2wt-% P and (2wt-% P +2wt-% Zn). This is mainly due to the increase in the slip of NO_2. It can be seen when comparing Figure 9 **A** and **C** that the sample that only contained 2wt-% P appears slightly more deactivated than the sample with the combination (2wt-% P+2wt-% Zn). The breakthrough in these two samples occurred much earlier in the lean phase than in the fresh catalyst. The slip of NO was significantly larger after impregnation with 2 wt-% phosphorous. However, as the lean phase proceeded, the poisoned samples approached saturation, and the excess slip of NO decreased in comparison with the fresh samples. Figure 9 **B** shows greater slip of NO_X for 2wt-% Zn than for the fresh catalyst. For the sample exposed to 2wt-% Zn, in contrast to the samples exposed to phosphorous (Figure 9 **A** and **C)**, the increased slip of NO is larger than the increased slip of NO_2, which is the opposite trend for phosphorous poisoned samples. This may indicate that poisoning by zinc interacts differently with the $Pt/Ba/Al_2O_3$ catalyst than phosphorous does.

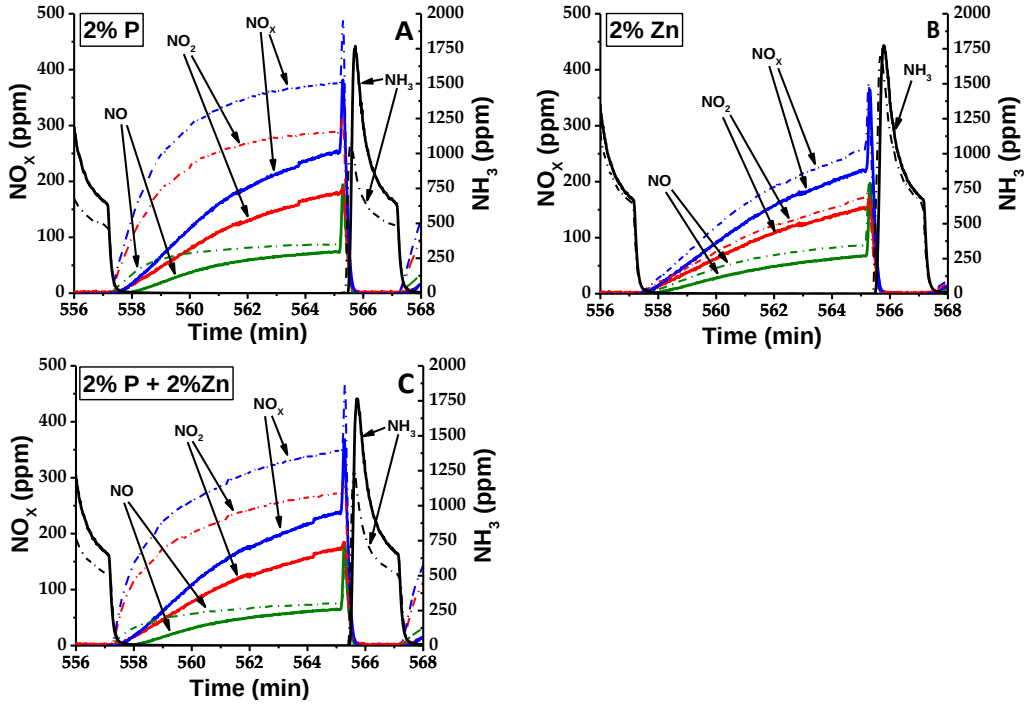

Figure 9. Lean/rich cycle at 350°C. Gas mixture lean phase: 400 ppm NO, 5% CO_2, 8% O_2, and 5% H_2O. Gas mixture rich phase: 400 ppm NO, 5% CO_2, 1% H_2, and 5% H_2O. **A)** Fresh and 2wt-% P, **B)** Fresh and 2wt-% Zn, and **C)** Fresh and (2wt-% P, 2wt-% Zn).

Figure 10 shows the second cycle segment, with NO_2 as the NO_X source and H_2 as the reducing agent for samples containing 2wt-% of poisoning species. A comparison of Figure 9 and Figure 10 shows that there were no significant differences when NO_2 instead of NO was used in the gas feed. This means that the oxidation of NO_X species was not inhibited by phosphorous to the

same extent as the storage of NO_2 on barium, which supports the previous observation. The formation of NH_3 during the rich phase decreased in both the first and the second cycle segments and occurred earlier in the rich phase. NH_3 is formed during the reduction of NO_X with H_2 as the reducing agent [17]. The concentration of NH_3 formed in the rich phase is related to several factors: (i) the reaction with H_2 and NO_X from the gas feed, (ii) the reaction with H_2 and stored NO_X on Al_2O_3 or BaO, (iii) the reaction of NH_3 with stored NO_X to form H_2O and N_2, which is seen in the SCR process [6,7]. Lietti et al. [17] have suggested that, when H_2 is used as a reducing agent, the breakthrough of NH_3 will occur when most of the stored NO_X has been reduced by H_2. Those authors showed that most N_2 had been formed before the breakthrough of NH_3. The breakthrough of NH_3 for all samples in Figure 9 and Figure 10 occurred earlier for the poisoned samples than for the fresh samples. This was likely related to less NO_X storage during the lean phase.

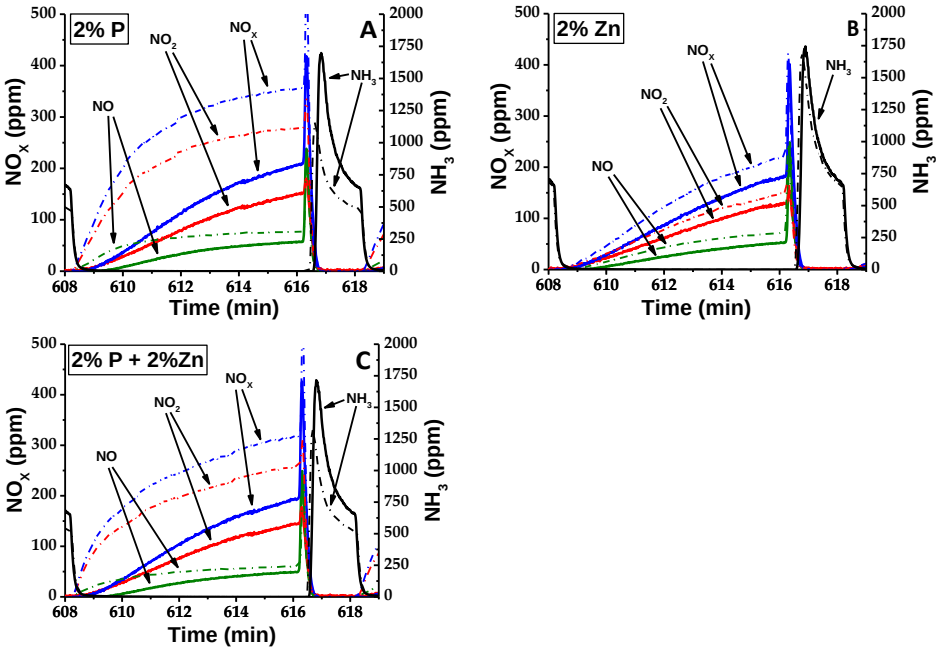

Figure 10. Lean/rich cycle at 350°C. Gas mixture lean phase: 400 ppm NO_2, 5% CO_2, 8% O_2, and 5% H_2O. Gas mixture rich phase: 400 ppm NO_2, 5% CO_2, 1% H_2, and 5% H_2O. **A)** Fresh and 2wt-% P, **B)** Fresh and 2wt-% Zn, and **C)** Fresh and (2wt-% P, 2wt-% Zn).

Figure 11 shows the third cycle segment for the samples containing 2 wt-% of poisoning species in which NO was used as the NO_X source and 1000 ppm C_3H_6 was used as the reducing agent. The deactivation during the lean phase is similar to what is shown in Figure 9 and Figure 10. However, an increase in NO_X slip was found both for fresh and poisoned samples. This is related to the reducing properties of C_3H_6 at 350°C. The reducing capacities of C_3H_6 were significantly better at 400°C than at 300°C [18], which means that the samples were not fully reduced during the rich phase at 350°C. This resulted in fewer barium sites available for NO_X storage during the lean phase. Figure 7 from the study of the gas-phase exposure of phosphorous

shows that the formation of NH_3 is rather low compared to when H_2 is used as the reducing agent.

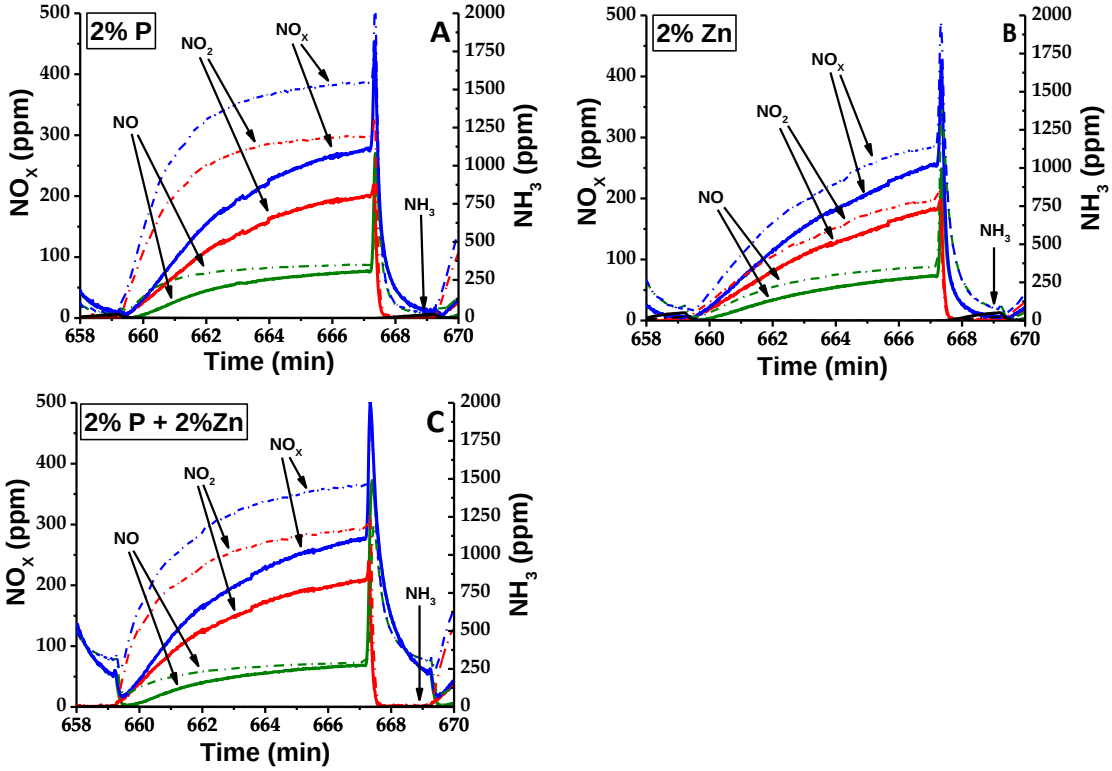

Figure 11. Lean/rich cycle at 350°C. Gas mixture lean phase: 400 ppm NO, 5% CO_2, 8% O_2, and 5% H_2O. Gas mixture rich phase: 400 ppm NO, 5% CO_2, 1000 ppm C_3H_6, and 5% H_2O. **A)** Fresh and 2wt-% P, **B)** Fresh and 2wt-% Zn, and **C)** Fresh and (2wt-% P, 2wt-% Zn).

To compare all six samples, all corresponding fresh samples were averaged and plotted together with the poisoned samples, as shown in Figure 14. A slight deactivation can be seen in the figure for samples that only contained Zn. The sample impregnated with 2wt-% Zn was more deactivated than the sample that only contained 1 wt-% Zn. However, the addition of P resulted in significantly more deactivation. It can be seen in the figure that the combination (1wt-%P+1wt-% Zn) was more deactivated than the samples that only contained 1wt-% P in all three cycle segments. This behavior did not apply to samples that contained 2 wt-% P and (2wt-%P+2wt-% Zn). In those samples, we observed the opposite trend from the samples that contained 1 wt-%, i.e. samples with the combination (2 wt-% P+2 wt-% Zn) appeared to be less deactivated than the samples with only 2 wt-% P. This trend was observed in all three cycle segments. This could indicate that zinc reacts with phosphorous to produce zinc phosphates, thereby freeing barium sites to participate in the NO_X storage mechanism during the lean phase. This experiment was repeated with another batch of $Pt/Ba/Al_2O_3$ (data not presented here). The trends for samples that contained both 1wt-% P and 2wt-% P were the same for the repeated

experiments. Another observation from these experiments is that increasing the poison level resulted in much greater poisoning.

NO_2-TPD was performed on samples in the flow reactor in Paper II, before and after the impregnation of P and Zn, in order to study the effect these species have on the storage of NO_2 and the desorption profiles of NO_X on the $Pt/BaAl_2O_3$ catalyst. Before the loading step, samples were pretreated in 1% H_2, 5% CO_2, and 5% H_2O at 400°C for 20 min. NO_2 was loaded in 500 ppm NO_2 and 5% H_2O at 100°C for 1h, which was followed by a short flush of the system with 5 % H_2O present. Thereafter, the temperature was increased from 100 to 500°C with a temperature ramp of 10°C/min.

NO_2 is favored at low temperatures, according to thermodynamic equilibrium, while NO dominates at higher temperatures, as can be seen in Figure 2. Lindholm et al. [23] have observed, when studying NO_2-TPD on $Pt/Ba/Al_2O_3$, that the release of NO_X in lower temperature regions is associated with storage on Al_2O_3, whereas the release of NO_X in higher temperature regions is associated with storage on Ba. The results from samples impregnated with 1wt-% are shown in Figure 12, and the results from samples impregnated with 2wt-% are shown in Figure 13. In the low temperature region, associated with storage on Al_2O_3, all samples exhibited a similar desorption trend, and the impregnation of poisoning species had a low or negligible impact on the release of NO_X in this region. We observed that, as the temperature reached 350°C, some poisoned samples started to deviate from the fresh catalyst; this can be seen in the samples in both Figures 12 and 13. The higher desorption temperature range is mainly associated with desorption from Ba. This would indicate that primarily Ba is affected by the poison and responsible for the increased NO_X slip during the NSR capacity tests. The trend that was observed from the lean/rich cycles, that the combination (2wt-%P+2wt-%Zn) stored more NO_X than 2wt-% P, can be seen in the NO_2-TPD measurements in Figure

13. It is also clear in the figures that samples impregnated with 2 wt-% Zn were less affected than samples impregnated with 2 wt-% P.

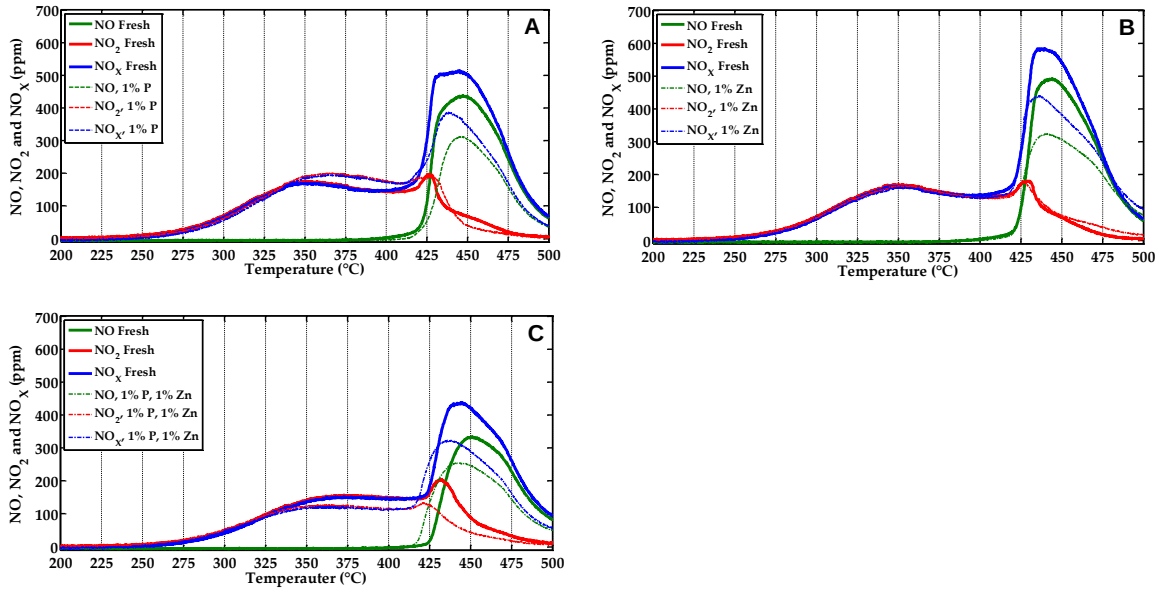

Figure 12. NO_2 TPD. Storage of NO_X at 100°C with a gas mixture of 500 ppm NO_2 and 5% H_2O, followed by flushing with 5% H_2O for 10 min, and, thereafter, a temperature ramp to 500°C with 10°C/min in 5%H2O A) Fresh and 1wt-% P, B) Fresh and 1wt-% Zn, and C) Fresh and (1wt-% P, 1wt-% Zn).

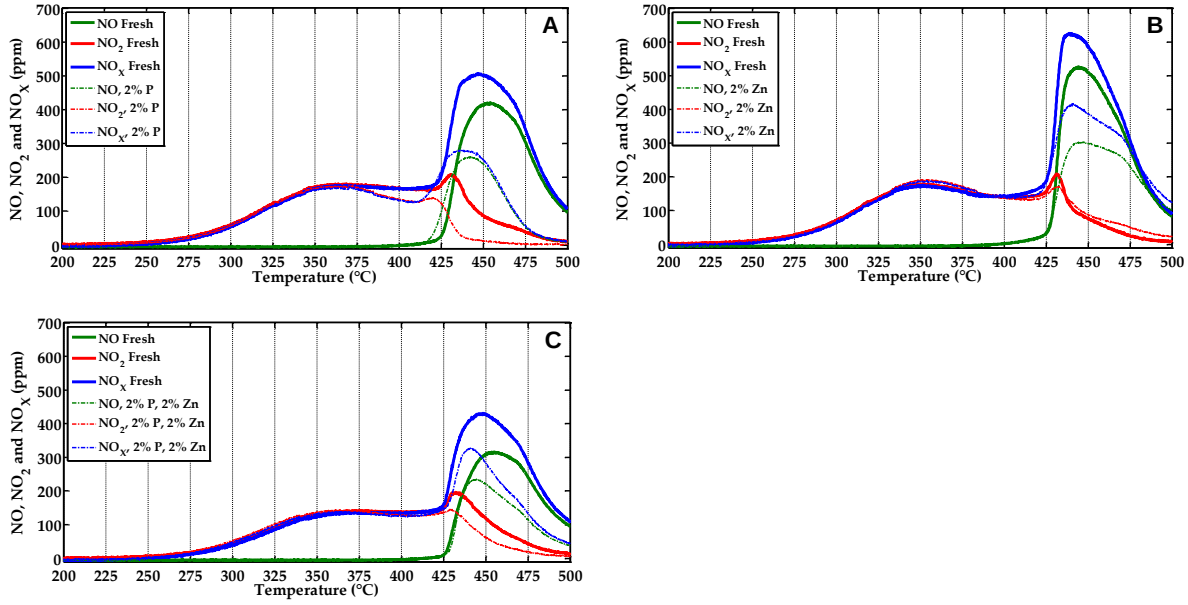

Figure 13. NO_2 TPD. Storage of NO_X at 100°C with a gas mixture of 500 ppm NO_2 and 5% H_2O, followed by flushing with 5% H_2O for 10 min, and, thereafter, a temperature ramp to

500°C in 5% H2O with 10°C/min **A)** Fresh and 2wt-% P, **B)** Fresh and 2wt-% Zn, and **C)** Fresh and (2wt-% P, 2wt-% Zn).

Comparing the methods in Paper I and Paper II, we observed a clear poisoning effect of phosphorus for both cases. However, the NO_X storage cycling for Paper I and Paper II were conducted at different temperatures and it is therefore not possible to compare the extent of the poisoning between the two studies. Another similarity is that for both cases the NO oxidation functionality was maintained, indicating that the noble metal was not/or only to a small degree poisoned with phosphorus and that the main poisoning is occurring on the storage component. From the NO_2 TPD for the samples impregnated with P and Zn, we observed that storage onto Ba was radically reduced whereas the storage onto Al_2O_3 mostly remained unchanged. Hence, we can conclude that that both Zn and P disturb the storage properties of Ba rather than the Al_2O_3 or noble metal.

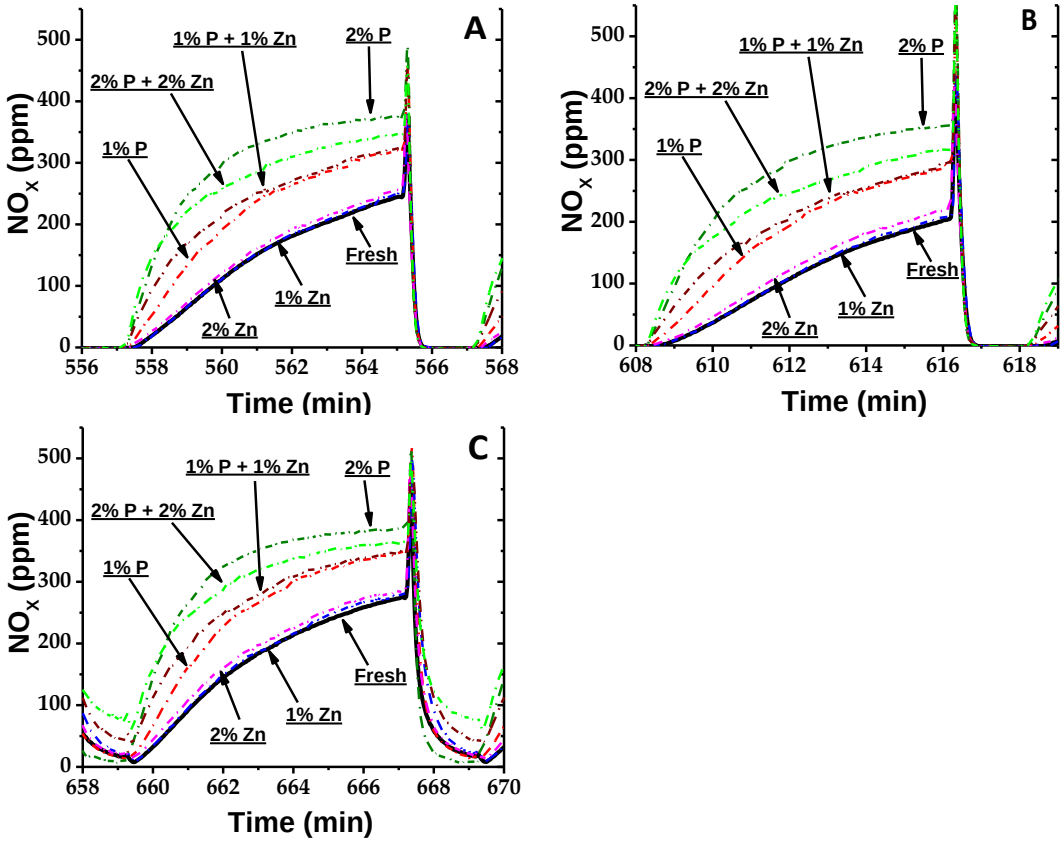

Figure 14. Lean/rich cycles at 350°C. An average of all fresh samples and the six poisoned samples. Gas mixture lean phase: 400 ppm **NOx**, 5% CO_2, 8% O_2, and 5% H_2O. Gas mixture rich phase: 400 ppm **NOx**, 5% CO_2, **reducing agent**, and 5% H_2O. **A)** 400 ppm NO and 1% H_2, **B)** 400 ppm NO_2 and 1% H_2, and **C)** 400 ppm NO and 1000 ppm C_3H_6.

4.1.2 Effect of P on surface area

It was observed that the phosphorous in field-aged catalysts deposited in an axial distribution [52,57,66]. Therefore, both samples in Paper I were divided into three sections, inlet, middle, and outlet. Each monolith section was crushed and ground to a powder. The BET surface area and pore volume for each section was compared to a freshly coated and degreened sample, which is shown in Table 4. Elemental analysis of each section using ICP-AES is also displayed in Table 4 for a comparison of P content and surface area. Results from BET surface area and pore volume indicate that both surface area and pore volume were the lowest at the inlet and the highest at the outlet. These results relate to the phosphorous content, which had the highest concentration at the inlet and the lowest at the outlet. Galisteo et al. [78] have studied wet impregnation of phosphorous on an LNT catalyst $Pt/Ba/Al_2O_3$, and they found that increased phosphorous content reduced the surface area. Indeed, the phosphorous content in our results correlate to a reduced BET surface area. An axial distribution of phosphorous, from inlet to outlet, is clear in the results in Table 4, which is in agreement with findings from the characterization of field-aged catalysts.

Table 4. Specific BET surface area and pore volume of sample "50 ppm, 34h," "100 ppm, 34h," and a fresh sample. Results compared with phosphorus content from ICP-AES measurements.

	P- Content, (wt-%)	S_{BET}(m^2/(g washcoat))*	V_P (cm^3/ (g washcoat))*
Fresh	-	134	0.46
50 ppm, 34h, inlet	2.2	98	0.36
50 ppm, 34h, middle	0.40	130	0.45
50 ppm, 34h, outlet	0.11	134	0.45
100 ppm, 34h, inlet	2.0	113	0.35
100 ppm, 34h, middle	0.38	123	0.39
100 ppm, 34h, outlet	0.07	132	0.39

4.1.3 Distribution of P and Zn on the LNT catalyst

In Paper I, EDX mapping and ESEM images from two different positions; 2mm from the front and 2 mm from the back of the monolith of the sample exposed to 50 ppm phosphorous for 34 hours, were acquired and are shown in Figures 15-16. Four elements were mapped for the chosen positions using EDX (P, Ba, Si, and Al). Silicon, which is one of the main components of the ceramic monolith substrate and is shown as green in both figures, is visible in the figures 2mm from the front and the back. Aluminium and barium, which make up most of the washcoat, are shown as grey and red in the figures. We observed that phosphorous, shown in yellow in the figures, was located more towards the surface of the washcoat in the image 2mm from the front (Figure 15). This was also observed by Bunting at al. [51] in their study of diesel oxidation catalysts. Interestingly, the results for the measurement 2 mm from the back (Figure 16) indicate that phosphorous are more dispersed into the washcoat and not located mainly towards the surface of the washcoat. The different patterns of accumulation could indicate that different

phosphorous species coexist in the washcoat.

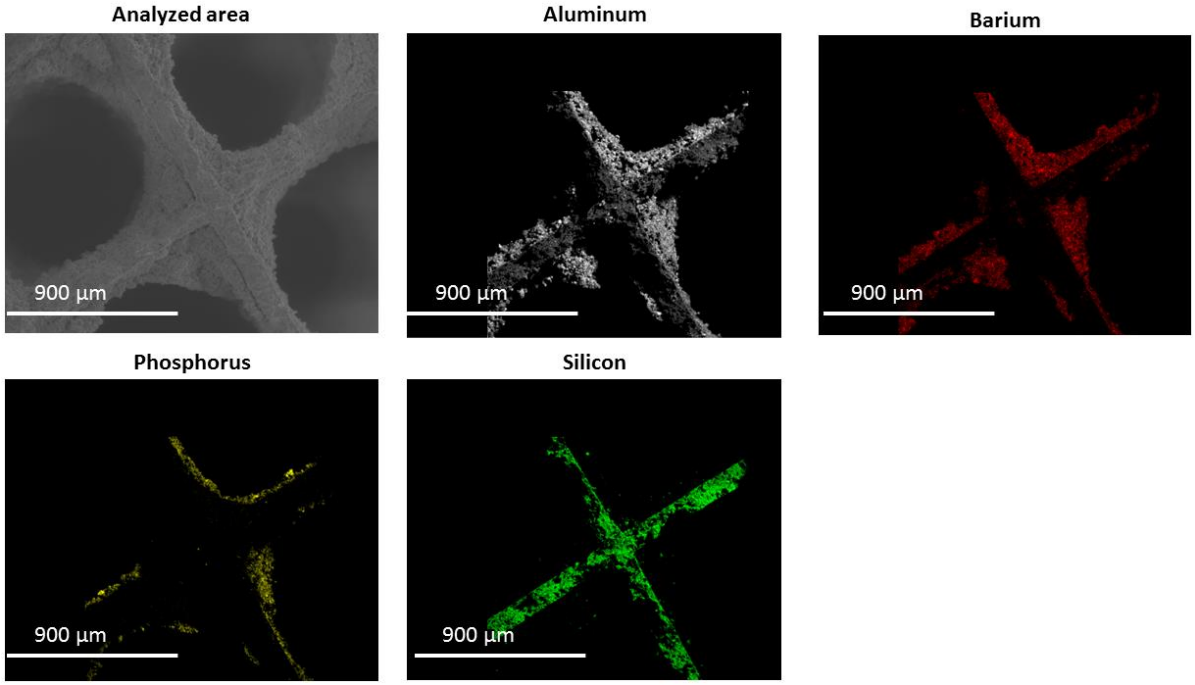

Figure 15. ESEM image (top row, left) and EDX elemental maps from the cross section 2 mm from the front of the Pt/Ba/Al_20_3 sample exposed to 50 vol.-ppm H_3PO_4, 8vol.% O_2, and 5 vol.%H_2O for 34 h.

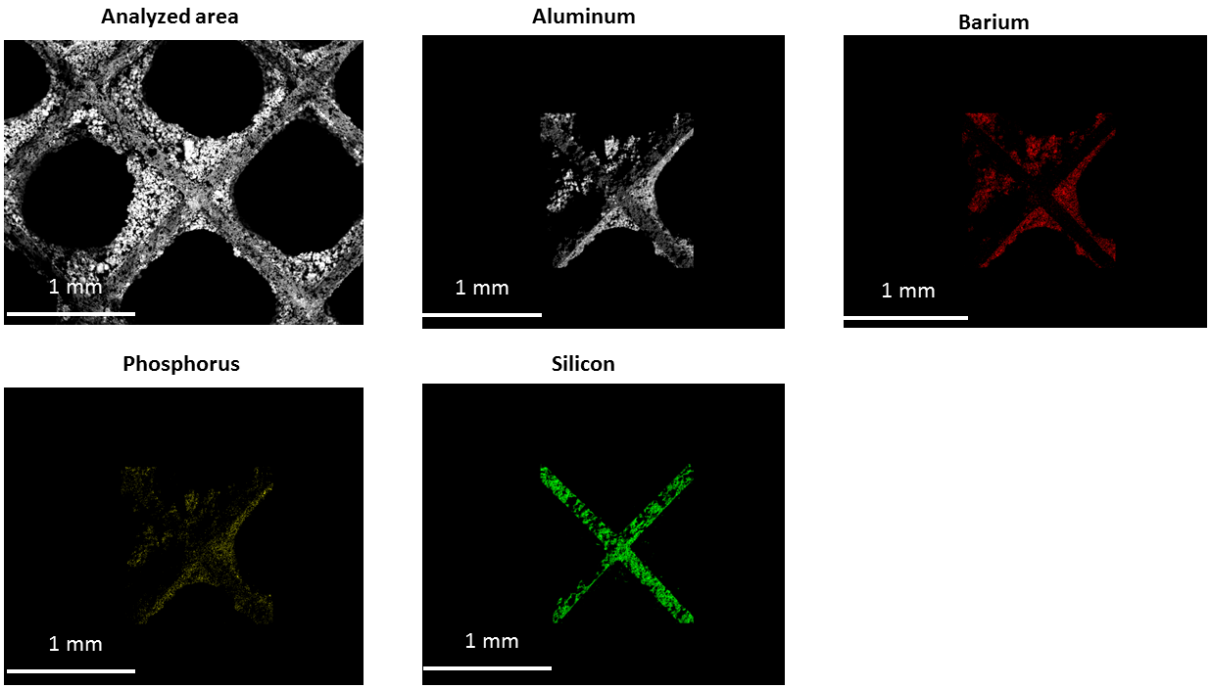

Figure 16. ESEM image (top row, left) and EDX elemental maps from the cross section 2 mm from the back of the Pt/Ba/Al_20_3 sample exposed to 50 vol.-ppm H_3PO_4, 8vol.% O_2, and 5 vol.%H_2O for 34 h.

In contrast to Paper I, Paper II used an impregnation method for poisoning, resulting in an even distribution of the poisons. All samples containing 2 wt.-% of poisoning species are characterized and mapped using STEM-EDX (see Figure 17). Images show areas where P, Zn, Ba, and Pt are present in the same region. For the sample containing 2 wt.-% P, it can be seen that both P and Ba coexist in the same region indicating that there might be an interaction between these two elements. In contrast to the sample with 2 wt.-% P, the sample with 2 wt.-% Zn did not indicate possible interactions between Zn and Ba. The sample containing both P and Zn at 2 wt.-% is shown in rows 3-5 in Figure 17, and also for this case the P and Ba appear to interact with each other in the same way as in the sample with only 2 wt.-% P in row 1. However, compared to when only Zn was present, here we can observe Zn located close to P, and thereby also to Ba. This may indicate that Zn and P either react with each other, forming for example zinc phosphates or that they form agglomerates. Both scenarios result in less P interacting with Ba, which provides more Ba available for NSR activity. This could further explain the results observed in Figure 14 where Zn reduced the aging effects caused by P on $Pt/Ba/Al_2O_3$.

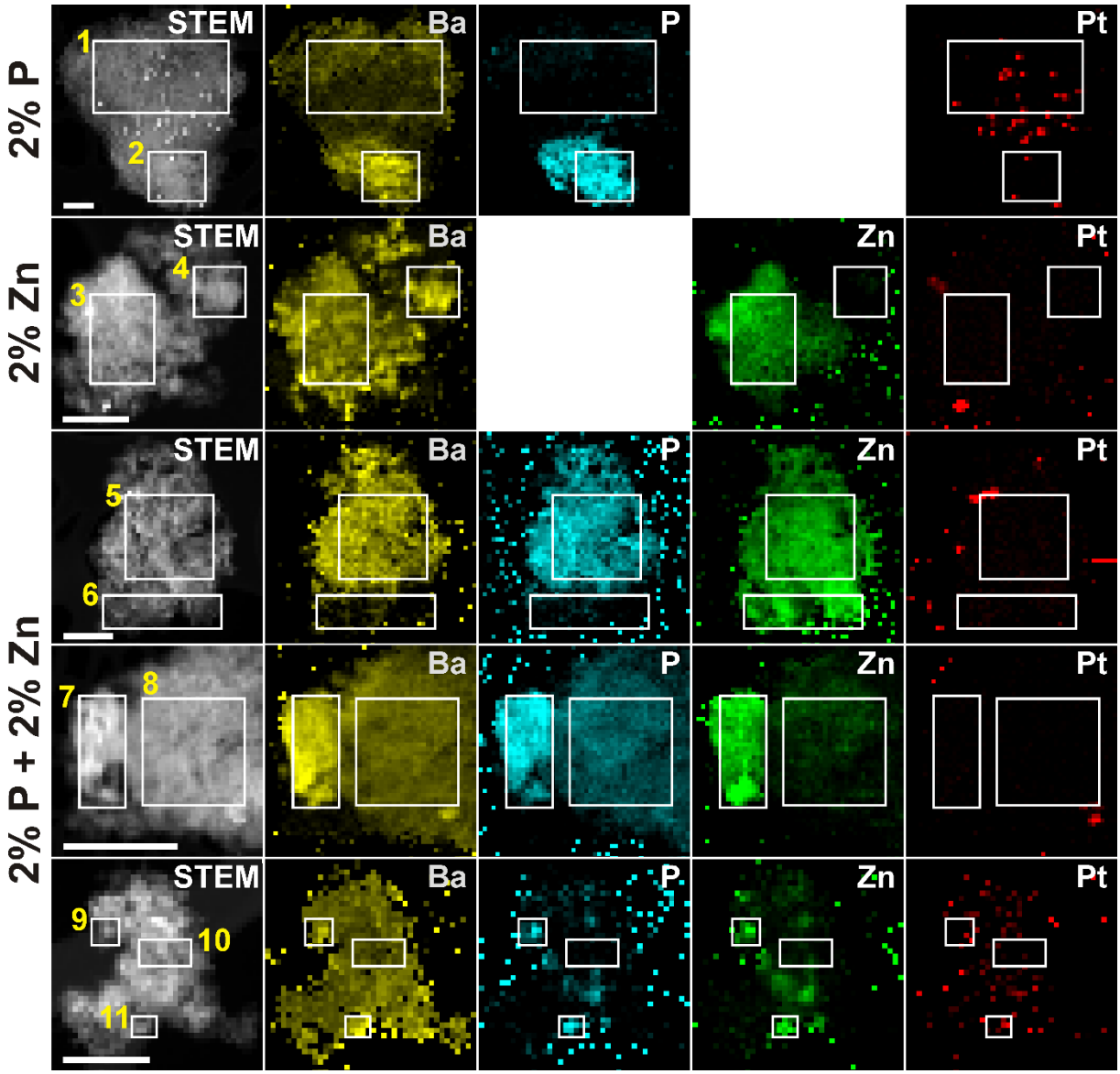

Figure 17. STEM images and EDX maps of samples impregnated with 2wt.-% poison. First row contains images from the sample with 2 wt.-% P. Second row contain images from the sample with 2wt.-% Zn. Rows 3-5 contain images from the sample with 2 wt.-% P and 2 wt.-% Zn. The white scale bar in the lower left corner of the STEM image in each row represents 200 nm.

For gas-phase exposure to phosphorous, as in Paper I, the distribution of phosphorous played a vital role. For real world application, the flow field of the exhaust gas inside of monolith channels determines how a foreign species, such as P, will be distributed over the washcoat. At the outlet of the samples in Paper I, the results indicated that P did diffuse into the washcoat. This could indicate that the wet impregnation in Paper II would be more comparable towards the rear end of a field-aged catalyst. However, the interaction between the elements in Paper II are more visible due to the approach, since the poisoning loading can be controlled in a more precise manner.

4.1.4 Phosphoric species formed after exposure

In Paper I, the surface compositions of the sample exposed to 50 vol. ppm H_3PO_4, 8vol.% O_2 and 5 vol.% H_2O for 34h were analysed using XPS. One channel was removed from the coated monolith, which was then measured at three different positions (inlet, middle, and outlet). Figure 18 **A** shows the overall spectrum for the measurements at inlet, middle, and outlet. The peaks of Al 2s and Ba 4p are both clear in the figure at the surface of all three measured positions. However, P 2s is significantly larger at the inlet than at the middle or outlet. This indicates a large presence of phosphorous species at the surface of the washcoat in the front of the catalyst. This result correlates well with the ICP results (Table 3) and with the results in Figures 15-16, which show a cross section over the washcoat at the front and at the end of the catalyst acquired using EXD mapping. Figure 18 **B** shows measurements with a higher resolution over P 2p. The positions of the peaks were corrected towards C 1s (284.8 eV) and normalized. The P 2s peak at the middle appears large due to the normalization, however, it was significantly lower than the peak at the inlet. We observed a shift in the center point of the P 2s peak for the inlet (135.3 eV) compared to the middle (134.5 eV). A deconvolution was done for both peaks in Figure 18 **B** and is shown in Figure 19. The phosphorous species considered for the deconvolution was P_4O_{10} ranging between 135 and 135.5 eV [109], PO_3^- ranging between 134 and 134, 5 eV [109] and PO_4^{3-} ranging between 132.1 and 132.9 eV [109]. The results from the deconvolution indicate that the shift in Figure 18 **B** was due to a larger amount of P_4O_{10} at the inlet of the catalyst, while the smaller phosphorous P 2s peak in Figure 19 **B** was dominated by PO_3^-. The formation of P_4O_{10} and PO_3^- was observed by Shwan et al. [75] when they studied gas-phase exposure to phosphoric acid on Fe-BEA. Andonova et al. [73] have also observed the formation of PO_3^- on Cu-BEA, caused by exposure to phosphoric acid in a similar way.

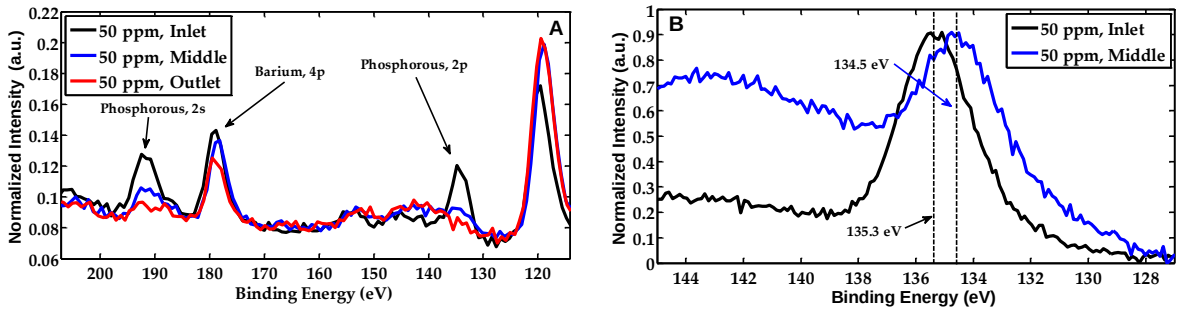

Figure 18. A) Normalized XPS spectra from the inlet, middle, and outlet sections of the Pt/Ba/Al_2O_3 sample exposed to 50 vol.-ppm H_3PO_4, 8vol.% O_2, and 5 vol.%H_2O for 34 h. **B)** Corresponding XPS spectra for the P 2p region from the inlet and middle sections of the sample.

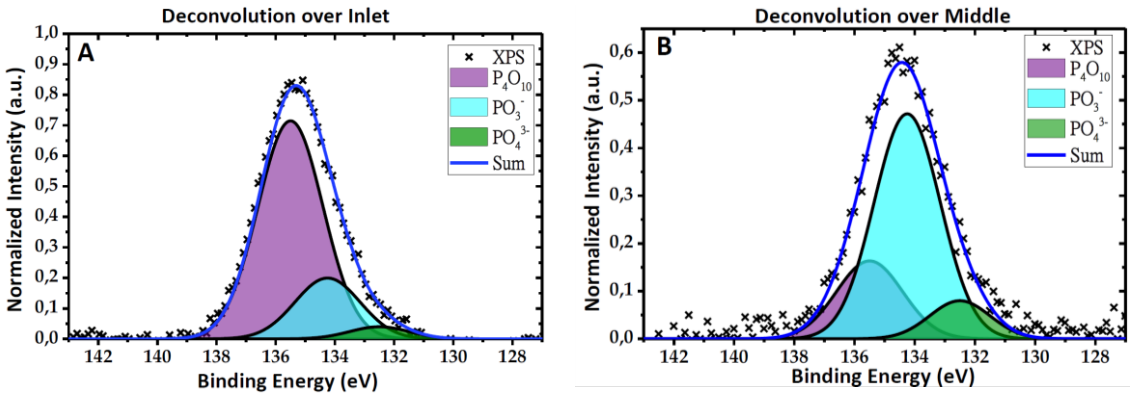

Figure 19. Deconvolution of the P 2p XPS spectra from the inlet (A) and middle (B) sections of the $Pt/Ba/Al_2O_3$ sample exposed to 50 vol.-ppm H_3PO_4, 8vol.% O_2, and 5 vol.% H_2O for 34 h. The considered phosphorous species are P_4O_{10}, PO_3^- and PO_4^{3-} .

XPS was performed in Paper II to understand the interactions between Zn and P on the $Pt/Ba/Al_2O_3$ catalyst. Figures with these measurements are shown in Paper II (Figure 8, Paper II). It is clearly visible in Figure 14 that Zn helped reduce the aging effect caused by P on the catalyst for high poisoning levels, Zn is observable in the same region in the STEM-EDX images in Figure 17, however, zinc phosphate was not possible to prove using XPS. Thus it is not clear exactly how phosphorous and zinc interacts with the LNT catalyst, but the flow reactor experiments clearly shows a reduced poisoning effect when combining P and Zn, compared to individual poisoning. Furthermore, TPD characterization results indicate that phosphorous mainly disturbs the properties of Ba in the LNT catalyst, and Zn possesses the capacity to reduce this effect.

4.1.5 Effect of Zn and P on crystallinity

In Paper II, samples 2 wt.-% P, 2 wt.-% Zn, and (2wt.-% Zn,2wt.-% P) were compared to a fresh sample in order to evaluate if changes in crystallinity could be observed after the poisoning process. Powder from crushed monoliths was used for all samples, including the fresh sample. Figure 20 shows the XRD results for these samples. Three different denotations are used to mark the peaks in the figure. These denotations are "#," which symbolizes cordierite, "Δ," which symbolizes Al_2O_3, and "●," which marks the Ba species. The positioning of the peaks associated with cordierite is the same for all samples in Figure 20 and the XRD spectra are normalized to the cordierite peak at 10° [110]. The support material, Al_2O_3, is rather amorphous, which resulted in a weak signal strength in XRD measurements. However, the peak visible at 54° can, nevertheless, be associated with the support material [111]. Lastly, two regions were marked for the Ba species. There are two twin peaks at 23 and 24°, and one peak at 33° in Figure 20. Different studies have associated these peaks with various Ba species, such as $BaCO_3$, $BaAl_2O_4$, and $Ba(NO_3)_2$ [78,111]. It can be observed that the peak positioned at 33° in all samples did not undergo considerable change after exposure to poisoning species. For the peaks at 23 and 24° in the samples containing P, however, it was observed that the intensity of the peaks decreased, indicating a loss of crystallinity for a certain Ba species. These results

further our understanding of the $Pt/Ba/Al_2O_3$ LNT catalyst, not only did Ba take different forms on the catalyst but P did, in fact, target certain crystalline forms of Ba more than others.

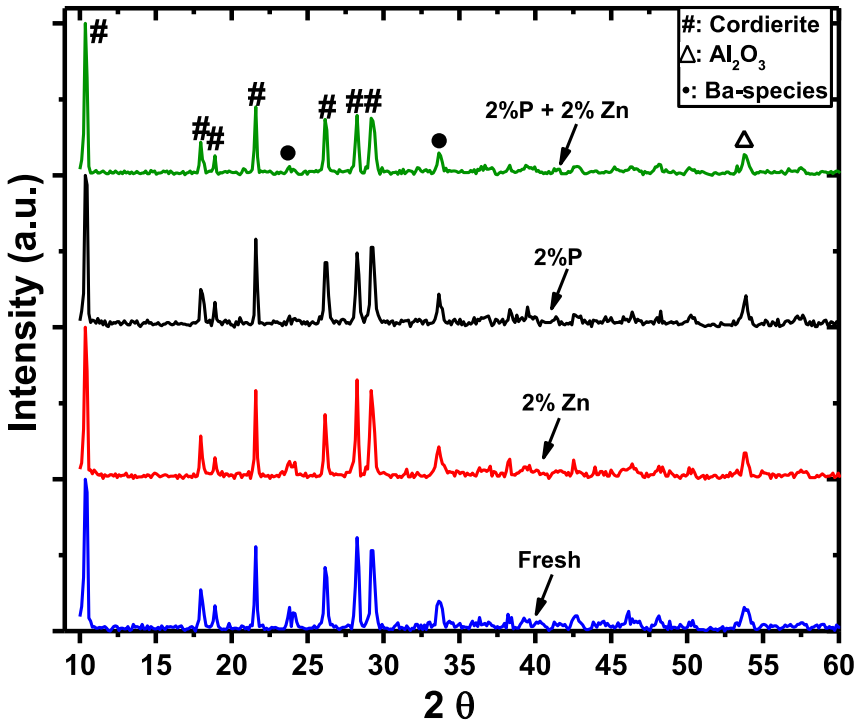

Figure 20. XRD patterns of samples 2% P, 2% Zn, 2% P + 2% Zn, and Fresh. "#" denotes cordierite, "Δ" denotes Al_2O_3, and "+" denotes Ba species.

4.2 Hydrocarbon Trap

The topic of Papers III and IV was hydrocarbon trapping under cold-start conditions. Both papers explored the addition of metal ions to a zeolite in order to improve the trapping ability of the zeolite. One of the major goals for these studies was to increase the temperature of desorption for toluene, propane, and propene and maintain a high adsorption quantity. Both Lewis acidity and ion size are relevant for that purpose and play an important role [101]. How the cation interreacts with a specific zeolite is, therefore, highly relevant.

The effect of promoting a zeolite beta with Fe, La, and Pd was studied and five samples were therefore prepared (Paper III). These samples were "Fe/BEA," "La/BEA," "Pd/BEA," "Fe/Pd/BEA," and "La/Pd/BEA" and were evaluated using toluene-TPD and propene-TPD experiments. These HC-trap formulations were characterized using TPO, XPS, STEM-EDX mapping, and in-situ DRIFTS.

The trapping ability of La ion-exchanged zeolites was studied further in Paper IV. Five promoted samples were used, where both the zeolite types were varied and the effect of different La loading were compared. The samples were "2% La/BEA," "6% La/BEA," "9% La/BEA," "2.5% La/ZSM-5," and "H-ZSM-5 + 2% La/BEA," which were compared to "H-BEA," "H-ZSM-5," and "H-SSZ-13." The HC-trapping ability of the samples was evaluated using toluene-

TPD, Propane-TPD, Propene-TPD, and a mixed TPD with all three different HC components. These samples were further characterized using XRD, in-situ DRIFTS, and BET.

4.2.1 Effect of HC-trap formulation on toluene adsorption

During the cold start of a vehicle, the aim is usually to reach light-off as quickly as possible. Therefore, the engine usually operates with a low air to fuel ratio. This results in unburned hydrocarbons in the exhaust. The most redundant HCs in the exhaust are ethene and methane, however, measured in number of carbon atoms, toluene is the major component [83]. For this reason, HC traps are often evaluated using toluene-TPD.

Shown in Figures 21 and 22 are the toluene and ethene concentrations during a dry-toluene TPD (Paper III). Both Lewis and Brønsted acid sites are available during adsorption in a dry atmosphere. It can be seen in Figure 21 **A** and **B** that all samples have a major desorption peak ranging from 100 to 180°C. This peak location is attributed to the storage of toluene on zeolite beta [95]. The adsorption capacity for toluene was increased in samples containing Pd, foremost Pd/BEA. Like the Pd-containing samples, the La/BEA sample had an increase in toluene adsorption capacity. It has been observed by Park et al. [91] as they mapped toluene adsorption on different ion-exchanged zeolites, that some ion-exchanged zeolites perform better than the "H" version. Figure 22 shows the desorption of ethene for the dry-toluene TPD. It can be concluded that toluene adsorbed onto zeolite beta may undergo cracking. Desorption of ethene ranged from 200 to 300°C, depending on the sample, with a larger degree of ethene desorption in sample BEA than in the other ones (Figure 22 **B**). It is known that the Brønsted acid sites play an important role in the industrial cracking of hydrocarbons in refinery operations [112]. This may explain why we observed a larger degree of cracking for H-BEA.

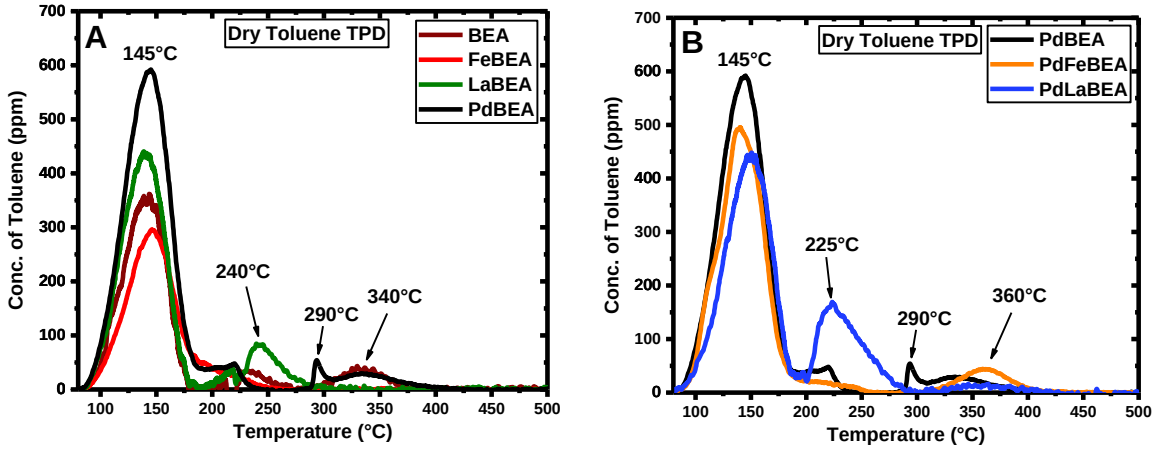

Figure 21. Dry-toluene-TPD experiments where toluene desorption is plotted against the corresponding desorption temperature for: **A**) BEA, Fe/BEA, La/BEA, and Pd/BEA; and **B**) Pd/BEA, Pd/Fe/BEA, and Pd/La/BEA.

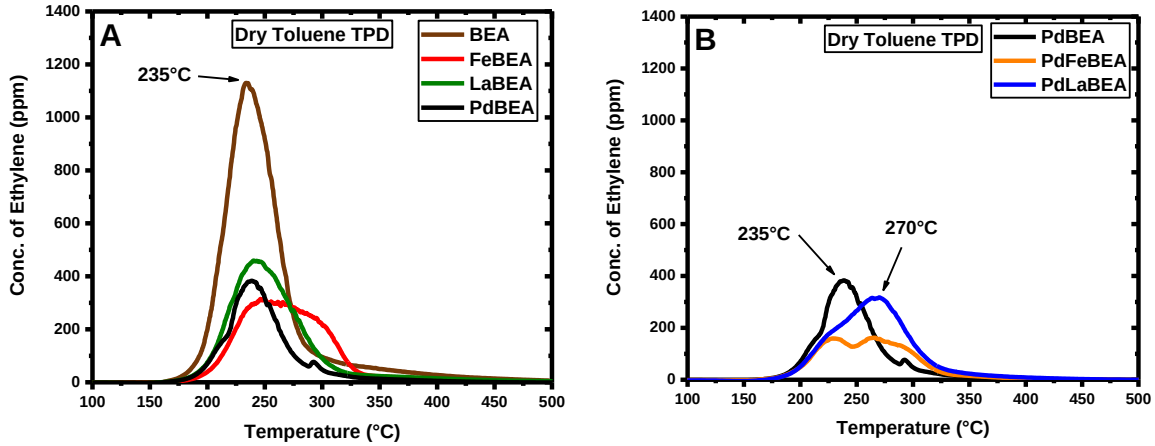

Figure 22. Dry-toluene-TPD experiments where ethene desorption is plotted against the corresponding temperature for: **A**) BEA, Fe/BEA, La/BEA, and Pd/BEA; and **B**) Pd/BEA, Pd/Fe/BEA, and Pd/La/BEA.

The adsorption of hydrocarbons can change considerably in wet conditions. When Burke et al. [106] studied hydrocarbon traps, they observed a significant loss of toluene adsorption capacity on zeolite beta in wet conditions. Wet-toluene TPD results are shown for the samples in Figure 23, and no significant difference in toluene desorption can be seen compared to Figure 21. However, it was observed in that the cracking of toluene into ethene was considerably reduced under wet conditions (Paper III). Moreover, the high temperature desorption of toluene vanished in the presence of water, and this could relate to water inhibition of the Brønsted acid sites. However, the main desorption peak, located at 100 to 180°C, may be more associated with Lewis acid sites, and this desorption peak is similar for dry and wet conditions and explains the similarities between Figures 21 and 23 [90,100].

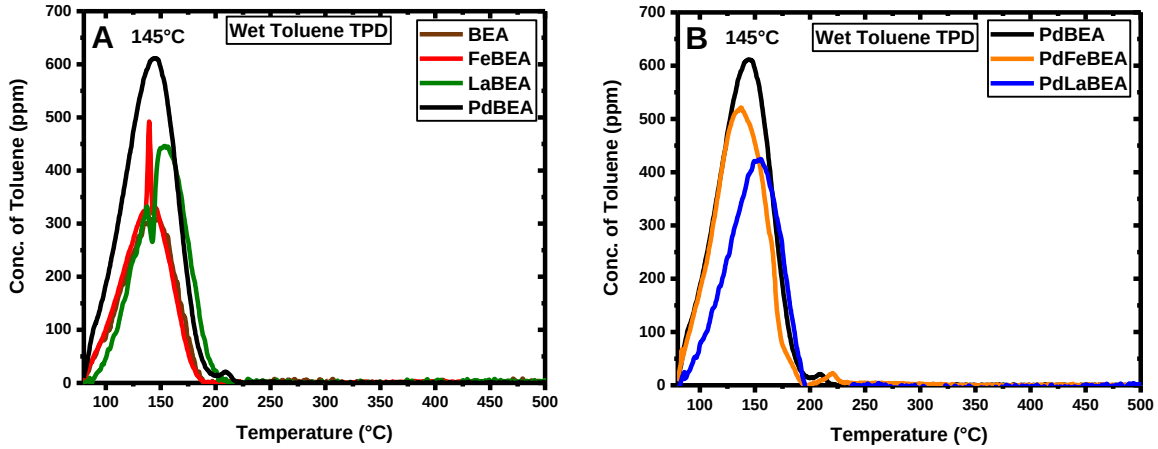

Figure 23. Wet-toluene-TPD experiments where toluene desorption is plotted against the corresponding temperature for: **A**) BEA, Fe/BEA, La/BEA, and Pd/BEA; and **B**) Pd/BEA, Pd/Fe/BEA, and Pd/La/BEA.

La-containing samples in Paper III exhibited a delayed temperature of desorption for toluene, which is very beneficial (see Figure 23). This provided motivation for Paper IV, where zeolites doped with La were studied further. A wet-toluene TPD experiment was performed on zeolites doped with La in various combinations, as shown in Figure 24. Comparing the results from the wet toluene- TPD experiment in Paper III, shown in Figure 23, with the wet-toluene TPD experiment from Paper IV in Figure 24, we can see that the temperature of desorption for toluene increases with lower La contents. Figure 24 **A** shows that a lower content of La improves HC-trapping ability, while the benefits of La decrease with higher La concentrations in zeolite beta. The samples with SSZ-13 and ZSM-5 as the support material instead of zeolite beta are shown in Figure 24 **B**. Zeolite SSZ-13 did not show any toluene desorption, which may be explained by the small pore diameter of the zeolite, hindering the toluene adsorption. There seemed to be a reduction of adsorption capacity in samples with zeolite ZSM-5 compared to zeolite beta, which has a larger pore diameter than zeolite ZSM-5, but ZSM-5 has a higher temperature of desorption, which is clearly beneficial. It has been shown by Park et al. [91] that toluene adsorption capacity increases with the zeolite ring and channel size, which explains the larger capacity found for zeolite beta than for ZSM-5. What can be observed for the sample (H-ZSM-5 + 2% La-BEA), is that the temperature of desorption more resembles zeolite beta but with an adsorption capacity that is drastically lower. Addition of La to zeolite ZSM-5, sample 2.5% La-ZSM-5, indicated a lower storage capacity than H-ZSM-5 in Figure 24, however, the temperature of desorption appears to be slightly increased compared to H-ZSM-5.

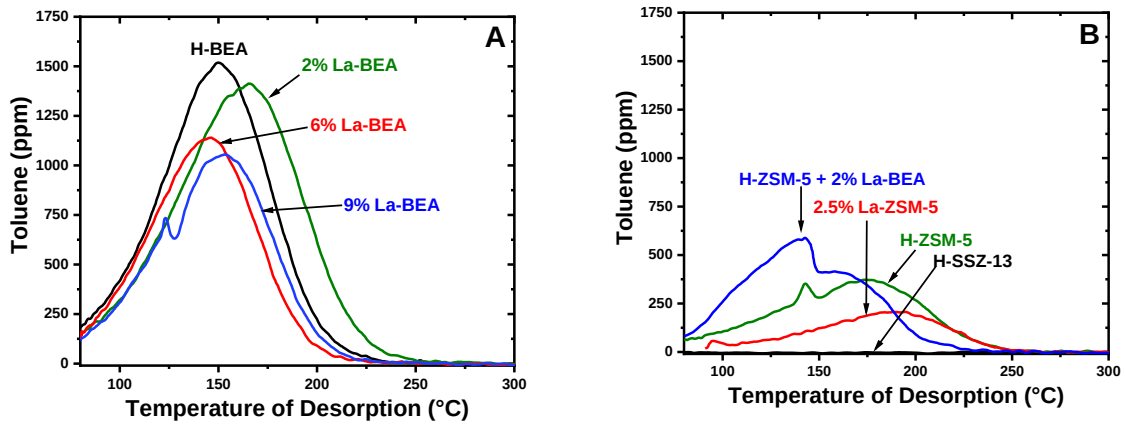

Figure 24. Wet-toluene TPD experiments where toluene desorption is plotted against the corresponding desorption temperature for: A) H-BEA, 2% La-BEA, 6% La-BEA, and 9% La-BEA; and B) SSZ-13, ZSM-5, 2% La-BEA, and ZSM-5 + 2% La-BEA

Comparing the toluene TPD experiments in Papers III and IV, we can see that many factors play important roles in the trapping of toluene. Water content in the exhaust negatively affects how many hydrocarbons that can be adsorbed onto an HC trap. Toluene, however, interacts with the Lewis acid sites of the ion-exchanged cations and charged oxygen in the zeolite framework. This enables the storage capacity to be maintained, even in wet conditions. The HC trapping of zeolite beta and ZSM-5 shows the effect and importance that pore size and pore volume have on HC-trapping mechanisms and performance. We also observed that the addition

of La provided benefits at low concentrations, but at higher loading, the benefits were reduced, both in terms of storage capacity and temperature of desorption.

4.2.2 Effect of HC-trap formulation on propane and propene adsorption

Toluene is, as mentioned above, the most common hydrocarbon in gasoline exhaust during a cold start, counting carbon atoms. However, the dry-toluene TPD results in Figure 22 show that toluene can undergo cracking when adsorbed to a zeolite, especially with a higher availability of Brønsted acid sites [112]. The most redundant hydrocarbon in gasoline exhaust during a cold start are ethene and methane [83]. For this reason, it is relevant to study the adsorption capacities of smaller alkanes and alkenes, such as propane and propene.

Dry-propene TPD experiments were performed on all samples in Paper III, and the results are shown in Figure 25. Even wet-propene TPD experiments were performed for this paper, but the results are not shown due to low levels of adsorption. Figure 25 **A** shows the desorption of propene for samples BEA, Fe/BEA, La/BEA, and Pd/BEA, and Figure 25 **B** shows samples Pd/BEA, Pd/Fe/BEA, and Pd/La/BEA. The temperature of desorption for propene for all samples was around 250°C. Pd reduced the total amount of propene desorbed from the zeolite in the dry-toluene TPD experiments, in contrast to the results shown in Figure 21 for toluene. A comparison of the propene desorption in Figure 25 with the ethene desorption in Figure 22 shows that these occur in the same temperature region. This indicates that TPD experiments with small alkenes have high comparability.

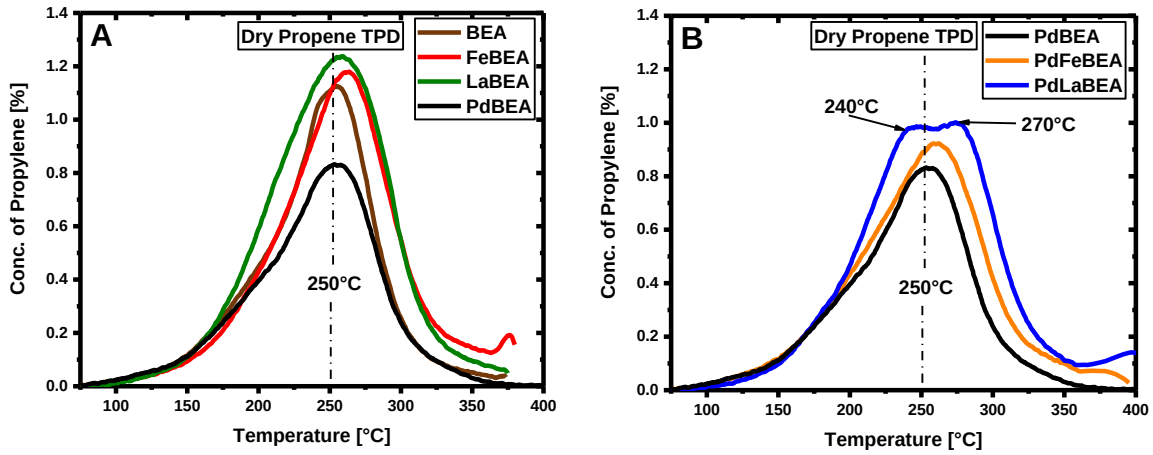

Figure 25. Dry-propene-TPD experiments where the concentration of propene is plotted against the corresponding temperature during the temperature ramp. The samples were pre-oxidized at 400°C.

Both propene and propane TPD experiments were performed on the samples in the study in Paper IV. Both TPD experiments were performed in the presence of 5% H_2O in the gas feed. The reason for performing wet TPD experiments is that they more resemble the real world application where vapor is always found in exhaust. Figure 26 shows the results for the propene TPD for all eight samples in the study, and Figure 27 shows the propane TPD results. A comparison of the zeolite beta samples in panel **A** of Figures 26 and 27, shows that the

desorption of both propene and propane was low, and the center of the desorption peaks was located from 150 to 180°C. This is in agreement with the study by Yoda et al. [113] who studied alkanes and alkenes activation energies and the heat of adsorption onto different zeolites and concluded that the C=C bond of alkenes interacts primarily with Brønsted acid sites. Azambre et al. [93] have studied HC trapping in both wet and dry conditions, and they observed strong water inhibitions associated with a low Si/Al ratio (i.e. large amount of Brønsted acid sites) in wet conditions but low water inhibitions with a high Si/Al ratio (i.e. low amount of Brønsted acid sites). Both studies align and help us understand why the adsorption of propene can be expected to be low in the presence of water.

The samples based on zeolite ZSM-5 and SSZ-13 shown in panel **B** in Figures 26 and 27 show less water inhibition than the samples containing zeolite beta, but it should be noted that water inhibition is significant for all samples. Samples based on zeolite ZSM-5 in the propene TPD experiment show a larger storage capacity of propene than the sample containing SSZ-13. However, the sample with SSZ-13 has a significantly higher temperature of desorption for propene in the figure, which may be associated with the smaller ring size of SSZ-13 compared to ZSM-5. In Figure 27 panel **B** shows an interesting feature of the wet-propane TPD experiments. The sample with SSZ-13 desorbed mainly propane. However, the samples containing ZSM-5 and zeolite beta released the adsorbed propane as propene. Sharma et al. [82] studied HC-trapping on zeolite beta and observed that propane can undergo reactions when adsorbed. This possibility aligns well with the reactions observed in Paper IV.

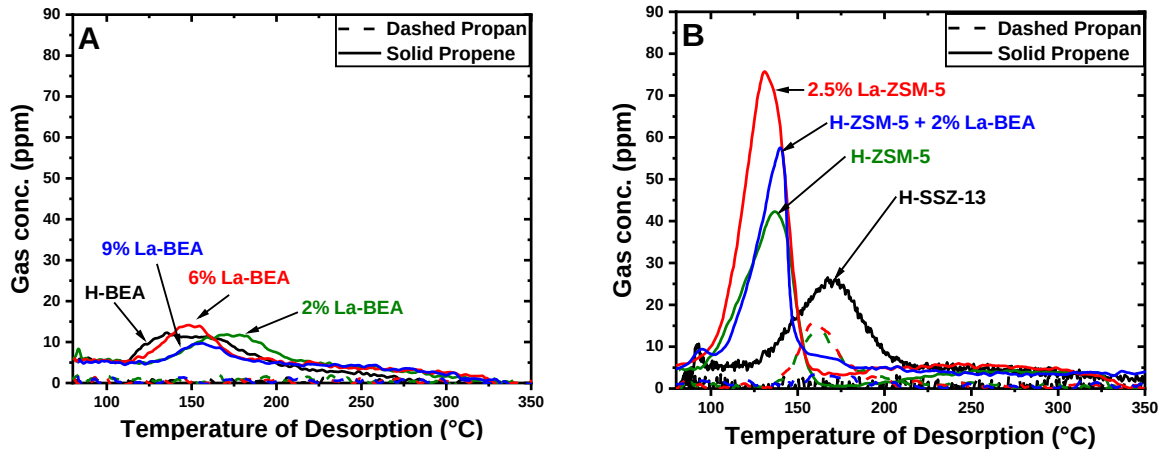

Figure 26. Wet-propene TPD experiments where propene and propane desorption are plotted against the corresponding desorption temperature for: A) H-BEA, 2% La-BEA, 6% La-BEA, and 9% La-BEA; and B) SSZ-13, ZSM-5, 2% La-BEA, and ZSM-5 + 2% La-BEA

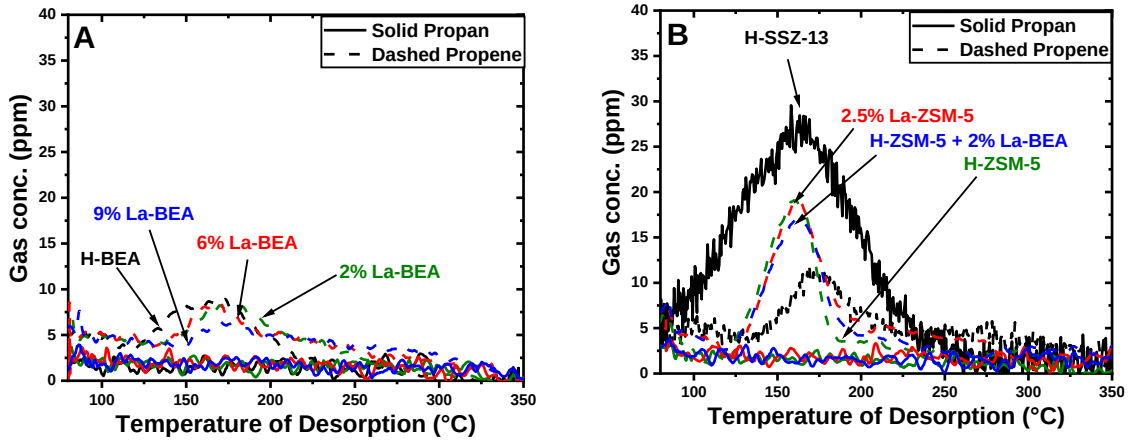

Figure 27. Wet-propane TPD experiments where propene and propane desorption is plotted against the corresponding desorption temperature for: A) H-BEA, 2% La-BEA, 6% La-BEA, and 9% La-BEA; and B) SSZ-13, ZSM-5, 2% La-BEA, and ZSM-5 + 2.5% La-BEA.

In summary, Papers III and IV show that water inhibition affects smaller hydrocarbons to a large extent and remains an important issue for HC traps, even in the future. Zeolite SSZ-13 has a lower adsorption capacity than zeolite ZSM-5 for propene, however, it provides a higher temperature of desorption than zeolite ZSM-5. Interestingly, SSZ-13 store larger amount of propane, compared to the other zeolites, however the amount was still low.

4.2.3 Interaction between hydrocarbons during HC adsorption

Mixed HC-TPD experiments were performed in Paper IV. Toluene, propene, and propane were all present in the loading step of the TPD, together with 5% H_2O. Shown in Figure 28 are the results from these mixed HC-TPD experiments. Panel **A** shows the toluene desorption, and panel **C** shows the propene and propane desorption for samples H-BEA, 2% La-BEA, 6% La-BEA, and 9% La-BEA. Panels **B** and **D** show the same hydrocarbons for H-ZSM-5, 2.5% La-ZSM-5, H-SSZ-13, and (H-ZSM-5 + 2% La-ZSM-5). What can be observed from panel A and B in Figure 28 is that the desorption quantities and patterns of toluene are preserved compared to the wet-toluene TPD results shown in Figure 24. These findings align with Azambre et al. [93] in their studies of mixed HC-TPD experiments. Their HC trap was exposed to propene, toluene, and decane, and over time, the larger hydrocarbons replaced the smaller ones inside the zeolite pores. Considering that toluene is significantly larger than both propene and propane, this could be expected to occur for both zeolite beta and ZSM-5.

The patterns of desorption in panels **C** and **D** in Figure 28 changed during the mixed HC-TPD experiments. This is especially true for the samples shown in panel **D**, where the desorption of propane and propene occurs at very different temperatures for samples containing zeolite-ZSM-5. These samples all have desorption peaks for propene at lower temperature followed by a desorption peak in a higher temperature range. The similarities between Figure 26 **B** and Figure 27 **B** with panel **D** in Figure 28 for sample SSZ-13 indicate that this sample was unaffected by the mixture of hydrocarbons. This could indicate that the presence of toluene primarily

contributes to this change of behavior in zeolite ZSM-5. Panel **D** shows that the temperature of desorption for both propene and propane in zeolite ZSM-5 is dependent on the mixture and sample composition. The temperature of desorption for propane was higher than the temperature for propene in all samples. A possible explanation for this behavior could be the Czaplewski effect [99]. This effect is based on the observations by Czaplewski et al. [99], who did HC-TPD experiments for propane and toluene alone and in a mixture. Those authors found that, in a mixture, propane was released at the same time as toluene, which desorbs at higher temperatures than propane alone. The reason for this was suggested to be attributed to a blocking effect caused by toluene, due to its size. Considering the propene TPD and propane TPD results alone, then, the blocking effect is not enough to explain the increase in both propane and propene. A hypothetical explanation for this phenomenon is that toluene introduces new temporary storage sites for propane inside the zeolite. Since the temperature of desorption and the adsorption capacity do not change as much for propene as for propane, there could possibly be intermolecular interaction between propane and toluene, which are both more hydrophobic than propene.

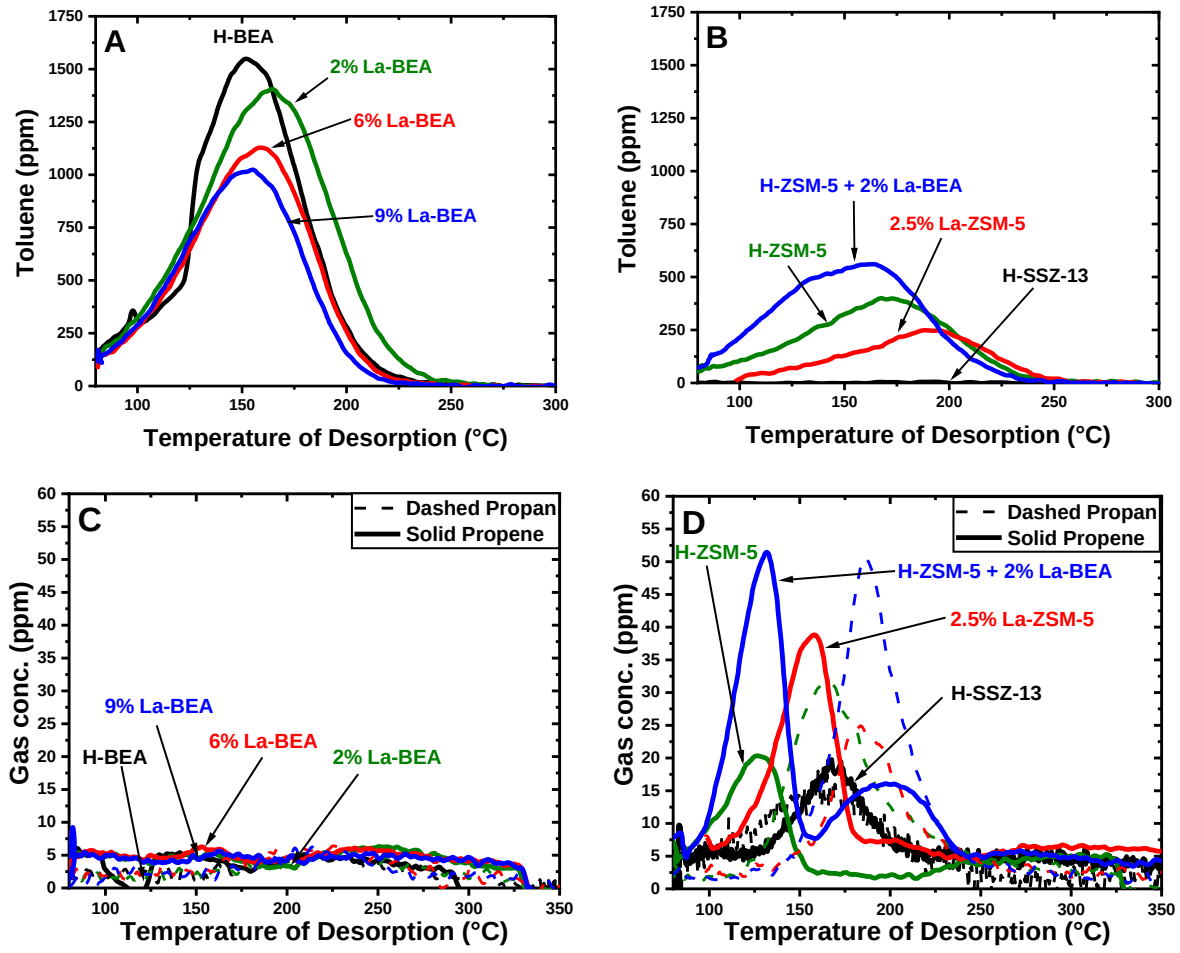

Figure 28. Combined HC-TPD experiments where Toluene (A and B), propene and propane (C and D) desorption is plotted against the corresponding desorption temperature for: A and C) H-BEA, 2% La-BEA, 6% La-BEA, and 9% La-BEA; and B and D) SSZ-13, ZSM-5, 2% La-BEA, and ZSM-5 + 2% La-BEA.

4.2.4 HC-storage sites introduced by Fe, La, and Pd

Adsorbed toluene was analysed in Paper III using in-situ DRIFTS. Washcoated samples were pre-oxidized and loaded identically to the dry-toluene TPD experiment (Figure 21) in a synthetic gas bench reactor. After the loading of toluene, samples were cooled to room temperature and removed from the reactor. Powder was scraped from these loaded samples and used for DRIFTS analysis. Experiments in DRIFTS were conducted in two steps. Firstly, a TPD was performed on toluene-loaded powder. Thereafter, the powder was oxidized at 400°C, then cooled to 80°C for a second TPD. The second TPD experiment was then subtracted from the first to eliminate peaks only associated with the sample. Results from these are shown in Figure 29, where spectra are taken from 80, 150, 250, and 350 °C.

Panels **A**, **C**, **E** and **G** show the wavenumbers in the region 4000-2000cm^{-1}. Five peaks are directly associated with toluene, 3088, 3063, 3030, 2920, and 2866 cm^{-1}. The first three peaks are associated with the C-H stretching vibrations of the aromatic ring of toluene, and the last two are assigned to asymmetric and symmetric C-H stretching vibrations of the methyl group, respectively [114,115]. See Paper III for the assignment of the other peaks visible in panels **A**, **C**, **E** and **G**. These five peaks are negative in their direction and this is due to that it is desorption that are occurring. Some toluene was desorbed from the surface of samples Pd/La/BEA and Pd/Fe/BEA already at 80°C. At 150°C, all samples exhibit these five negative peaks, which are associated with the vibrations of the toluene molecule. This is reasonable given that all samples had their largest desorption peak in this temperature region in the toluene-TPD experiment in Figure 21.

Three peaks are associated with toluene in panels **B**, **D**, **F,** and **H**, with wavenumbers in the region 2000-1000cm^{-1}. These three peaks are 1602, 1494, and 1294cm^{-1} and the two first peaks are assigned to in-plane skeleton vibrations of the phenyl ring, and the last peak is assigned to symmetric vibrations of C-C [116–118]. Similar to the high wavenumber region, these peaks start to be visible at 80°C in the Pd/La/BEA and Pd/Fe/BEA samples. As the temperature reaches 150°C, these negative peaks become visible in all the samples. Two peaks are seen in the region around 1575 cm^{-1} for all samples in Figure 21, except Fe/BEA and BEA. These two peaks have their strongest magnitude around 250°C, which is in the same region the desorption of ethene was observed for the dry-toluene TPD experiment (Figure 22). A possible explanation for these peaks could be that they are temporary storage sites during the cracking of toluene into smaller hydrocarbons. Another possible explanation for these peaks could be that they provide an additional storage site for toluene that activates at higher temperatures. Liu et al. studied Ag-ZSM-5 [89] and observed that the addition of Ag^+ to zeolite ZSM-5 provided new adsorption peaks for toluene. These peaks were located in this region and were assigned to phenyl-Ag^+. Therefore, it is likely that similar behavior could occur after the addition of Pd and La to zeolite beta.

Similar to these results in Paper III, as in-situ DRIFTS was performed in Paper IV, the dual peaks around wavenumber 1575cm^{-1} could be observed clearly for samples doped with La. Doping of a zeolite would supposedly provide a given zeolite with new potential storage sites.

Therefore, such peaks would be expected to appear whether or not the cation improves the zeolite ability to trap toluene.

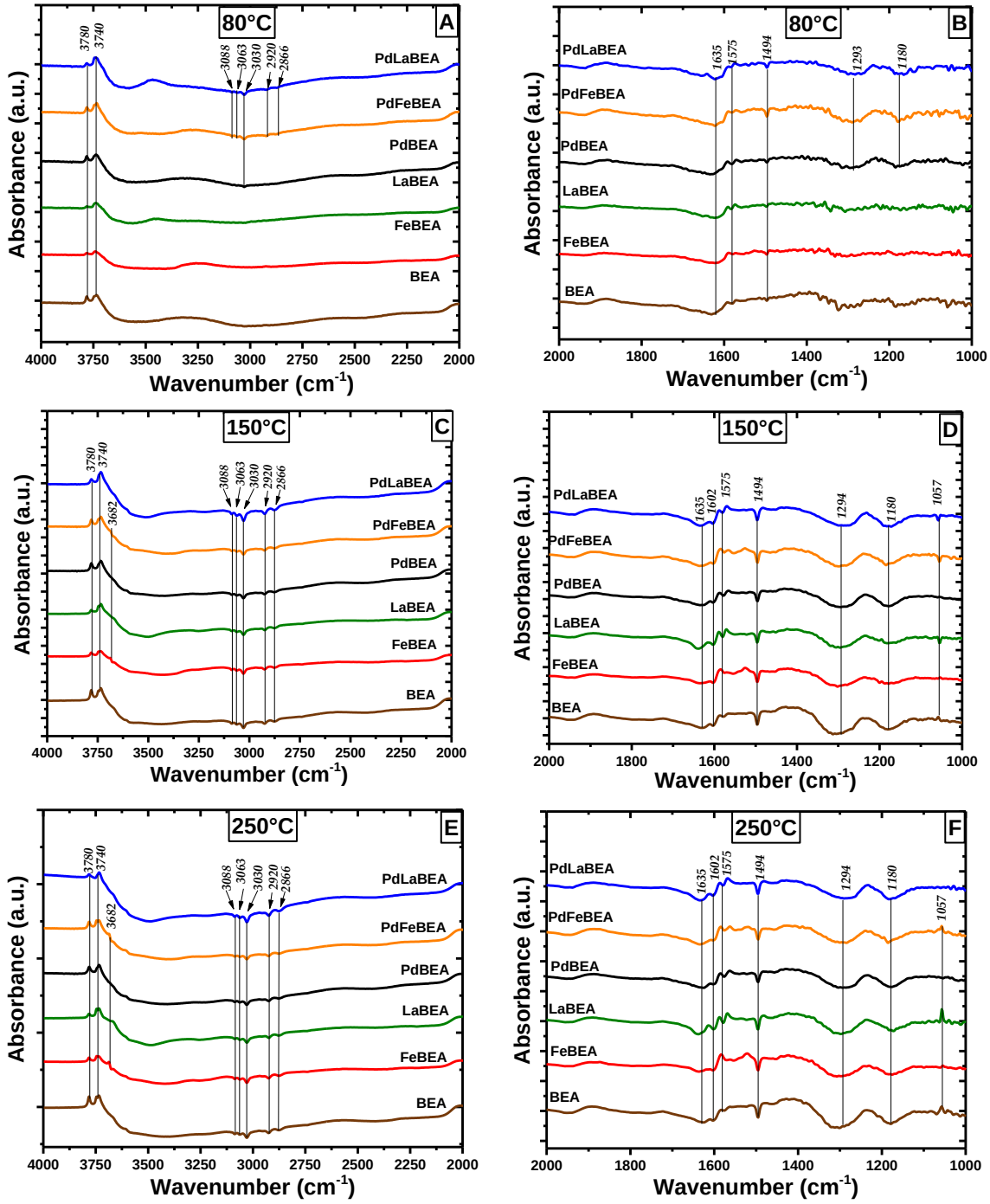

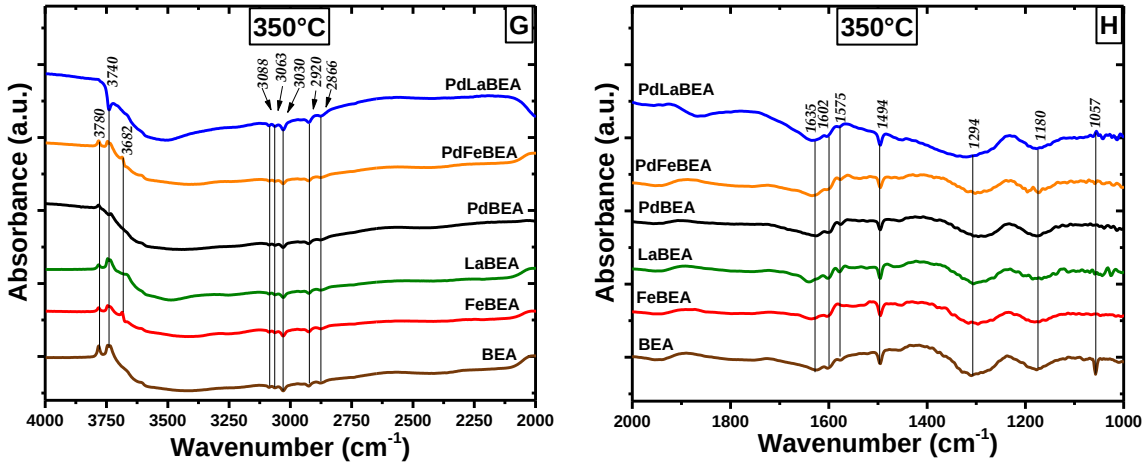

Figure 29. DRIFTS spectra during dry-toluene TPD experiments. A stepwise measurement from 80-350°C with only argon present in the gas feed. Panels A, C, E, and G show the wavenumber region 4000-2000 cm^{-1}. Panels B, D, F, and H show the wavenumber region 2000-1000 cm^{-1}.

4.2.5 Impact of crystallinity on zeolite beta with impregnation of La

Paper IV shows that the addition of lower amounts of La onto zeolite beta improved the zeolite (Figure 24 **A**). However, as the concentration of La increased, the positive effects were lost. All samples were then measured with XRD to further understand the loss of HC-storage capacity. The XRD spectra for H-BEA, 2% La-BEA, 6% La-BEA, and 9% La-BEA are shown in Figure 30 **A** and **B**. The intensity of the samples with a high La loading was reduced, in contrast to H-BEA. A shift towards a higher 2θ was found for the samples with a higher La loading. No clear shift was found for sample 2% La-BEA. A shift toward a higher 2θ, or contra reflection angles, indicates that the shell size of the zeolite structure has decreased [119]. 2% La-BEA loaded with toluene was measured with XRD to further examine the effect of La on crystallinity. The results are shown in Figure 30 **C**. In contrast to the high La loadings, the loading of toluene onto the zeolite shifted the XRD spectra to a lower 2θ. This indicates that toluene expands the shell size of the zeolite. Therefore, the addition of La to a zeolite framework may help stabilize and preserve the crystallinity of the framework during HC trapping.

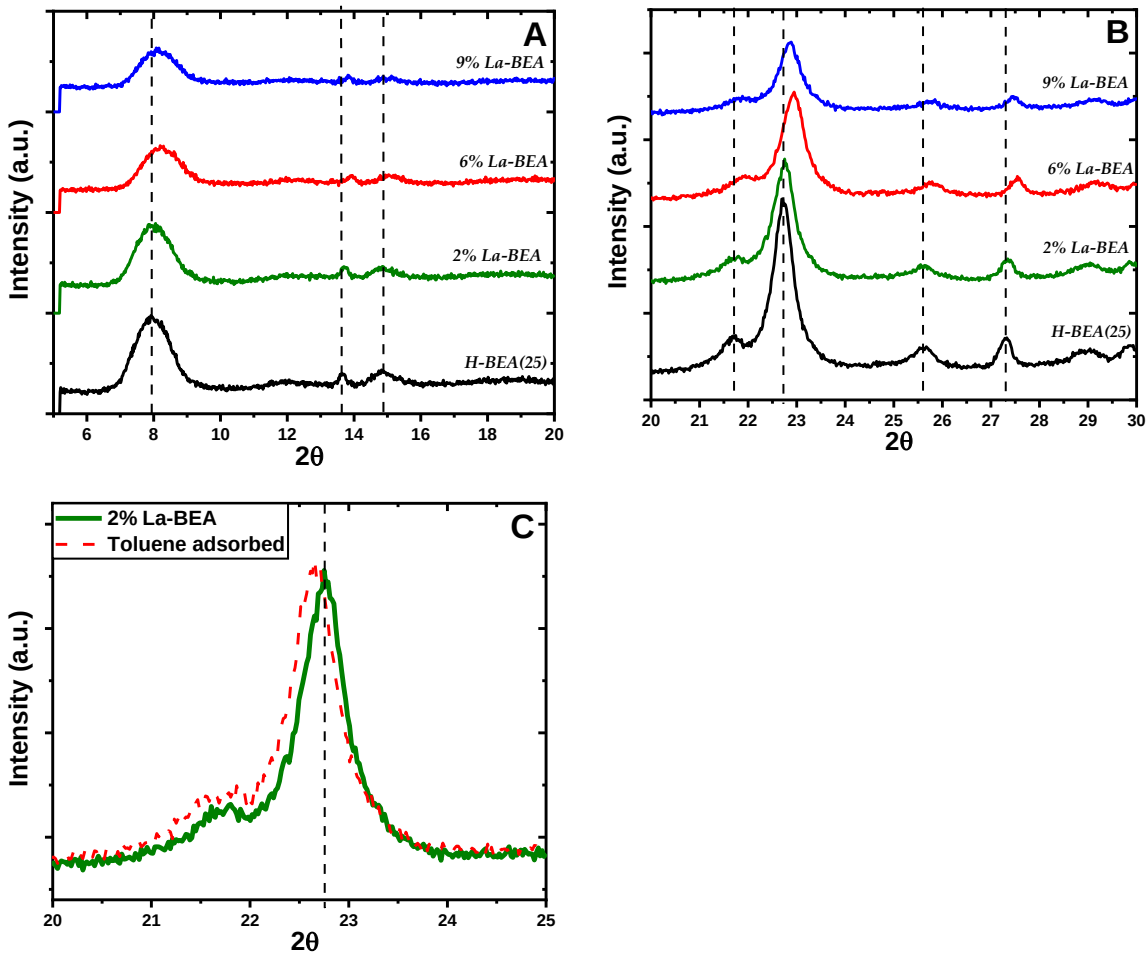

Figure 30. XRD patterns from H-BEA, 2% La-BEA, 6% La-BEA, 9% La-BEA, and 2% La-BEA loaded with toluene. In panel A) the range 5-20 2θ, in panel B) the range 20-40 2θ, and in panel C) the 2% La-BEA and toluene loaded 2% La-BEA are plotted in the range 20-25 2θ.

5 Conclusions

This thesis dealt with exhaust-gas abatement. Papers I and II examined the aging of an LNT catalyst, mainly the effect of P and Zn on the model catalyst $Pt/Ba/Al_2O_3$. The relevance of P and Zn derives from the oil lubricants (ZPPD) used to extend the lifespan of engines in vehicles. Papers III and IV examined hydrocarbon trapping during the cold start of gasoline engines. A large part of pollutants is released during a cold start since the catalyst has not reached light-off. For this reason, the topic of hydrocarbon trapping is relevant for the development of future exhaust-gas abatement.

P was introduced in Papers I and II either through gas-phase exposure or wet impregnation, and Zn was introduced only through wet impregnation. P was mainly located on the surface of the washcoat and in high concentrations at the inlet of the monolith in the gas-phase exposure. However, P was present in a smaller amount in the outlet than in the inlet, but the results indicated that it was more diffused into the washcoat of the LNT catalyst. Results from XPS showed a shift in the oxidation state of P in a comparison of the inlet and outlet of the washcoated monolith structure. At the inlet of the coated monolith, phosphorous was mainly present in the form of P_4O_{10}, however, in the middle, the dominating phosphorous species was PO_3^-. This indicate that different poisoning effects can be present simultaneously. Results from both poisoning methods indicate that P mainly affects the Ba. NSR experiments indicate that during lean phase, the Pt maintained its catalytic properties in the presence of P. Moreover, NO_2 TPD indicated that the storage onto Al_2O_3 was unaffected by P and Zn whilst storage onto Ba was significantly decreased.

The effect of individual and combined poisoning of P and Zn was studied, since both of them are main components in ZDDP, a common oil lubricant for vehicles. This was done by wet impregnation technique, which has the advantage of that the poison amount can be precisely steered. However, the P and Zn will be well distributed over the whole wash-coat, which is not the case for gas phase poisoning. A significant proportion of the deactivation of the catalyst in the gas-phase exposure might be from blockage as well as from the poisoning of the active sites. This is due to a high concentrations of P at the inlet-surface of the washcoat. There are large similarities between the methods of poisoning, such as the breakthrough of NO_X during lean phase, which occurs earlier and with a larger magnitude for both cases. Moreover, that the Pt sites seems not or only to a minor extent be deactivated.

In Paper II, it was found that Zn by itself reduced the NSR capacities of the $Pt/Ba/Al_2O_3$ catalyst, although to a much smaller extent compared to P, and only for higher Zn loadings (2 wt%). Interestingly, combined with P, Zn could reduce the larger deactivation caused by P on the catalyst, for the case with high poisoning loading. The reason for this may stem from a possible interaction between the two species, e.g. the formation of zinc phosphates which could reduce the poisoning of the barium.

Zeolites were doped with different cations and metals in the studies of HC-trapp material. In Paper III, Pd was combined with Fe and La onto zeolite beta to study possibilities for the improvement of HC trapping. It was found that Pd considerably increased the adsorption capacity of toluene for zeolite beta. The addition of La provided an increase in the temperature of desorption for zeolite beta and a slight increase in adsorption capacity, whereas Fe did not provide much of an altered behavior compared to pure zeolite beta. The positive effects caused by Pd and La were verified with DRIFTS experiments, which indicated that the addition of these metals provided zeolite beta with new potential storage sites for hydrocarbons. Paper IV examined the addition of La in different concentrations onto zeolite beta, and it was added to zeolite ZSM-5 for comparison. It was found that there is an optimal amount of La in the zeolite; at 2 wt-% La had positive effects on zeolite beta in terms of the temperature of desorption and the storage capacity for toluene. These effects were lost at 6 and 9 wt-% of La onto zeolite beta. Results from XRD indicated that the impregnation of zeolite beta with La at high loading (6 and 9 wt %) decreased the crystallinity of the zeolite structure and reduced the cell volume and this could explain the negative effect of increasing the La loading to much. Moreover, zeolite ZSM-5 had a lower storage capacity for toluene than zeolite beta, however, the temperature of desorption increased, which may be related to the ring size of the zeolite. The addition of La to zeolite ZSM-5 indicated some improvement of the temperature of desorption of toluene but did slightly reduce the total adsorption capacity. This behavior resembles what was observed for addition of La to zeolite beta in regards to the increased temperature of desorption.

An interesting dynamic was observed between toluene and propane in zeolite ZSM-5 in mixed HC adsorption experiments. Comparing TPD experiments when propene, propane, and toluene are alone and together indicated an increase in HC storage capacity. In a mixed TPD experiment, the propene remained almost the same. However, the propane storage capacity increased as did the temperature of desorption. Possible reasons for this could be that toluene reduces the mass-transport of propane in zeolite ZSM-5. However, it is also possible that propane interacts with toluene and is maintained longer in the system for that reason.

6 Future Work

There are several possibilities for further studies of the aging of an LNT catalyst in terms of phosphorous and zinc poisoning. It would be interesting to further study why phosphorous is present in different forms over the washcoat of the catalyst when introduced through the gas-phase. Also, the interaction observed between Zn and P in Paper II would be interesting to further examine. Moreover, to study if there are possibilities to take advantage of the interaction between these elements in order to reduce the deactivation of P on LNT catalysts. Since these foreign substances are usually introduced to the system in the gas-phase in the real application, it would be interesting to map the effects of the different regions of P in the washcoat. Would Zn have an impact similar to wet impregnation if it was introduced in the gas-phase? These are all interesting possibilities to study on the topic of the zinc and phosphorous poisoning of LNT catalysts.

There are several possibilities for further studies of hydrocarbon trapping during cold In this work it was found that the crystallinity was a key component for incorporation of La into zeolite beta. Therefore, this might also be the limiting factor for other cations in HC trapping purposes. It would therefore be interesting to study the correlation between crystallinity, through XRD measurements, and HC storage capacity as well as the temperature of desorption for different cations with different cation loadings. Furthermore, since there are clear interactions between different HC species during the adsorption, such interactions could be used for further improvements of the cold start. Water inhibition was clearly one of the greater issues observed in the studies of hydrocarbon trapping for smaller molecules. The data in Paper III indicated that water hinders most hydrocarbons from adsorbing, except larger and more hydrophobic HC species. Finding ways to prevent water inhibition would greatly benefit this field.

7 References

1. Guerreiro, C.; Gonzalez Ortiz, A.; de Leeuw, F.; Viana, M.; Horalek, J. *Air quality in Europe — 2016 report*; 2016; ISBN 9789292138240.

2. Takahashi, N.; Shinjoh, H.; Iijima, T.; Suzuki, T.; Yamazaki, K.; Yokota, K.; Suzuki, H.; Miyoshi, N.; Matsumoto, S.; Tanizawa, T.; et al. The new concept 3-way catalyst for automotive lean-burn engine: NOx storage and reduction catalyst. *Catal. Today* **1996**, *27*, 63–69.

3. Epling, W.S.; Campbell, L.E.; Yezerets, A.; Currier, N.W.; Parks, J.E. Overview of the fundamental reactions and degradation mechanisms of NOx storage/reduction catalysts. *Catal. Rev. Sci. Eng.* **2004**, *46*, 163–245.

4. Matsumoto, S. Recent advances in automobile exhaust catalysts. *Catal. Today* **2004**, *90*, 183–190.

5. Nova, I.; Castoldi, L.; Lietti, L.; Tronconi, E.; Forzatti, P.; Prinetto, F.; Ghiotti, G. NOx adsorption study over Pt-Ba/alumina catalysts: FT-IR and pulse experiments. *J. Catal.* **2004**, *222*, 377–388.

6. Partridge, W.P.; Choi, J.S. NH3 formation and utilization in regeneration of Pt/Ba/Al2O3 NOx storage-reduction catalyst with H2. *Appl. Catal. B Environ.* **2009**, *91*, 144–151.

7. Lindholm, A.; Currier, N.W.; Li, J.; Yezerets, A.; Olsson, L. Detailed kinetic modeling of NOx storage and reduction with hydrogen as the reducing agent and in the presence of CO2 and H2O over a Pt/Ba/Al catalyst. *J. Catal.* **2008**, *258*, 273–288.

8. Park, J.H.; Park, S.J.; Nam, I.S.; Yeo, G.K.; Kil, J.K.; Youn, Y.K. A fast and quantitative assay for developing zeolite-type hydrocarbon trap catalyst. *Microporous Mesoporous Mater.* **2007**, *101*, 264–270.

9. Kim, M.Y.; Kyriakidou, E.A.; Choi, J.S.; Toops, T.J.; Binder, A.J.; Thomas, C.; Parks, J.E.; Schwartz, V.; Chen, J.; Hensley, D.K. Enhancing low-temperature activity and durability of Pd-based diesel oxidation catalysts using ZrO2 supports. *Appl. Catal. B Environ.* **2016**, *187*, 181–194.

10. Du, S.; Tang, W.; Guo, Y.; Binder, A.; Kyriakidou, E.A.; Toops, T.J.; Wang, S.; Ren, Z.; Hoang, S.; Gao, P.X. Understanding low temperature oxidation activity of nanoarray-based monolithic catalysts: from performance observation to structural and chemical insights. *Emiss. Control Sci. Technol.* **2017**, *3*, 18–36.

11. Hazlett, M.J.; Epling, W.S. Spatially resolving CO and C 3 H 6 oxidation reactions in a Pt/Al 2 O 3 model oxidation catalyst. *Catal. Today* **2016**, *267*, 157–166.

12. Ikeda, Y.; Sobue, K.; Tsuji, S.; Matsumoto, S. Development of NOx storage-reduction Three-way catalyst for D-4 Engines. *SAE Tech. Pap.* **1999**, *1999-01–12*.

13. Clayton, R.D.; Harold, M.P.; Balakotaiah, V.; Wan, C.Z. Pt dispersion effects during NOx storage and reduction on Pt/BaO/Al2O3 catalysts. *Appl. Catal. B Environ.* **2009**, *90*, 662–676.

14. Andonova, S.; Marchionni, V.; Lietti, L.; Olsson, L. Enhanced low temperature NO x reduction performance over bimetallic Pt/Rh-BaO lean NO x trap catalysts. *Top. Catal.* **2013**, *56*, 68–74.

15. Clayton, R.D.; Harold, M.P.; Balakotaiah, V. Selective catalytic reduction of NO by H2 in O2 on Pt/BaO/Al2O3 monolith NOx storage catalysts. *Appl. Catal. B Environ.* **2008**, *81*, 161–181.

16. Lietti, L.; Artioli, N.; Righini, L.; Castoldi, L.; Forzatti, P. Pathways for N_2 and N_2O Formation during the Reduction of NO_x over Pt–Ba/Al_2O_3 LNT Catalysts Investigated by Labeling Isotopic Experiments. *Ind. Eng. Chem. Res.* **2012**, *51*, 7597–7605.

17. Lietti, L.; Nova, I.; Forzatti, P. Role of ammonia in the reduction by hydrogen of NOx stored over Pt-Ba/Al2O3 lean NOx trap catalysts. *J. Catal.* **2008**, *257*, 270–282.

18. Olsson, L.; Fridell, E.; Skoglundh, M.; Andersson, B. Mean field modelling of NOx storage on Pt/BaO/Al2O3. *Catal. Today* **2002**, *73*, 263–270.

19. Casapu, M.; Grunwaldt, J.D.; Maciejewski, M.; Krumeich, F.; Baiker, a.; Wittrock, M.; Eckhoff, S. Comparative study of structural properties and NOx storage-reduction behavior of Pt/Ba/CeO2 and Pt/Ba/Al2O3. *Appl. Catal. B Environ.* **2008**, *78*, 288–300.

20. Malpartida, I.; Guerrero-Pérez, M.O.; Herrera, M.C.; Larrubia, M. a.; Alemany, L.J. MS-FTIR reduction stage study of NSR catalysts. *Catal. Today* **2007**, *126*, 162–168.

21. Kobayashi, T.; Yamada, T.; Kayano, K. Study of NOx Trap Reaction by Thermodynamic Calculation. *SAE Tech. Pap. Ser.* **1997**, 970745.

22. Ando, H.; Tamura, Y.; Kikuchi, S.; Okada, K.; Koga, K. Development of Advanced Emission-Control Technologies for Gasoline Direct- Injection Engines. *SAE Tech. Pap. 2001-01-0254* **2001**, *2001*.

23. Lindholm, A.; Currier, N.W.; Dawody, J.; Hidayat, A.; Li, J.; Yezerets, A.; Olsson, L. The influence of the preparation procedure on the storage and regeneration behavior of Pt and Ba based NOx storage and reduction catalysts. *Appl. Catal. B Environ.* **2009**, *88*, 240–248.

24. Shimizu, K. ichi; Saito, Y.; Nobukawa, T.; Miyoshi, N.; Satsuma, A. Effect of supports on formation and reduction rate of stored nitrates on NSR catalysts as investigated by in situ FT/IR. *Catal. Today* **2008**, *139*, 24–28.

25. Lindholm, A.; Currier, N.W.; Fridell, E.; Yezerets, A.; Olsson, L. NOx storage and reduction over Pt based catalysts with hydrogen as the reducing agent. Influence of H2O and CO2. *Appl. Catal. B Environ.* **2007**, *75*, 78–87.

26. Xu, J.; Harold, M.P.; Balakotaiah, V. Microkinetic modeling of steady-state NO/H2/O2 on Pt/BaO/Al2O3 NOx storage and reduction monolith catalysts. *Appl. Catal. B Environ.* **2009**, *89*, 73–86.

27. Olsson, L.; Fridell, E. The Influence of Pt Oxide Formation and Pt Dispersion on the

Reactions NO2⇔NO+1/2 O2 over Pt/Al2O3 and Pt/BaO/Al2O3. *J. Catal.* **2002**, *210*, 340–353.

28. Corbos, E.C.; Courtois, X.; Can, F.; Marécot, P.; Duprez, D. NOx storage properties of Pt/Ba/Al model catalysts prepared by different methods. *Appl. Catal. B Environ.* **2008**, *84*, 514–523.

29. Nova, I.; Castoldi, L.; Lietti, L.; Tronconi, E.; Forzatti, P. How to control the selectivity in the reduction of NOx with H2 over Pt-Ba/Al2O3 Lean NOx Trap catalysts. In Proceedings of the Topics in Catalysis; 2007; Vol. 42–43, pp. 21–25.

30. Salasc, S.; Skoglundh, M.; Fridell, E. A comparison between Pt and Pd in NOx storage catalysts. *Appl. Catal. B Environ.* **2002**, *36*, 145–160.

31. Andonova, S.; Marchionni, V.; Borelli, M.; Nedyalkova, R.; Lietti, L.; Olsson, L. Mechanistic investigations of the promoting role of Rh on the NSR performance of NOx storage BaO-based catalysts. *Appl. Catal. B Environ.* **2013**, *132–133*, 266–281.

32. Ji, Y.; Choi, J.S.; Toops, T.J.; Crocker, M.; Naseri, M. Influence of ceria on the NOx storage/reduction behavior of lean NOx trap catalysts. *Catal. Today* **2008**, *136*, 146–155.

33. Kašpar, J.; Fornasiero, P.; Graziani, M. Use of CeO 2-based oxides in the three-way catalysis. *Catal. Today* **1999**, *50*, 285.

34. Lietti, L.; Forzatti, P.; Nova, I.; Tronconi, E. NOxstorage reduction over Pt-Ba/γ - Al2O3catalyst. *J. Catal.* **2001**, *204*, 175–191.

35. Hodjati, S.; Bernhardt, P.; Petit, C.; Pitchon, V.; Kiennemann, A. Removal of NO x : Part I . Sorption / desorption processes on barium aluminate. *Appl. Catal.* **1998**, *19*, 209–219.

36. Olsson, L.; Persson, H.; Fridell, E.; Skoglundh, M.; Andersson, B. A Kinetic Study of NO Oxidation and NO x Storage on Pt/Al2O3 and Pt/BaO/Al2O3. *J. Phys. Chem. B* **2001**, *105*, 6895–6906.

37. Nova, I.; Tronconi, E. *Urea-SCR Technology for deNOx After Treatment of Diesel Exhausts*; 2014; ISBN 978-1-4899-8070-0.

38. Olsson, L.; Westerberg, B.; Persson, H.; Fridell, E.; Skoglundh, M.; Andersson, B. A Kinetic Study of Oxygen Adsorption/Desorption and NO Oxidation over Pt/Al2O3 Catalysts. *J. Phys. Chem. B* **1999**, *103*, 10433–10439.

39. Perng, C.C.Y.; Easterling, V.G.; Harold, M.P. Fast lean-rich cycling for enhanced NOxconversion on storage and reduction catalysts. *Catal. Today* **2014**, *231*, 125–134.

40. Epling, W.S.; Campbell, G.C.; Parks, J.E. The effects of CO2 and H2O on the NOx destruction performance of a model NOx storage/reduction catalyst. *Catal. Letters* **2003**, *90*, 45–56.

41. Li, Y.; Roth, S.; Dettling, J.; Beutel, T. Effects of lean / rich timing and nature of reductant on the performance of a NO x trap catalyst. *Top. Catal.* **2001**, *16/17*, 139–144.

42. Abdulhamid, H.; Fridell, E.; Skoglundh, M. Influence of the type of reducing agent (H2,CO,C3H6 and C3H8)onthe reduction of stored NOX in a Pt/BaO/Al2O3 model catalyst. *Top. Catal.* **2004**, *30*, 161–168.

43. Bamwenda, G. The role of the metal during NO2 reduction by C3H6 over alumina and

silica-supported catalysts. *J. Mol. Catal. A Chem.* **1997**, *126*, 151–159.

44. Sedlmair, C.; Seshan, K.; Jentys, A.; Lercher, J.A. Studies on the deactivation of NOx storage-reduction catalysts by sulfur dioxide. *Catal. Today* **2002**, *75*, 413–419.

45. Piacentini, M.; Maciejewski, M.; Baiker, a. NOx storage-reduction behavior of Pt-Ba/MO2 (MO2 = SiO2, CeO2, ZrO2) catalysts. *Appl. Catal. B Environ.* **2007**, *72*, 105–117.

46. Tonkyn, R.G.; Disselkamp, R.S.; Peden, C.H.F. Nitrogen release from a NOx storage and reduction catalyst. *Catal. Today* **2006**, *114*, 94–101.

47. Ji, Y.; Easterling, V.; Graham, U.; Fisk, C.; Crocker, M.; Choi, J.S. Effect of aging on the NO x storage and regeneration characteristics of fully formulated lean NO x trap catalysts. *Appl. Catal. B Environ.* **2011**, *103*, 413–427.

48. Andersson, J.; Antonsson, M.; Eurenius, L.; Olsson, E.; Skoglundh, M. Deactivation of diesel oxidation catalysts: Vehicle- and synthetic aging correlations. *Appl. Catal. B Environ.* **2007**, *72*, 71–81.

49. Bartholomew, C.H. Mechanism of catalyst deactivation. *Appl. Catal. A Gen.* **2001**, *212*, 17–60.

50. Stanmore, B.R.; Brilhac, J.F.; Gilot, P. The oxidation of soot: A review of experiments, mechanisms and models. *Carbon N. Y.* **2001**, *39*, 2247–2268.

51. Bunting, B.G.; More, K.; Lewis, S.; Toops, T. Phosphorous Poisoning and Phosphorous Exhaust Chemistry with Diesel Oxidation Catalysts. *SAE Tech. Pap.* **2005**, *2005*.

52. Bodek, K.M.; Wong, V.W. The Effects of Sulfated Ash , Phosphorus and Sulfur on Diesel Aftertreatment Systems – A Review. *Sae Pap. 2007-01-1922* **2007**, 1–21.

53. Umeno, T.; Hanzawa, M.; Hayashi, Y.; Hori, M. Development of New Lean NOx Trap Technology with High Sulfur Resistance. *SAE Int.* **2014**.

54. Le Phuc, N.; Corbos, E.C.; Courtois, X.; Can, F.; Marecot, P.; Duprez, D. NOx storage and reduction properties of Pt/CexZr1-xO2 mixed oxides: Sulfur resistance and regeneration, and ammonia formation. *Appl. Catal. B Environ.* **2009**, *93*, 12–21.

55. Huang, H.Y.; Long, R.Q.; Yang, R.T. A highly sulfur resistant Pt-Rh/TiO2/Al2O3 storage catalyst for NOx reduction under lean-rich cycles. *Appl. Catal. B Environ.* **2001**, *33*, 127–136.

56. Hochhauser, A.M.; Schleyer, C.H.; Yeh, L.I.; Rickeard, D.J. Impact of Fuel Sulfur on Gasoline and Diesel Vehicle Emissions. *SAE Tech. Pap. Ser.* **2006**, 776–790.

57. Rokosz, M.J.; Chen, A.E.; Lowe-Ma, C.K.; Kucherov, a. V.; Benson, D.; Paputa Peck, M.C.; McCabe, R.W. Characterization of phosphorus-poisoned automotive exhaust catalysts. *Appl. Catal. B Environ.* **2001**, *33*, 205–215.

58. Angove, D.E.; Cant, N.W. Position dependent phenomena during deactivation of three-way catalytic converters on vehicles. *Catal. Today* **2000**, *63*, 371–378.

59. Beck, D.; Monroe, D.; DiMaggio Craig; Sommers, J. Impact of Oil-Derived Catalyst Poisons on FTP Performance of LEV Catalyst Systems. *SAE Tech. Pap.* **1997**.

60. Wang, L.; Wang, L.; Li, G.; Xu, X. The Effect of ZDDP Type on Phosphorus Volatility:

Engine Oil Performance on Sequence IIIG and Field Tests. **2013**.

61. Guevremont, J.M.; Guinther, G.; Jao, T.; Herlihy, T.; White, R.; Howe, J. Total Phosphorus Detection and Mapping in Catalytic Converters. *SAE Tech. Pap.* **2007**.

62. Uy, D.; O'Neill, A.E.; Xu, L.; Weber, W.H.; McCabe, R.W. Observation of cerium phosphate in aged automotive catalysts using Raman spectroscopy. *Appl. Catal. B Environ.* **2003**, *41*, 269–278.

63. Williamson, W.B.; Perry, J.; Gandhi, H.S.; Bomback, J.L. Effects of oil phosphorus on deactivation of monolithic three-way catalysts. *Appl. Catal.* **1985**, *15*, 277–292.

64. Beck, D.D.; Sommers, J.W.; DiMaggio, C.L. Axial characterization of oxygen storage capacity in close-coupled lightoff and underfloor catalytic converters and impact of sulfur. *Appl. Catal. B Environ.* **1997**, *11*, 273–290.

65. Beck, D.; Monroe, D.; DiMaggio Craig; Sommers, J. Axial Characterization of Lightoff and Underfloor Catalytic Converters Vehicle-Aged on a 5.7 L Corvette. *SAE Tech. Pap.* **1995**.

66. Sumida, H.; Koda, Y.; Sadai, A.; Ichikawa, S.; Kyogoku, M.; Takato, M.; Miwa, Y. Analysis of Phosphorus Poisoning on Exhaust Catalysts from Compact-Class Vehicle. *SAE Tech. Pap.* **2004**, *2004-01–01*.

67. Larese, C.; Galisteo, F.; Granados, M.; Mariscal, R.; Fierro, J.; Lambrou, P.; Efstathiou, a Effects of the CePO on the oxygen storage and release properties of CeO and CeZrO solid solution. *J. Catal.* **2004**, *226*, 443–456.

68. Larese, C.; Cabello Galisteo, F.; López Granados, M.; Mariscal López, R.; Fierro, J.L.G.; Lambrou, P.S.; Efstathiou, a. M. Effects of calcination temperature on the stability of CePO4 detected in vehicle-aged commercial three-way catalysts. *Appl. Catal. B Environ.* **2004**, *48*, 113–123.

69. López Granados, M.; Galisteo, F.C.; Lambrou, P.S.; Mariscal, R.; Sanz, J.; Sobrados, I.; Fierro, J.L.G.; Efstathiou, a. M. Role of P-containing species in phosphated CeO2 in the deterioration of its oxygen storage and release properties. *J. Catal.* **2006**, *239*, 410–421.

70. Christou, S.Y.; Efstathiou, A.M. The effects of P-poisoning of CexZr1-xO2 on the transient oxygen storage and release kinetics. *Top. Catal.* **2013**, *56*, 232–238.

71. Eaton, S.J.; Bunting, B.G.; Toops, T.J. The Roles of Phosphorus and Soot on the Deactivation of Diesel Oxidation Catalysts. **2009**.

72. Kröger, V.; Lassi, U.; Kynkäänniemi, K.; Suopanki, A.; Keiski, R.L. Methodology development for laboratory-scale exhaust gas catalyst studies on phosphorus poisoning. *Chem. Eng. J.* **2006**, *120*, 113–118.

73. Andonova, S.; Vovk, E.; Sjöblom, J.; Ozensoy, E.; Olsson, L. Chemical deactivation by phosphorous under lean hydrothermal conditions over Cu/BEA NH3-SCR catalysts. *Appl. Catal. B Environ.* **2014**, *147*, 251–263.

74. Shwan, S.; Olsson, L.; Skoglundh, M.; Jansson, J. Kinetic Modeling of Fe-BEA as NH3-SCR Catalyst—Effect of Phosphorous. *AIChe* **2014**, *61*, 215–223.

75. Shwan, S.; Jansson, J.; Olsson, L.; Skoglundh, M. Chemical deactivation of Fe-BEA as NH3-SCR catalyst-Effect of phosphorous. *Appl. Catal. B Environ.* **2013**, *147*, 111–123.

76. Yamazaki, K.; Suzuki, T.; Takahashi, N.; Yokota, K.; Sugiura, M. Effect of the addition of transition metals to Pt / Ba / Al 2 O 3 catalyst on the NO x storage-reduction catalysis under oxidizing conditions in the presence of SO 2. *Appl. Catal. B Environ.* **2001**, *30*, 459–468.

77. Togawa, S.; Nemoto, S.; Yamamoto, H.; Nakamura, K.; Miura, M.; Hashimoto, T.; Yoshida, S.; Matsuura, K. Impact of Oil-derived Sulfur and Phosphorus on Diesel NOx Storage Reduction Catalyst – JCAP II Oil WG Report. *SAE Int.* **2006**.

78. Cabello Galisteo, F.; López Granados, M.; Martín Alonso, D.; Mariscal, R.; Fierro, J.L.G. Loss of NOx storage capacity of Pt-Ba/Al2O3 catalysts due to incorporation of phosphorous. *Catal. Commun.* **2008**, *9*, 327–332.

79. Christou, S.Y.; García-Rodríguez, S.; Fierro, J.L.G.; Efstathiou, a. M. Deactivation of Pd/Ce 0.5Zr 0.5O 2 model three-way catalyst by P, Ca and Zn deposition. *Appl. Catal. B Environ.* **2012**, *111–112*, 233–245.

80. Chen, H.-Y.; Mulla, S.; Weigert, E.; Camm, K.; Ballinger, T.; Cox, J.; Blakeman, P. Cold Start Concept (CSC^{TM}): A Novel Catalyst for Cold Start Emission Control. *SAE Int. J. Fuels Lubr.* **2013**, *6*, 2013-01–0535.

81. Westermann, A.; Azambre, B. Impact of the Zeolite Structure and Acidity on the Adsorption of Unburnt Hydrocarbons Relevant to Cold Start Conditions. *J. Phys. Chem. C* **2016**, *120*, 25903–25914.

82. Sharma, M.; Shane, M. Hydrocarbon-Water Adsorption and Simulation of Catalyzed Hydrocarbon Traps. *Catal. Today* **2016**, *267*, 82–92.

83. Rao, K.N.; Kim, M.; Song, J.; Na, S.; Sik, H.; Heesung, H. Cold-Start Hydrocarbon Speciation and Trap Materials for Gasoline Engines. **2018**, 1–8.

84. Wesson, P.J.; Snurr, R.Q. Modified temperature programmed desorption evaluation of hydrocarbon trapping by CsMOR zeolite under cold start conditions. *Microporous Mesoporous Mater.* **2009**, *125*, 35–38.

85. Yoshimoto, R.; Hara, K.; Okumura, K.; Katada, N.; Niwa, M. Analysis of toluene adsorption on na-form zeolite with a temperature-programmed desorption method. *J. Phys. Chem. C* **2007**, *111*, 1474–1479.

86. Kanazawa, T. Development of hydrocarbon adsorbents, oxygen storage materials for three-way catalysts and NOx storage-reduction catalyst. *Catal. Today* **2004**, *96*, 171–177.

87. Moor, B.A. De; Gobin, O.C.; Lercher, J.A.; Marin, G.B. Adsorption of C2 - C8. **2011**, 1204–1219.

88. Blakeman, P.G.; Burkholder, E.M.; Chen, H.Y.; Collier, J.E.; Fedeyko, J.M.; Jobson, H.; Rajaram, R.R. The role of pore size on the thermal stability of zeolite supported Cu SCR catalysts. *Catal. Today* **2014**, *231*, 56–63.

89. Liu, X.; Lampert, J.K.; Arendarskiia, D.A.; Farrauto, R.J. FT-IR spectroscopic studies of hydrocarbon trapping in Ag+-ZSM-5 for gasoline engines under cold-start conditions. *Appl. Catal. B Environ.* **2001**, *35*, 125–136.

90. Westermann, A.; Azambre, B.; Finqueneisel, G.; Da Costa, P.; Can, F. Evolution of unburnt hydrocarbons under "cold-start" conditions from adsorption/desorption to

conversion: On the screening of zeolitic materials. *Appl. Catal. B Environ.* **2014**, *158–159*, 48–59.

91. Park, J.H.; Park, S.J.; Ahn, H.A.; Nam, I.S.; Yeo, G.K.; Kil, J.K.; Youn, Y.K. Promising zeolite-type hydrocarbon trap catalyst by a knowledge-based combinatorial approach. *Microporous Mesoporous Mater.* **2009**, *117*, 178–184.

92. Spoto, G.; Bordiga, S.; Ricchiardi, G.; Scarano, D.; Zecchina, A.; Borello, E. IR study of ethene and propene oligomerization on H-ZSM-5: Hydrogen-bonded precursor formation, initiation and propagation mechanisms and structure of the entrapped oligomers. *J. Chem. Soc. Faraday Trans.* **1994**, *90*, 2827–2835.

93. Azambre, B.; Westermann, A.; Finqueneisel, G.; Can, F.; Comparot, J.D. Adsorption and desorption of a model hydrocarbon mixture over HY zeolite under dry and wet conditions. *J. Phys. Chem. C* **2015**, *119*, 315–331.

94. Luo, J.; Mccabe, R.W.; Dearth, M.A.; Gorte, R.J. Transient Adsorption Studies of Automotive Hydrocarbon Traps. *AICHE J.* **2014**, *60*, 2875–2881.

95. Kang, S.B.; Kalamaras, C.; Balakotaiah, V.; Epling, W. Hydrocarbon Trapping over Ag-Beta Zeolite for Cold-Start Emission Control. *Catal. Letters* **2017**, *147*, 1355–1362.

96. Daldoul, I.; Auger, S.; Picard, P.; Nohair, B.; Kaliaguine, S. Effect of temperature Ramp on hydrocarbon desorption profiles from zeolite ZSM-12. *Can. J. Chem. Eng.* **2016**, *94*, 931–937.

97. Yamamoto, S.; Matsushita, K.; Satomi, E.; Takaya, M. In-line hydrocarbon (HC) adsorber system for cold start emissions. *SAE Tech. Pap.* **2000**, *01*.

98. Goralski, C.T.; Chanko, T.; Lupescu, J.; Ganti, G. Experimental and modeling investigation of catalyzed hydrocarbon trap performance. *SAE Tech. Pap.* **2000**.

99. Czaplewski, K.F.; Reitz, T.L.; Kim, Y.J.; Snurr, R.Q. One-dimensional zeolites as hydrocarbon traps. *Microporous Mesoporous Mater.* **2002**, *56*, 55–64.

100. Sarshar, Z.; Zahedi-Niaki, M.H.; Huang, Q.; Eić, M.; Kaliaguine, S. MTW zeolites for reducing cold-start emissions of automotive exhaust. *Appl. Catal. B Environ.* **2009**, *87*, 37–45.

101. Takamitsu, Y.; Ariga, K.; Yoshida, S.; Ogawa, H.; Sano, T. Adsorption of toluene on alkali metal ion-exchanged zsm-5 and β-zeolites under humid conditions. *Bull. Chem. Soc. Jpn.* **2012**, *85*, 869–876.

102. Serra, R.M.; Miró, E.E.; Bolcatto, P.; Boix, A. V. Experimental and theoretical studies about the adsorption of toluene on ZSM5 and mordenite zeolites modified with Cs. *Microporous Mesoporous Mater.* **2012**, *147*, 17–29.

103. Choudhary, V.R.; Srinivasan, K.R.; Singh, A.P. Temperature-programmed desorption of aromatic hydrocarbons on silicalite-I and ZSM-5-type zeolites. *Zeolites* **1990**, *10*, 16–20.

104. Xu, L.; Lupescu, J.; Cavataio, G.; Guo, K.; Jen, H. The Impacts of Pd in BEA Zeolite on Decreasing Cold-Start NMOG Emission of an E85 Fuel Vehicle. *SAE Int. J. Fuels Lubr.* **2018**, *11*, 239–246.

105. Lupescu, J.; Xu, L.; Jen, H.-W.; Harwell, A.; Company, F.M.; Nunan, J.; Alltizer, C.; Denison Umicore, G. A New Catalyzed HC Trap Technology that Enhances the

Conversion of Gasoline Fuel Cold-Start Emissions. *SAE Tech. Pap. 2018-01-0938* **2018**, 2018–1.

106. Burke, N.R.; Trimm, D.L.; Howe, R.F. The effect of silica:alumina ratio and hydrothermal ageing on the adsorption characteristics of BEA zeolites for cold start emission control. *Appl. Catal. B Environ.* **2003**, *46*, 97–104.

107. Yamashita, T.; Hayes, P. Analysis of XPS spectra of Fe2+ and Fe3+ ions in oxide materials. *Appl. Surf. Sci.* **2008**, *254*, 2441–2449.

108. De Abreu Goes, J.E.; Olsson, L.; Berggrund, M.; Kristoffersson, A.; Gustafson, L.; Hicks, M. Performance Studies and Correlation between Vehicle- and Rapid- Aged Commercial Lean NOx Trap Catalysts. *SAE Int. J. Engines* **2017**, *10*, 2017-01–0940.

109. J.F. Moulder, W. Stickle, P.E. Sobol, K.D. Bomben *Handbook of X-ray Photoelectron Spectroscopy*; Perkin Elmer Corporation, Eden Prairie, MN, 1992;

110. Larese, C.; Cabello Galisteo, F.; López Granados, M.; Mariscal, R.; Fierro, J.L.G.; Furió, M.; Fernández Ruiz, R. Deactivation of real three way catalysts by CePO4 formation. *Appl. Catal. B Environ.* **2003**, *40*, 305–317.

111. Luo, J.Y.; Meng, M.; Zha, Y.Q.; Xie, Y.N.; Hu, T.D.; Zhang, J.; Liu, T. A comparative study of Pt/Ba/Al2O3 and Pt/Fe-Ba/Al2O3 NSR catalysts: New insights into the interaction of Pt-Ba and the function of Fe. *Appl. Catal. B Environ.* **2008**, *78*, 38–52.

112. Huber, G.W.; Corma, A. Synergies between bio- and oil refineries for the production of fuels from biomass. *Angew. Chemie - Int. Ed.* **2007**, *46*, 7184–7201.

113. Yoda, E.; Kondo, J.N.; Domen, K. Detailed process of adsorption of alkanes and alkenes on zeolites. *J. Phys. Chem. B* **2005**, *109*, 1464–1472.

114. Sanati, M.; Andersson, A. DRIFT study of the oxidation and the ammoxidation of toluene over a TiO2(B)-supported vanadia catalyst. *J. Mol. Catal.* **1993**, *81*, 51–62.

115. Li, X.; Zhu, Z.; Zhao, Q.; Wang, L. Photocatalytic degradation of gaseous toluene over ZnAl2O4 prepared by different methods: A comparative study. *J. Hazard. Mater.* **2011**, *186*, 2089–2096.

116. Du, J.; Qu, Z.; Dong, C.; Song, L.; Qin, Y.; Huang, N. Low-temperature abatement of toluene over Mn-Ce oxides catalysts synthesized by a modified hydrothermal approach. *Appl. Surf. Sci.* **2018**, *433*, 1025–1035.

117. Nagao, M.; Suda, Y. Adsorption of Benzene, Toluene, and Chlorobenzene on Titanium Dioxide. *Langmuir* **1989**, *5*, 42–47.

118. Wang, M.; Zhang, F.; Zhu, X.; Qi, Z.; Hong, B.; Ding, J.; Bao, J.; Sun, S.; Gao, C. DRIFTS evidence for facet-dependent adsorption of gaseous toluene on TiO2 with relative photocatalytic properties. *Langmuir* **2015**, *31*, 1730–1736.

119. Peng, X.; Schlamp, M.C.; Kadavanich, A. V.; Alivisatos, A.P. Epitaxial growth of highly luminescent CdSe/CdS core/shell nanocrystals with photostability and electronic accessibility. *J. Am. Chem. Soc.* **1997**, *119*, 7019–7029.